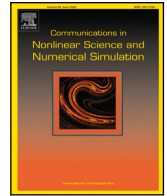




Contents lists available at [ScienceDirect](https://www.sciencedirect.com)

# Communications in Nonlinear Science and Numerical Simulation

journal homepage: [www.elsevier.com/locate/cnsns](http://www.elsevier.com/locate/cnsns)

Research paper

## Semi-analytical attitude propagation for earth orbiting objects

I. Cavallari , J. Feng, M. Vasile \*

Aerospace Centre of Excellence, University of Strathclyde, 75 Montrose Street, G11XJ, Glasgow, UK

### ARTICLE INFO

#### Keywords:

Attitude dynamics  
Celestial mechanics  
Space objects  
Perturbation theory  
Semi-analytical propagation

### ABSTRACT

This paper presents the development of a semi-analytical theory for the long-term propagation of the attitude motion of Earth-orbiting objects with arbitrary shape. The attitude dynamics includes the effects of gravity-gradient, residual magnetic, and light-pressure torques. The equations of motion are expressed in Sadov variables. The equations of motion are averaged over the Sadov angles and the orbital mean anomaly and a combination of Lie transformations is applied to transform from non-averaged to mean attitude variables. It will be shown how this technique can be used to estimate the approximation error and improve the accuracy of the averaged solution. Furthermore, we introduce an alternative set of variables, that removes one of the singularities in the formulation in Sadov variables. The results of the numerical tests demonstrate that the proposed semi-analytical theory, provides a good balance between accuracy and computational cost.

### 1. Introduction

While perturbation techniques are widely applied to study the orbital dynamics of artificial satellites or celestial bodies, the development of analytical or semi-analytical theories for studying the attitude dynamics is less frequent. It is worth recalling the works by Ferrandiz and Sansaturio [1], Vallejo [2], Elipe and Vallejo [3], Lara and Ferrer [4], Lara [5] who deal with the rotational dynamics of triaxial bodies under the effect of the gravity-gradient torque. The Hamiltonian nature of the problem allows them to apply the classical Lie series technique (see [6]) consisting of the iterative composition of Lie transformations to obtain a normal form suitable to study the dynamics over long periods of time. One of the main advantages of this method is that the transformation from non-averaged to mean attitude variables can be analytically determined. Not only is this useful to reverse the transformation, but also to compute the initial value of the mean variables, which is fundamental to compute an accurate evolution of the mean attitude motion. In the remainder of the paper we will use the term *osculating* to indicate the non-averaged variables. The Lie series approach is adopted also by Lara et al. [7], San Juan et al. [8], Mohammed et al. [9], who deal with the case of axisymmetric bodies under the effect of different conservative torques. Zanardi and Vilhena de Moraes [10] treat a similar case adding the effects of non-conservative perturbations, which make the rotational problem non-Hamiltonian. The authors mix the Lie series technique with a successive approximations approach. Benson and Scheeres [11,12] deal with the problem of artificial triaxial objects, along geosynchronous orbits, perturbed by light pressure. The problem is completely non-Hamiltonian and the authors develop a semi-analytical model by averaging the equations of attitude motion over the fast variables. Garcia et al. [13] use a similar technique for the perturbations coming from the residual magnetic and eddy current torques.

All previous works in the literature deal with specific perturbations, specific geometries, or specific orbital regimes. The work in this paper proposes a more general averaged model suitable to propagate the attitude dynamics of both triaxial and axisymmetric objects in Earth orbit under the combined effect of gravity gradient, residual magnetic, and light pressure torques.

\* Corresponding author.

E-mail address: [massimiliano.vasile@strath.ac.uk](mailto:massimiliano.vasile@strath.ac.uk) (M. Vasile).

<https://doi.org/10.1016/j.cnsns.2024.108549>

Received 1 May 2024; Received in revised form 13 December 2024; Accepted 13 December 2024

Available online 21 December 2024

1007-5704/© 2024 The Authors. Published by Elsevier B.V. This is an open access article under the CC BY license (<http://creativecommons.org/licenses/by/4.0/>).

The semi-analytical theory, proposed in this paper, is developed by averaging the equations of attitude motion over the fast attitude variables and the orbital mean anomaly. To determine the required transformation from the osculating to the averaged vector field, we apply a method similar to the one described in Barrio and Palacià [14]. It is a generalised Lie series technique suitable for problems with both Hamiltonian and non-Hamiltonian terms. In this paper we will cover the general case of triaxial bodies. The action–angle variables for the general case of triaxial bodies are the so-called *Sadov variables*, introduced almost contemporary by Sadov [15] and Kinoshita [16]. The use of action–angle variables is advantageous because it is straightforward to identify the fast attitude variables over which the equations of motion are to be averaged. The disadvantage is that the dynamic equations expressed in Sadov angles contain Jacobi elliptic functions, which makes computing the Lie transformations more complicated. In this paper, we follow the method suggested by Vallejo [2] and Elipe and Vallejo [3] and expand the Jacobi elliptic functions in Fourier series before applying the Lie transformations. The generators of Lie transformations, combined to transform the osculating variables in mean variables, are also used to compute higher-order correction terms to be added to the averaged equations to increase their accuracy.

This paper extends the results in [17], with more in depth theoretical developments and an analysis of accuracy and limits of applicability. In Section 2, we briefly introduce the Andoyer–Serret and Sadov action–angle variables. In Sections 3 and 4, we write the equations of attitude motion in Sadov variables and the models of the external torques acting on an Earth-orbiting object. In Section 5 we describe the procedure to derive the averaged dynamical model and the computation of the higher-order corrections required to increase the accuracy of the propagation. In the same section, we propose a new set of variables that avoids one of the singularities in the equations of motion. The model is developed assuming constant orbital parameters, except for the mean anomaly. However, over long periods of time, the effects of various perturbations on the orbital dynamics are not negligible. Thus, in Section 6 we introduce the coupling of the attitude averaged model with an orbital averaged model accounting for orbit perturbations. In Section 7 we present some numerical simulations, in which the averaged attitude dynamics is compared to the high-precision propagation of the full non-averaged attitude and orbital dynamics. Finally, Section 8 contains the analysis of the accuracy of the semi-analytical propagation.

## 2. Attitude representation

The classical sets of attitude variables, such as the Andoyer–Serret variables, describe the orientation of a reference frame embedded in the rotating body with respect to a reference frame with fixed axes. In particular, the Andoyer–Serret variables are employed when the rotating reference frame is in principal axes of inertia. In this work, we take a geocentric equatorial reference frame  $EXYZ$  as inertial reference frame, with the  $Z$  axis pointing towards the Earth's north pole. Furthermore, we consider a rotating reference frame  $Oxyz$  centred in the satellite centre of mass with principal axes of inertia. The  $z$  axis is the axis of maximum inertia and the  $x$  axis is the axis of minimum inertia so that  $A \leq B \leq C$  where

$$\begin{aligned} A &= \int (y^2 + z^2) dm, \\ B &= \int (x^2 + z^2) dm, \\ C &= \int (x^2 + y^2) dm, \end{aligned}$$

with  $dm$  a mass element. Thus, the classical sets of attitude variables are used to describe the orientation of  $Oxyz$  with respect to  $OXYZ$ , i.e. with respect to the inertial reference frame translated into the satellite's centre of mass. The physical meaning of the Sadov variables is less straightforward. They are action–angle variables for the torque-free problem when triaxial bodies are considered and derive from a canonical transformation of the Andoyer–Serret variables.

After briefly reviewing the classical Andoyer–Serret variables, we introduce the main steps of the canonical transformation leading to the Sadov variables, following the work by Lara and Ferrer [4].

### 2.1. Andoyer–Serret variables

The Andoyer–Serret variables  $(L, G, H, l, g, h)$  are canonical variables for the description of attitude motion. Variables  $(L, G, H)$  are the momenta conjugated to the angles  $(l, g, h)$ . Let  $\mathbf{G}$  be the angular momentum of the satellite and  $\gamma$  the plane perpendicular to  $\mathbf{G}$ . Consider also the intersections between the planes  $OXY$  and  $\gamma$  and between the planes  $Oxy$  and  $\gamma$ , which can be respectively identified by the unit vectors

$$\hat{e}_{lG} = \frac{\hat{e}_Z \times \mathbf{G}}{\|\hat{e}_Z \times \mathbf{G}\|}, \quad \hat{e}_{hG} = \frac{\mathbf{G} \times \hat{e}_z}{\|\mathbf{G} \times \hat{e}_z\|},$$

with  $\hat{e}_Z$  and  $\hat{e}_z$  the unit vectors in the direction of the  $Z$  and  $z$  axes. Variable  $G$  is the magnitude of  $\mathbf{G}$ ,  $L$  is the projection of  $\mathbf{G}$  on the  $z$  axis,  $H$  is the projection of  $\mathbf{G}$  on the  $Z$  axis,  $l \in (0, 2\pi)$  is the angle between  $\hat{e}_{lG}$  and the  $x$  axis,  $g \in (0, 2\pi)$  is the angle between  $\hat{e}_{lG}$  and  $\hat{e}_{hG}$ , and  $h \in (0, 2\pi)$  is the angle between the  $X$  axis and  $\hat{e}_{lG}$ . These variables describe a set of five rotations from  $OXYZ$  to  $Oxyz$  (see Fig. 1): a rotation around the  $Z$  axis by the angle  $h$ ; a rotation around  $\hat{e}_{lG}$  by the angle  $\delta \in (0, \pi)$ , defined as

$$\delta = \arccos\left(\frac{H}{G}\right),$$

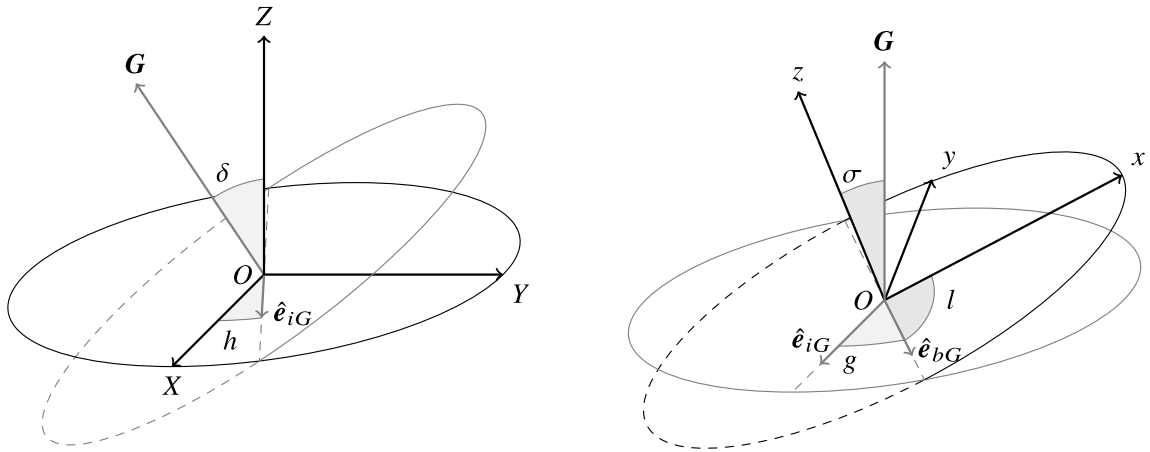


Fig. 1. The rotation angles described by the Andoyer–Serret variables to describe the orientation of the rotating frame  $Oxyz$  with respect to the reference frame  $OXYZ$ . In the figure,  $G$  is the angular momentum of the satellite.

a rotation around  $G$  by the angle  $g$ , a rotation around  $\hat{e}_{bi}$  by the angle  $\sigma \in (0, \pi)$ , equal to

$$\sigma = \arccos\left(\frac{L}{G}\right),$$

and a rotation around the  $z$  axis by the angle  $l$ . The rotation matrix is

$$\mathbf{R}_{i2b} = \mathbf{R}_l \mathbf{R}_\sigma \mathbf{R}_g \mathbf{R}_\delta \mathbf{R}_h,$$

with

$$\begin{aligned} \mathbf{R}_h &= \begin{bmatrix} \cos h & \sin h & 0 \\ -\sin h & \cos h & 0 \\ 0 & 0 & 1 \end{bmatrix}, & \mathbf{R}_\delta &= \begin{bmatrix} 1 & 0 & 0 \\ 0 & \cos \delta & \sin \delta \\ 0 & -\sin \delta & \cos \delta \end{bmatrix}, & \mathbf{R}_g &= \begin{bmatrix} \cos g & \sin g & 0 \\ -\sin g & \cos g & 0 \\ 0 & 0 & 1 \end{bmatrix}, \\ \mathbf{R}_\sigma &= \begin{bmatrix} 1 & 0 & 0 \\ 0 & \cos \sigma & \sin \sigma \\ 0 & -\sin \sigma & \cos \sigma \end{bmatrix}, & \mathbf{R}_l &= \begin{bmatrix} \cos l & \sin l & 0 \\ -\sin l & \cos l & 0 \\ 0 & 0 & 1 \end{bmatrix}. \end{aligned} \tag{1}$$

The Hamiltonian of the torque-free problem in the Andoyer–Serret variables is

$$H = \frac{1}{2} \left( \frac{\sin^2 l}{A} + \frac{\cos^2 l}{B} \right) (G^2 - L^2) + \frac{L^2}{2C}, \tag{2}$$

(see [18]). For axisymmetric bodies with  $A = B$ , the Andoyer–Serret variables become action–angle variables, as  $H$  depends on the momenta only. For axisymmetric bodies with  $C = B$  the same is true if one considers an alternative rotating frame  $Ox'y'z'$ , with  $x'$  the axis of maximum inertia and  $z'$  the axis of minimum inertia, such that

$$\begin{aligned} A' &= \int (y'^2 + z'^2) dm = C, \\ B' &= \int (x'^2 + z'^2) dm = B, \\ C' &= \int (x'^2 + y'^2) dm = A. \end{aligned} \tag{3}$$

## 2.2. Sadov variables

The canonical transformation  $(L, G, H, l, g, h) \mapsto (J_l, J_g, J_h, \psi_l, \psi_g, \psi_h)$ , from the Andoyer–Serret variables to the Sadov variables, derives from the generating function

$$S(J_l, J_g, J_h, l, g, h, t) = -t\Phi(J_l, J_g) + hJ_h + gJ_g + \mathcal{W}(l, J_l, J_g),$$

in which  $t$  is the time variable, the function  $\Phi(J_l, J_g)$  is the new targeted Hamiltonian depending only on the new momenta, and  $\mathcal{W}(l, J_l, J_g)$  is the characteristic function fulfilling the Hamilton–Jacobi equation

$$\left( \frac{\sin^2 l}{A} + \frac{\cos^2 l}{B} \right) \left( J_g^2 - \left( \frac{\partial \mathcal{W}}{\partial l} \right)^2 \right) + \frac{1}{C} \left( \frac{\partial \mathcal{W}}{\partial l} \right)^2 = 2\Phi(J_l, J_g). \tag{4}$$

From (4), it follows that

$$\mathcal{W} = J_g \int \sqrt{Q} dl, \quad Q = \frac{\sin^2 l/A + \cos^2 l/B - 1/J_d}{\sin^2 l/A + \cos^2 l/B - 1/C},$$

where

$$J_d = \frac{J_g^2}{2\Phi}$$

is the dynamic moment of inertia (see [12]). By performing the change of coordinates

$$\sin l = \frac{\cos \lambda}{\sqrt{1 + \kappa \sin^2 \lambda}}, \quad \cos l = -\frac{\sqrt{1 + \kappa} \sin \lambda}{\sqrt{1 + \kappa \sin^2 \lambda}}, \tag{5}$$

and introducing the function

$$\mu(J_l, J_g) = \frac{A}{C} \kappa \frac{C - J_d}{J_d - A}, \tag{6}$$

where  $\kappa$  is a constant depending on the moments of inertia. i.e.

$$\kappa = \frac{C(B - A)}{A(C - B)}, \tag{7}$$

we have that

$$Q = \frac{\kappa(1 - \mu \sin^2 \lambda)}{\kappa + \mu}, \quad \frac{\partial Q}{\partial(1/J_d)} = \frac{AC(1 + \kappa \sin^2 \lambda)}{A - C}, \quad dl = \frac{\sqrt{1 + \kappa}}{1 + \kappa \sin^2 \lambda} d\lambda,$$

and

$$\Phi(J_g, J_l) = \frac{J_g^2}{2AC} \frac{\kappa A + \mu C}{\kappa + \mu}. \tag{8}$$

Thus,

$$L = \frac{\partial S}{\partial l} = J_g \sqrt{\frac{\kappa}{\kappa + \mu}} \sqrt{1 - \mu \sin^2 \lambda}, \tag{9}$$

$$G = \frac{\partial S}{\partial g} = J_g, \tag{10}$$

$$H = \frac{\partial S}{\partial h} = J_h, \tag{11}$$

$$\psi_l = \frac{\partial S}{\partial J_l} = -\frac{J_g}{2} \frac{\sqrt{\kappa(1 + \kappa)}}{(\kappa + \mu)^{3/2}} F(\lambda, \mu) \frac{\partial \mu}{\partial J_l}, \tag{12}$$

$$\psi_g = \frac{\partial S}{\partial J_g} = g + \sqrt{\kappa + \mu} \sqrt{\frac{1 + \kappa}{\kappa}} \left( \Pi(-\kappa, \lambda, \mu) - \frac{F(\lambda, \mu)}{\kappa + \mu} \left( \mu + \frac{J_g}{2} \frac{\kappa}{\kappa + \mu} \frac{\partial \mu}{\partial J_g} \right) \right), \tag{13}$$

$$\psi_h = \frac{\partial S}{\partial J_h} = h, \tag{14}$$

where  $F(\lambda, \mu)$  is the incomplete elliptic integral of first kind and  $\Pi(-\kappa, \lambda, \mu)$  is the incomplete elliptic integrals of third kind, defined as:

$$F(\lambda, \mu) = \int_0^\lambda \frac{d\vartheta}{\sqrt{1 - \mu \sin^2 \vartheta}}, \quad \Pi(-\kappa, \lambda, \mu) = \int_0^\lambda \frac{d\vartheta}{(1 + \kappa \sin^2 \vartheta) \sqrt{1 - \mu \sin^2 \vartheta}},$$

(see [19]). The new canonical variables  $\psi_l$  and  $\psi_g$  are angles only if they fulfil conditions

$$\oint \psi_l = 2\pi, \quad \oint \psi_g = 2\pi. \tag{15}$$

Considering that  $F(0, \mu) = 0$ ,  $F(2\pi, \mu) = 4K(\mu)$ ,  $\Pi(-\kappa, 0, \mu) = 0$  and  $\Pi(-\kappa, 2\pi, \mu) = 4\Pi(-\kappa, \mu)$ , where  $K(\mu)$  and  $\Pi(-\kappa, \mu)$  are the following complete integrals of the first and third kind, i.e.

$$K(\mu) = F(\pi/2, \mu), \quad \Pi(-\kappa, \mu) = \Pi(-\kappa, \pi/2, \mu),$$

the conditions in (15) applied to  $\psi_l$  in (12) and  $\psi_g$  in (13) imply that:

$$\frac{\partial \mu}{\partial J_l} = -\frac{\pi}{J_g} \frac{1}{\zeta^{\frac{3}{2}}} \frac{\kappa}{\sqrt{1 + \kappa}} \frac{1}{K(\mu)}, \tag{16}$$

$$\frac{\partial \mu}{\partial J_g} = \frac{2\kappa (\Pi(-\kappa, \mu) - (1 - \zeta)K(\mu))}{J_g K(\mu) \zeta^2}, \tag{17}$$

with

$$\zeta = \frac{\kappa}{\kappa + \mu}. \tag{18}$$

As explained by Lara and Ferrer [4], in order to find a particular solution of the partial differential system composed by Eqs. (16) and (17), it is convenient to introduce the constraint  $\mu = \mu(J_l/J_g)$ , for which

$$J_l \frac{\partial \mu}{\partial J_l} + J_g \frac{\partial \mu}{\partial J_g} = 0,$$

so that relation

$$\frac{J_l}{J_g} = \frac{2}{\pi} \sqrt{\frac{1+\kappa}{\zeta}} (\Pi(-\kappa, \mu) - (1-\zeta)K(\mu))$$

holds true. It follows that the Sadov variables are:

$$\begin{aligned} J_l &= \frac{2G}{\pi} \sqrt{\frac{1+\kappa}{\zeta}} (\Pi(-\kappa, \mu) - (1-\zeta)K(\mu)), \\ J_g &= G, \\ J_h &= H, \\ \psi_l &= \frac{\pi}{2} \frac{F(\lambda, \mu)}{K(\mu)}, \\ \psi_g &= g + \sqrt{\frac{1+\kappa}{\zeta}} \left( \Pi(-\kappa, \lambda, \mu) - \frac{\Pi(-\kappa, \mu)}{K(\mu)} F(\lambda, \mu) \right), \\ \psi_h &= h, \end{aligned} \tag{19}$$

where the value of  $\mu$  is given by Eq. (6). The rotation matrix from  $OXYZ$  to  $Oxyz$  in Sadov variables can be written by, first, considering that the angle  $\lambda$  corresponds to the Jacobi amplitude

$$\lambda = \text{am}(u, \mu),$$

with

$$u = \frac{2K(\mu)\psi_l}{\pi}, \tag{20}$$

as it follows from the definition of  $\psi_l$  in (19), so that

$$\begin{aligned} g &= \psi_g + \delta g, \quad \sin l = \text{cn}(u, \mu) \text{dnk}^{-\frac{1}{2}}, \quad \cos l = -\sqrt{1+\kappa} \text{sn}(u, \mu) \text{dnk}^{-\frac{1}{2}}, \\ \cos \sigma &= \frac{I}{G} = \sqrt{\zeta} \text{dn}(u, \mu), \quad \sin \sigma = \sqrt{1-\zeta} \text{dnk}^{\frac{1}{2}}, \end{aligned} \tag{21}$$

where  $\text{cn}(u, \mu)$  is the Jacobi elliptic cosine,  $\text{sn}(u, \mu)$  is the Jacobi elliptic sine,  $\text{dn}(u, \mu)$  is the Jacobi elliptic delta amplitude, and

$$\delta g = -\sqrt{\frac{1+\kappa}{\zeta}} \left( \Pi(-\kappa, \text{am}(u, \mu), \mu) - u \frac{\Pi(-\kappa, \mu)}{K(\mu)} \right), \tag{22}$$

$$\text{dnk} = 1 + \kappa \text{sn}^2(u, \mu), \tag{23}$$

as it follows from Eqs. (5), (9) and the definition of  $\psi_g$  in (19). Thus, from (1) it is straightforward to see that the rotation matrix is

$$\mathbf{R}_{i2b} = \mathbf{R}_b \mathbf{R}_\delta \mathbf{R}_{\psi_h}, \tag{24}$$

where  $\mathbf{R}_{\psi_h} = \mathbf{R}_h|_{h=\psi_h}$ ,  $\mathbf{R}_\delta$  with

$$\delta = \delta(J_h, J_g) = \arccos(J_h/J_g),$$

and  $\mathbf{R}_b = (b_{ij})_{i=1..3, j=1..3}$  with elements

$$b_{11} = -(\sqrt{\zeta} \sin(\psi_g + \delta g) \text{cn}(u, \mu) \text{dn}(u, \mu) + \sqrt{1+\kappa} \cos(\psi_g + \delta g) \text{sn}(u, \mu) \text{dnk}^{-\frac{1}{2}}), \tag{25}$$

$$b_{12} = -(\sqrt{1+\kappa} \sin(\psi_g + \delta g) \text{sn}(u, \mu) - \sqrt{\zeta} \cos(\psi_g + \delta g) \text{dn}(u, \mu) \text{cn}(u, \mu) \text{dnk}^{-\frac{1}{2}}), \tag{26}$$

$$b_{13} = \sqrt{1-\zeta} \text{cn}(u, \mu), \tag{27}$$

$$b_{21} = -(\cos(\psi_g + \delta g) \text{cn}(u, \mu) - \sqrt{1+\kappa} \sqrt{\zeta} \sin(\psi_g + \delta g) \text{sn}(u, \mu) \text{dn}(u, \mu) \text{dnk}^{-\frac{1}{2}}), \tag{28}$$

$$b_{22} = -(\sqrt{1+\kappa} \sqrt{\zeta} \cos(\psi_g + \delta g) \text{sn}(u, \mu) \text{dn}(u, \mu) + \sin(\psi_g + \delta g) \text{cn}(u, \mu) \text{dnk}^{-\frac{1}{2}}), \tag{29}$$

$$b_{23} = -\sqrt{1-\zeta} \sqrt{1+\kappa} \text{sn}(u, \mu), \tag{30}$$

$$b_{31} = \sqrt{1-\zeta} \sin(\psi_g + \delta g) \text{dnk}^{\frac{1}{2}}, \tag{31}$$

$$b_{32} = -\sqrt{1-\zeta} \cos(\psi_g + \delta g) \text{dnk}^{\frac{1}{2}}, \tag{32}$$

$$b_{33} = \sqrt{\zeta} \text{dn}(u, \mu). \tag{33}$$

Note that the canonical transformation leading to the Sadov variables can be suitably performed only if:

$$B \leq J_d \leq C; \tag{34}$$

and

$$L > 0. \tag{35}$$

Indeed, since  $|L| < G$ , from (9), we have that  $Q \in (0, 1)$  which implies condition (34). Moreover, since  $J_g > 0$ , from (9) it also follows condition (35). When the disequality (34) is fulfilled, the satellite is in a *short axis mode (SAM)*, with the largest components of its angular velocity along its shortest axis, corresponding to the axis of maximum inertia. Instead, when  $A < J_d < B$ , the satellite is in a *long axis mode (LAM)*, with the largest components of its angular velocity along its longest axis, which is the axis of minimum inertia. In this case, the set of Sadov variables can be introduced considering the alternative rotating reference frame  $Ox'y'z'$  discussed in Section 2.1. The transformation can be applied as described using Andoyer–Serret variables defined with respect to  $Ox'y'z'$  and replacing  $A, B, C$  with  $A', B', C'$ , given in (3). Similarly, if disequality (35) is not fulfilled, it is sufficient to consider the alternative reference frame  $Ox_0y_0z_0$  with the  $y_0$  and  $z_0$  axes in the opposite directions of the  $y$  and  $z$  axes.

The transformation to Sadov variables can be applied also in the case of axisymmetric bodies such that either  $A = B$  or  $B = C$ , which correspond to  $\kappa = 0$  and  $\mu = 0$ . On the contrary, if  $A = B = C$  the transformation is not well defined and the Andoyer–Serret variables should be employed as action–angle variables.

### 3. Attitude dynamics in Sadov variables

When propagating the attitude dynamics, it is convenient to employ a set of modified Sadov variables, in which the momentum  $J_l$  is replaced by either  $\mu$  or  $\zeta$ . Indeed, as one can simply verify in the torque-free problem given the Hamiltonian in (8), the equations of motion depend only implicitly on  $J_l$  through  $\mu$  and  $\zeta$ . For axisymmetric bodies, while  $\mu$  is equal to zero,

$$\lim_{\kappa \rightarrow 0} \zeta = \frac{C(J_d - A)}{J_d(C - A)},$$

as it follows from Eqs. (6) and (18). Thus, while the value of  $\mu$  can be immediately inferred from the value of  $\zeta$ , the inverse is not possible. For this reason, we select  $\zeta$ . This choice becomes advantageous when non-conservative external torques act on the satellite, since  $\mu$  and  $\zeta$  may vary in time. When the satellite is affected by both a total conservative torque with potential energy  $\mathcal{V}$  and total non-conservative torque  $\mathbf{M}$ , setting  $s = (\zeta, J_g, J_h, \psi_l, \psi_g, \psi_h)$ , we have that the equations of motion become

$$\frac{ds}{dt} = \mathbf{A} \nabla_s \Phi + \mathbf{A} \nabla_s \mathcal{V} + \mathbf{B} \mathbf{M}, \tag{36}$$

where  $\nabla_s$  is the gradient operator,

$$\mathbf{A} = \begin{bmatrix} 0 & \mathbf{I} \\ -\mathbf{I}^\top & 0 \end{bmatrix}, \tag{37}$$

with

$$\mathbf{I} = \begin{bmatrix} -\frac{\pi}{J_g K(\mu)} \sqrt{\frac{\zeta}{1+\kappa}} & \frac{2(\Pi(-\kappa, \mu) - (1-\zeta)K(\mu))}{J_g K(\mu)} & 0 \\ 0 & -1 & 0 \\ 0 & 0 & -1 \end{bmatrix},$$

and

$$\mathbf{B} = \begin{bmatrix} -\frac{2\zeta}{J_g} b_{13} & -\frac{2\zeta(1-\mu)}{J_g(1+\kappa)} b_{23} & \frac{2(1-\zeta)}{J_g} b_{33} \\ b_{13} & b_{23} & b_{33} \\ \cos \delta b_{13} + \sin \delta b_{12} & \cos \delta b_{23} + \sin \delta b_{22} & \cos \delta b_{33} + \sin \delta b_{32} \\ -\frac{\pi S_x}{2J_g K(\mu)(1-\mu)} & -\frac{\pi S_y}{2J_g K(\mu)} & -\frac{\pi S_z}{2J_g K(\mu)(1-\mu)} \\ \frac{\mathcal{T} S_x}{1-\mu} - \frac{b_{11} \cos \delta}{J_g \sin \delta} & \mathcal{T} S_y - \frac{b_{21} \cos \delta}{J_g \sin \delta} & \frac{\mathcal{T} S_z}{1-\mu} - \frac{b_{31} \cos \delta}{J_g \sin \delta} \\ \frac{b_{11}}{J_g \sin \delta} & \frac{b_{21}}{J_g \sin \delta} & \frac{b_{31}}{J_g \sin \delta} \end{bmatrix}, \tag{38}$$

with

$$\mathcal{T} = \frac{(\Pi(-\kappa, \mu) - (1-\zeta)K(m)) \sqrt{1+\kappa}}{J_g K(\mu) \sqrt{\zeta}}, \tag{39}$$

$$S_x = \frac{\text{dn}(u, \mu) \text{sn}(u, \mu) - \text{cn}(u, \mu) \text{zn}(u, \mu)}{\sqrt{1-\zeta}}, \tag{40}$$

$$S_y = \frac{\text{dn}(u, \mu) \text{cn}(u, \mu) + \text{sn}(u, \mu) \text{zn}(u, \mu)}{\sqrt{1+\kappa} \sqrt{1-\zeta}}, \tag{41}$$

$$S_z = \frac{\text{dn}(u, \mu) \text{zn}(u, \mu) - \mu \text{cn}(u, \mu) \text{sn}(u, \mu)}{\sqrt{\zeta}}, \tag{42}$$

and  $zn(u, \mu)$  the Jacobi zeta function. Eqs. (36) to (42) are derived in Appendix A.

Note that, when the new set of variables  $s$  are employed,  $\mu$  is only a function  $\zeta$  and  $u$  is a function of  $\zeta$  and  $\psi_l$ .

#### 4. External torques

At medium and high altitudes, Earth satellites are mostly affected by the gravity-gradient, the residual magnetic, and the light pressure torques (see [20]). Typically, the light pressure has smaller effects. However, since the magnitude of the gravity gradient and the residual magnetic torques decrease with the geocentric distance of the satellite, the light pressure becomes more and more significant at increasing altitudes.

##### 4.1. Gravity-gradient torque

The Earth's gravity generates a conservative torque acting on the satellites. As suggested by Liu and Chen [21], this torque can be modelled by considering the Earth as a perfectly spherical body, so that its potential energy results equal to:

$$V_g = \frac{3\mu_\oplus}{2r^3} (A\alpha_1^2 + B\alpha_2^2 + C\alpha_3^2), \quad (43)$$

with

$$(\alpha_1, \alpha_2, \alpha_3)^T = \mathbf{R}_{12b} \frac{\mathbf{r}}{r}.$$

In the above equations,  $\mu_\oplus$  is the Earth's gravitational parameters,  $\mathbf{r}$  is the geocentric position vector of the satellite's centre of mass, and  $r = |\mathbf{r}|$ .

##### 4.2. Residual magnetic torque

The residual magnetic torque arises from the interaction between the Earth's magnetic field and the intrinsic magnetic moment of an orbiting object, due, for example, to parasitic magnetic induction (see [13]). Similarly to the gravity-gradient torque, it is a conservative torque. As proposed by Liu and Chen [21], the magnetic flux density of the Earth can be approximated by using a simplified model, in which the geomagnetic dipole is aligned with the Earth's polar axis, so that

$$\mathbf{B}_\oplus = \frac{\mu_m}{r^3} \left( \hat{\mathbf{e}}_Z - 3 \left( \hat{\mathbf{e}}_Z \cdot \frac{\mathbf{r}}{r} \right) \frac{\mathbf{r}}{r} \right),$$

where  $\mu_m = 10^{17}$  Wb m is the Earth's magnetic dipole strength. The potential energy reads:

$$V_m = -\mathbf{I}_m \cdot \mathbf{R}_{12b} \mathbf{B}_\oplus. \quad (44)$$

where  $\mathbf{I}_m$  is the intrinsic magnetic moment of the object.

##### 4.3. Light pressure torque

The light pressure torque is a non-conservative torque caused by the resultant of the light pressure force acting on different surfaces of an object. As suggested by Benson and Scheeres [12], the light pressure force can be computed by modelling a complex object as the composition of  $n_f$  facets and summing up the forces acting on each facet. The force acting on the  $i$ th facet is:

$$\mathbf{f}_{lp_i} = -P_{lp} S_i (c_{a,i} \hat{\mathbf{u}} + c_{d,i} \hat{\mathbf{n}}_i + c_{s,i} (\hat{\mathbf{u}} \cdot \hat{\mathbf{n}}_i) \hat{\mathbf{n}}_i) \max(\hat{\mathbf{u}} \cdot \hat{\mathbf{n}}_i, 0). \quad (45)$$

$P_{lp}$  is the light pressure given by

$$P_{lp} = \tilde{P}_{lp} \left( \frac{1 \text{ au}}{|\mathbf{r}_\odot - \mathbf{r}|} \right)^2,$$

with  $\tilde{P}_{lp} = 4.56 \cdot 10^{-6}$  kg/s<sup>2</sup> m its value at 1 astronomical unit (au) and  $\mathbf{r}_\odot$  the geocentric position vector of the Sun (see [10]).  $S_i$  is the area of the  $i$ th facet,  $\hat{\mathbf{n}}_i$  is its outer-pointing normal unit vector, and  $c_{a,i}$ ,  $c_{d,i}$  and  $c_{s,i}$  are coefficients depending on its optical properties. In particular, given the total reflectivity  $\rho_i$  of the facet and the fraction  $s_i$  of  $\rho_i$  that is specular, relations

$$c_{a,i} = 1 - \rho_i s_i, \quad c_{d,i} = \frac{2}{3} (1 - s_i) \rho_i, \quad c_{s,i} = 2 \rho_i s_i.$$

hold (see [10]). Furthermore,

$$\hat{\mathbf{u}} = \mathbf{R}_{12b} \frac{\mathbf{r}_\odot - \mathbf{r}}{|\mathbf{r}_\odot - \mathbf{r}|},$$

(see [12]). Following [12], some simplifications are adopted. The satellite-to-Sun vector is approximated by the geocentric position vector of the Sun so that

$$\hat{\mathbf{u}} \sim \tilde{\mathbf{u}} = \mathbf{R}_{12b} \frac{\mathbf{r}_\odot}{|\mathbf{r}_\odot|}, \quad (46)$$

and

$$P_{lp} \sim \tilde{P}_{lp} \left( \frac{1 \text{ au}}{|r_{\odot}|} \right)^2.$$

Moreover,

$$\max(\hat{\mathbf{u}} \cdot \hat{\mathbf{n}}_i, 0) \sim g_i = \frac{1}{3\pi} + \frac{1}{2}(\tilde{\mathbf{u}} \cdot \hat{\mathbf{n}}_i) + \frac{4}{3\pi}(\tilde{\mathbf{u}} \cdot \hat{\mathbf{n}}_i)^2.$$

It follows that the light pressure force can be approximated as

$$\mathbf{f}_{lp} \sim -\tilde{P}_{lp} \left( \frac{1 \text{ au}}{|r_{\odot}|} \right)^2 \sum_{i=1}^{n_f} S_i g_i (c_{a,i} \tilde{\mathbf{u}} + c_{d,i} \hat{\mathbf{n}}_i + c_{s,i} (\tilde{\mathbf{u}} \cdot \hat{\mathbf{n}}_i) \hat{\mathbf{n}}_i), \quad (47)$$

and, consequently, the light pressure torque can be modelled as

$$\mathbf{M}_{lp} \sim -\tilde{P}_{lp} \left( \frac{1 \text{ au}}{|r_{\odot}|} \right)^2 \sum_{i=1}^{n_f} S_i g_i \rho_i \times (c_{a,i} \tilde{\mathbf{u}} + c_{d,i} \hat{\mathbf{n}}_i + c_{s,i} (\tilde{\mathbf{u}} \cdot \hat{\mathbf{n}}_i) \hat{\mathbf{n}}_i), \quad (48)$$

with  $\rho_i$  the vector from the centre of mass of an object to the centroid of the  $i$ th facet.

The effect of the Earth's shadow, which may become relevant over long periods of time, is included by multiplying  $\mathbf{M}_{lp}$  by a *shadow function*, which is equal to either zero when the satellite is in shadow or one when the satellite is in sunlight (see [22]). A natural choice would be the function:

$$v_s(Y) = \begin{cases} 0 & \text{if } Y_1 \leq Y \leq Y_2, \\ 1 & \text{otherwise,} \end{cases}$$

where  $Y$  is the satellite's eccentric longitude, and  $Y_1$  and  $Y_2$  are the values of  $Y$  at the entrance and the exit of the shadow region, respectively. However, when propagating the dynamics, it is more convenient to use a smooth function. Thus, we multiply  $\mathbf{M}_{lp}$  by the Fourier expansion of  $v_s(Y)$  truncated at the 20-th harmonic:

$$v_s(Y) \sim \tilde{v}_s(Y) = 1 - \frac{Y_2 - Y_1}{2\pi} - \sum_{k=1}^{20} \frac{\sin(k(Y - Y_1)) - \sin(k(Y - Y_2))}{\pi k}. \quad (49)$$

The algorithm proposed by Valk and Lemaître [23] can be employed to compute the values  $Y_1$  and  $Y_2$ .

## 5. Averaged model

If the effect of external torques can be considered a perturbation of the torque-free motion, perturbation techniques can be applied to derive an averaged model suitable to study the attitude dynamics over long timescales. The equations of attitude motion (36) can be shortly written as

$$\frac{ds}{dt} = \mathbf{A} \nabla_s \Phi + \mathbf{F}_{et}(s), \quad (50)$$

where  $\mathbf{F}_{et}(s)$  is the vector field depending on all the external torques acting on the object, defined as:

$$\mathbf{F}_{et}(s) = \mathbf{A} \nabla_s (V_g + V_m) + \mathbf{B} \mathbf{M}_{lp} v_s, \quad (51)$$

where

$$v_s = \begin{cases} 1 & \text{if the satellite is considered always in light,} \\ \tilde{v}_s & \text{if the Earth's shadow effects are taken into account,} \end{cases}$$

see Eqs. (43), (44), (48) and (49). If the satellite was not affected by any external torque, the only non-constant attitude variables would be the angles  $\psi_l$  and  $\psi_g$ . Furthermore, if the orbital perturbations are also neglected, the only non-constant orbital element is the orbital mean anomaly  $M$ . Under the hypothesis that the external torques are perturbations of the free-torque problem, all the other attitude variables in  $s$  are expected to have a slower evolution in comparison to  $\psi_l$ ,  $\psi_g$  and  $M$ , i.e. their time derivatives are expected to remain close to zero and be smaller than the time derivatives of  $\psi_l$ ,  $\psi_g$  and  $M$ . Thus,  $\psi_l$ ,  $\psi_g$ , and  $M$  are the fast variables of the problem in our derivations (see [4,8]). Averaging over the fast variables allows one to retain only the long-period terms in the equations of motion. This average is equivalent to performing the transformation of variables close to the identity

$$s(t) = \bar{s}(t) + \mathbf{W}(\bar{s}(t), t), \quad (52)$$

transforming (50) into

$$\frac{d\bar{s}(t)}{dt} = \mathbf{A} \nabla_s \Phi + \bar{\mathbf{F}}_{et}(\bar{s}) + \mathbf{R}, \quad (53)$$

and neglecting the remainder  $\mathbf{R}$ , whose magnitude is hopefully significantly smaller than  $|\bar{\mathbf{F}}_{et}|$ . This leads to the approximation:

$$\frac{d\bar{s}(t)}{dt} \sim \frac{d\bar{s}(t)}{dt} = \mathbf{A} \nabla_s \Phi + \bar{\mathbf{F}}_{et}. \quad (54)$$

The averaged model gives the dynamical evolution of the mean attitude variables  $\bar{s}$ . Transformation (52) is computed with a Lie series technique. The same technique can be used to compute a higher-order correction term, to be included in the model:

$$\frac{d\bar{s}(t)}{dt} \sim \mathbf{A} \nabla_s \Phi + \bar{\mathbf{F}}_{et} + \bar{\mathbf{R}}_p. \quad (55)$$



The term  $\bar{\mathbf{R}}_p$  corresponds to the average of the largest terms of  $\mathbf{R}$  over the fast variables. Eqs. (55) are characterised by a smaller number of terms than the original Eqs. (50), and, thus, are faster to integrate. The averaging process is performed under the hypothesis that the fast angles are not resonant. Furthermore, the satellite is assumed to be fast-rotating and moving along a Keplerian orbit. The orbit is defined by the equinoctial elements  $E = (a, P_1, P_2, Q_1, Q_2)$ , where  $a$  is the semi-major axis of the orbit, and

$$\begin{aligned} P_1 &= e \sin(\omega + \Omega), \\ P_2 &= e \cos(\omega + \Omega), \\ Q_1 &= \tan\left(\frac{I}{2}\right) \sin \Omega, \\ Q_2 &= \tan\left(\frac{I}{2}\right) \cos \Omega, \end{aligned}$$

with  $e, I, \omega$  and  $\Omega$  the orbital eccentricity, inclination, argument of the perigee and longitude of the node, respectively. In the following, we will describe the procedure to analytically solve the integral

$$\bar{F}_{\text{et}} = \frac{1}{8\pi^3} \int_0^{2\pi} \int_0^{2\pi} \int_0^{2\pi} F_{\text{et}} d\psi_g d\psi_l dM, \tag{56}$$

which corresponds to deriving the first-order averaged model. Then, we will present how the Lie series technique can be used to derive the transformation from non-averaged to mean variables and compute higher-order correction terms. Finally, we will discuss the singularities appearing in the averaged model and a way to handle them, through the use of non-singular variables.

### 5.1. Averaging procedure

The average of the terms due to conservative torques can be computed from the average of the corresponding potential energies as  $\mathbf{A}\nabla_s (\bar{V}_g + \bar{V}_m)$ , with

$$\bar{V}_g = \frac{1}{8\pi^3} \int_0^{2\pi} \int_0^{2\pi} \int_0^{2\pi} V_g d\psi_g d\psi_l dM, \tag{57}$$

$$\bar{V}_m = \frac{1}{8\pi^3} \int_0^{2\pi} \int_0^{2\pi} \int_0^{2\pi} V_m d\psi_g d\psi_l dM. \tag{58}$$

Thus, determining  $\bar{F}_{\text{et}}$  in (56) implies to compute (57), (58) and the integral

$$\frac{1}{8\pi^3} \int_0^{2\pi} \int_0^{2\pi} \int_0^{2\pi} \mathbf{B}\mathbf{M}_{\text{lp}} v_s d\psi_g d\psi_l dM.$$

All the terms in  $\mathbf{B}\mathbf{M}_{\text{lp}} v_s, V_g$  and  $V_m$  can be expressed as the product of three factors: a function of the slow variables ( $\zeta, J_g, J_h, \psi_h$ ); a function of the fast angles ( $\psi_l, \psi_g$ ) and  $\zeta$ ; a function of the orbital elements. Thus, the generic term to be averaged has the form

$$f = F(\zeta, J_g, J_h, \psi_h) f_a(\zeta, \psi_l, \psi_g) f_o(E, M).$$

From (43), (44) and (48), it is clear that  $V_g, V_m$  and  $\mathbf{M}_{\text{lp}}$  depend on the Sadov fast angles only through the elements  $b_{ij}$  of the rotation matrix  $\mathbf{R}_{2\text{tb}}$  in (24). Instead, the dependence of  $\mathbf{B}$  in (38) on  $(\psi_l, \psi_g)$  occurs through both the  $b_{ij}$  elements and the terms  $S_x, S_y, S_z$  (see (40)–(42)). It follows that  $f_a$  has the form

$$f_a = F_a(\zeta) \sin^i(\psi_g + \delta g) \cos^j(\psi_g + \delta g) \text{dn}^o(u, \mu) \text{sn}^s(u, \mu) \text{cn}^k(u, \mu) \text{dn}^k \frac{p_i + p_j}{2} \text{zn}^{u'}(u, \mu), \tag{59}$$

with  $w \in [0, 1], i, j, o, s, k$  natural numbers,  $p_i$  an integer number with the same parity as  $i$  and  $p_j$  and integer number with the same parity as  $j$ . Because of the form of  $f$  and  $f_a$ , to analytically compute

$$\bar{f} = \frac{1}{8\pi^3} \int_0^{2\pi} \int_0^{2\pi} \int_0^{2\pi} f d\psi_g d\psi_l dM,$$

it is convenient to apply the procedure described in the following:

#### (i) Average over $\psi_g$

As a first step, the average  $\langle f \rangle_{\psi_g}$  of  $f$  over  $\psi_g$  is computed:

$$\langle f \rangle_{\psi_g} = F f_o \langle f_a \rangle_{\psi_g}, \quad \langle f_a \rangle_{\psi_g} = \frac{1}{2\pi} \int_0^{2\pi} f_a d\psi_g.$$

It can be proved that

**Proposition 1.** *If either the natural number  $i$  or the natural number  $j$  in Eq. (59) is odd,  $\langle f_a \rangle_{\psi_g} = 0$ . Otherwise, if both  $i$  and  $j$  are even numbers,*

$$\langle f_a \rangle_{\psi_g} = \bar{F}_a(\zeta) \text{dn}^o(u, \mu) \text{sn}^s(u, \mu) \text{cn}^k(u, \mu) \text{dn}^k \text{zn}^u(u, \mu),$$

with  $p$  an integer number and

$$\bar{F}_a(\zeta) = F_a(\zeta) \sum_{d=0}^{\frac{i}{2}} \binom{\frac{i}{2}}{d} (-1)^d \prod_{v=0}^{d+\frac{j}{2}-1} \frac{2d+j-2v-1}{2d+j-2v}.$$

The proof of Proposition 1 is given in Appendix B. Observe that the resulting  $\langle f \rangle_{\psi_g}$  depends on  $\psi_l$  only through Jacobi elliptic functions, as the trigonometric functions depending on  $\delta_g$  disappear. This makes  $\langle f \rangle_{\psi_g}$  easier to be averaged over  $\psi_l$  than  $f$ .

**(ii) Average over  $\psi_l$**

As a second step, the average  $\langle f \rangle_{\psi_g, \psi_l}$  of  $\langle f \rangle_{\psi_g}$  over  $\psi_l$  is determined, i.e.

$$\langle f \rangle_{\psi_g, \psi_l} = F f_o \bar{f}_a = F f_o \frac{\tilde{F}_a \mathcal{J}}{4K(\mu)},$$

where

$$\mathcal{J} = \int_0^{4K(\mu)} \text{dn}^o(u, \mu) \text{sn}^s(u, \mu) \text{cn}^k(u, \mu) \text{dn}^p \text{zn}^w(u, \mu) \text{du}.$$

It is possible to show that

**Proposition 2.** *If  $w = 1$  and either  $s$  or  $k$  are even,  $\mathcal{J} = 0$ . Otherwise, if  $w = 1$  and both  $s$  or  $k$  are odd,*

$$\mathcal{J} = \int_0^{4K(\mu)} \left( \int \text{dn}^o(u, \mu) \text{sn}^s(u, \mu) \text{cn}^k(u, \mu) \text{dn}^p \text{du} \right) \cdot \left( \frac{E(\mu)}{K(\mu)} - \text{dn}^2(u, \mu) \right) \text{du},$$

with  $E(\mu)$  the complete elliptic integral of second kind, i.e.

$$E(\mu) = \int_0^{\frac{\pi}{2}} \sqrt{1 - \mu \sin^2 \vartheta} \text{d}\vartheta.$$

Thus, the computation of  $\mathcal{J}$  implies solving integrals with the form

$$\int \text{dn}^v(u, \mu) \text{sn}^s(u, \mu) \text{cn}^k(u, \mu) \text{dn}^p \text{du},$$

with  $v$  natural number. This can be easily done with the support of a symbolic manipulator, such as MAPLE. The proof of Proposition 2 is given in Appendix C.

**(iii) Average over  $M$**

Finally, the average over  $M$  is computed:

$$\bar{f} = F \bar{f}_a \frac{1}{2\pi} \int_0^{2\pi} f_o \text{d}M.$$

Since the dependence of the external torques or their potential energies on  $M$  is implicit through geometrical angles, such as the true longitude  $\Lambda$  or the eccentric longitude  $Y$ ,  $\bar{f}$  is computed as either

$$\bar{f} = \frac{F \bar{f}_a}{2\pi} \int_0^{2\pi} \frac{f_o \eta^3}{(1 + P_1 \sin \Lambda + P_2 \cos \Lambda)^2} \text{d}\Lambda$$

or

$$\bar{f} = \frac{F \bar{f}_a}{2\pi} \int_0^{2\pi} f_o (1 - P_1 \sin Y - P_2 \cos Y) \text{d}Y.$$

with

$$\eta = \sqrt{1 - P_1^2 - P_2^2}.$$

For example, one can note that the light pressure torque  $\mathbf{M}_{lp}$  in (48) is independent of the mean anomaly. The dependence on  $M$  is introduced when  $\mathbf{M}_{lp}$  is multiplied by the shadow function in (49), which indeed depends on the eccentric longitude. Instead, it is convenient to express the gravity-gradient and the residual magnetic torques potential energies in terms of the true longitude, by using

$$\mathbf{r} = r \begin{bmatrix} \frac{(1-Q_1^2+Q_2^2) \cos \Lambda + 2Q_1 Q_2 \sin \Lambda}{1+Q_1^2+Q_2^2} \\ \frac{(1+Q_1^2-Q_2^2) \sin \Lambda + 2Q_1 Q_2 \cos \Lambda}{1+Q_1^2+Q_2^2} \\ \frac{-2Q_1 \cos \Lambda + 2Q_2 \sin \Lambda}{1+Q_1^2+Q_2^2} \end{bmatrix}, \quad r = \frac{a\eta^2}{1 + P_1 \sin \Lambda + P_2 \cos \Lambda},$$

in (43) and (44). This simplifies computing  $\bar{f}$  analytically. Indeed, the resulting integrands depend on the geometrical angles through trigonometric functions always at the numerator.

**5.2. Lie transformations and the higher-order correction term**

As already discussed, the semi-analytical propagation does not give the evolution of the osculating attitude variables  $s$ , but the one of the mean attitude variables  $\bar{s}$ . Deriving a transformation (52) between these two sets of variables is necessary to compute

the initial value of  $\bar{s}$ . This is done by using a Lie series technique, based on the combination of Lie transformations. In particular, a method similar to the one in Barrio and Palacià [14] is employed in this paper. The Lie transformation from a set of variables  $s^{(0)}$  to a new set  $s^{(1)}$  is given by

$$s^{(0)} = \sum_{i=0}^{\infty} \frac{1}{i!} \mathcal{L}_W^i s^{(1)}, \tag{60}$$

where  $\mathcal{L}_W s^{(1)}$  is the Lie derivative of  $s^{(1)}$  with respect to the vector field  $W$ , called generator, and

$$\mathcal{L}_W^i(s^{(1)}) = \underbrace{\mathcal{L}_W (\mathcal{L}_W (\dots (\mathcal{L}_W s^{(1)})))}_{i \text{ times}}.$$

Henrard [24] shows that, as a consequence of the transformation, a vector field  $F(s^{(0)})$  becomes

$$F'(s^{(1)}) = \sum_{i=0}^{\infty} \frac{1}{i!} \mathcal{L}_W^i F(s^{(0)}) \Big|_{s^{(0)=s^{(1)}},$$

with

$$\mathcal{L}_W^i F(s^{(0)}) = \underbrace{\mathcal{L}_W (\mathcal{L}_W (\dots (\mathcal{L}_W F(s^{(0)})))}_{i \text{ times}},$$

where

$$\mathcal{L}_W \cdot = \frac{\partial \cdot}{\partial s^{(0)}} W - \frac{\partial W}{\partial s^{(0)}}.$$

is the so-called *Lie operator*. In the following, to simplify the notation, we drop the subscripts here employed to distinguish the variables before and after the Lie transformation.

The dependence of the attitude equations of motion in (50) on the Sadov fast angles through the Jacobi elliptic function makes it extremely difficult to compute the generators of the Lie transformations leading to the averaged model (54). Thus, a Fourier expansion of the Jacobi elliptic functions in (50) is performed, applying the method by Abad et al. [25] and Vallejo [2], summarised in Appendix D. This allows us to express the dependence of the equations of motion on  $(\psi_l, \psi_g)$  through trigonometric functions, which are easier to handle. It is also convenient to introduce a dummy action  $J_M$  conjugated to the mean anomaly  $M$ , extending  $s$  to the set

$$\bar{s} = (\zeta, J_g, J_h, \psi_l, \psi_g, \psi_h, J_M, M),$$

to obtain an autonomous system. The equations of motion become

$$\frac{d\bar{s}}{dt} = \bar{A} \nabla_{\bar{s}} (\Phi + nJ_M + V_g + V_m) + \bar{B} M_{lp} v_s,$$

where  $n$  is the orbital mean motion, i.e.

$$n = \sqrt{\frac{\mu_{\oplus}}{a^3}}, \tag{61}$$

and

$$\bar{A} = \begin{bmatrix} \mathbf{A} & 0 \\ 0 & \mathbf{J} \end{bmatrix}, \quad \bar{B} = \begin{bmatrix} \mathbf{B} & 0 \\ 0 & 0 \end{bmatrix}, \quad \mathbf{J} = \begin{bmatrix} 0 & -1 \\ 1 & 0 \end{bmatrix}. \tag{62}$$

To keep track of the different relative sizes of the terms characterising the vector field during the successive application of Lie transformations, we introduce the *book-keeping parameter*  $\epsilon$  (see [26]). This is a formal parameter whose numerical value is equal to one and whose powers are used to assess the sizes of the terms. The higher the power of  $\epsilon$ , the smaller the order of magnitude of the term multiplied by it. Because of the hypothesis of a fast-rotating satellite, we have

$$\frac{d\bar{s}}{dt} = \bar{A} \nabla_{\bar{s}} \Phi + \epsilon \bar{A} \nabla_{\bar{s}} (nJ_M) + \epsilon^2 \bar{A} \nabla_{\bar{s}} (V_g + V_m) + \epsilon^2 \bar{B} M_{lp} v_s.$$

Three successive Lie transformations are applied to transform  $\bar{s}$  into  $\bar{\bar{s}} = (\bar{\bar{s}}, \bar{J}_M, M)$ , with  $\bar{J}_M$  the transformed ‘mean’ dummy action:

1. The generator  $W_1$  of the first transformation is given by the sum of two generators  $W_{1NH}$  and  $W_{1H}$ , used to deal with the parts of the vectorial field depending on non-conservative and conservative torques, respectively:

$$W_1 = W_{1NH} + W_{1H}.$$

$W_{1NH}$  fulfils

$$\mathcal{L}_{W_{1NH}} \bar{A} \nabla_{\bar{s}} \Phi + \epsilon^2 \bar{B} M_{lp} v_s = \epsilon^2 Z_2, \quad Z_2 = \frac{1}{4\pi^2} \int_0^{2\pi} \int_0^{2\pi} \bar{B} M_{lp} v_s d\psi_g d\psi_l.$$

Instead,  $W_{1H} = \bar{A} \nabla_{\bar{s}} \chi_1$ , with  $\chi_1$  fulfilling

$$-n_{\psi_l} \frac{\partial \chi_1}{\partial \psi_l} - n_{\psi_g} \frac{\partial \chi_1}{\partial \psi_g} + \epsilon^2 (V_g + V_m) = \epsilon^2 Z_2, \quad Z_2 = \frac{1}{4\pi^2} \int_0^{2\pi} \int_0^{2\pi} (V_g + V_m) d\psi_g d\psi_l,$$

where

$$n_{\psi_l} = -\pi \sqrt{\frac{\zeta}{1+\kappa}} \frac{J_g}{2AC} \frac{C-A}{K(\mu)} \tag{63}$$

and

$$n_{\psi_g} = \left( \Pi(-\kappa, \mu) + \frac{A}{C-A} K(\mu) \right) \frac{J_g(C-A)}{AC K(\mu)} \tag{64}$$

respectively represent the angular speed of  $\psi_l$  and  $\psi_g$  in the torque-free problem. The transformed vectorial field is

$$\frac{d\bar{s}^{(1)}}{dt} = \bar{\mathbf{A}} \nabla_{\bar{s}} \Phi + \varepsilon \bar{\mathbf{A}} \nabla_{\bar{s}} (nJ_M) + \varepsilon^2 \bar{\mathbf{A}} \nabla_{\bar{s}} \mathcal{Z}_2 + \varepsilon^2 \bar{\mathcal{Z}}_2 + \mathcal{O}(\varepsilon^3). \tag{65}$$

Let us remark that the average of  $\bar{\mathbf{W}}_1$  over  $(\psi_l, \psi_g)$  is equal to zero.

2. Denoting by  $Z_{2,i}$ ,  $i = 1 \dots 8$ , the components of  $\mathbf{Z}_2$ , the generator of the second transformation is

$$\mathbf{W}_2 = \frac{2\varepsilon^2}{n_{\psi_g}^2} \begin{bmatrix} n_{\psi_g} \Delta Z_{2,1} \arctan\left(\tan \frac{\psi_g}{2}\right), \\ n_{\psi_g} \Delta Z_{2,2} \arctan\left(\tan \frac{\psi_g}{2}\right) \\ 0 \\ \left(\frac{\partial n_{\psi_l}}{\partial \zeta} \Delta Z_{2,1} + \frac{\partial n_{\psi_l}}{\partial J_g} \Delta Z_{2,2}\right) \left(\arctan^2\left(\tan \frac{\psi_g}{2}\right) - \frac{\pi^2}{12}\right) \\ \left(\frac{\partial n_{\psi_g}}{\partial \zeta} \Delta Z_{2,1} + \frac{\partial n_{\psi_g}}{\partial J_g} \Delta Z_{2,2}\right) \left(\arctan^2\left(\tan \frac{\psi_g}{2}\right) - \frac{\pi^2}{12}\right) \\ 0 \\ 0 \\ 0 \end{bmatrix},$$

with

$$\Delta Z_{2,1} = Z_{2,1} - \bar{Z}_{2,1}, \quad \bar{Z}_{2,1} = \frac{1}{2\pi} \int_0^{2\pi} Z_{2,1} dM, \tag{66}$$

$$\Delta Z_{2,2} = Z_{2,2} - \bar{Z}_{2,2}, \quad \bar{Z}_{2,2} = \frac{1}{2\pi} \int_0^{2\pi} Z_{2,2} dM, \tag{67}$$

The vector field in (65) is transformed into

$$\frac{d\bar{s}^{(2)}}{dt} = \bar{\mathbf{A}} \nabla_{\bar{s}} \Phi + \varepsilon \bar{\mathbf{A}} \nabla_{\bar{s}} (nJ_M) + \varepsilon^2 \bar{\mathbf{A}} \nabla_{\bar{s}} \mathcal{Z}_2 + \varepsilon^2 \bar{\mathcal{Z}}_2 + \mathcal{O}(\varepsilon^3),$$

where  $\bar{\mathcal{Z}}_2 = (\bar{Z}_{2,1}, \bar{Z}_{2,2}, Z_{2,3}, Z_{2,4}, Z_{2,5}, Z_{2,6}, Z_{2,7}, Z_{2,8})^T$ .

3. The generator  $\mathbf{W}_3$  of the last Lie transformation is

$$\mathbf{W}_3 = \mathbf{W}_{3\text{NH}} - \bar{\mathbf{W}}_{3\text{NH}} + \mathbf{W}_{3\text{H}} - \bar{\mathbf{W}}_{3\text{H}}.$$

Here,  $\mathbf{W}_{3\text{NH}}$  fulfils

$$\mathcal{L}_{\mathbf{W}_{3\text{NH}}} \bar{\mathbf{A}} \nabla_{\bar{s}} (nJ_M) + \varepsilon^2 \bar{\mathcal{Z}}_2 = \varepsilon^2 \bar{\mathcal{Z}}_2, \quad \bar{\mathcal{Z}}_2 = \frac{1}{2\pi} \int_0^{2\pi} \bar{\mathcal{Z}}_2 dM,$$

and  $\bar{\mathbf{W}}_{3\text{NH}}$  is the average of  $\mathbf{W}_{3\text{NH}}$  over  $M$ . Instead,  $\mathbf{W}_{3\text{H}} = \bar{\mathbf{A}} \nabla_{\bar{s}} \chi_3$ , with  $\chi_3$  fulfilling

$$-n \frac{\partial \chi_3}{\partial M} \varepsilon + \varepsilon^2 \mathcal{Z}_2 = \varepsilon^2 \bar{\mathcal{Z}}_2, \quad \bar{\mathcal{Z}}_2 = \frac{1}{2\pi} \int_0^{2\pi} \bar{\mathcal{Z}}_2 dM,$$

and

$$\bar{\mathbf{W}}_{3\text{H}} = \bar{\mathbf{A}} \nabla_{\bar{s}} \left( \frac{1}{2\pi} \int_0^{2\pi} \chi_3 dM \right).$$

The transformed vector field is

$$\frac{d\bar{s}^{(3)}}{dt} = \bar{\mathbf{A}} \nabla_{\bar{s}} \Phi + \varepsilon \bar{\mathbf{A}} \nabla_{\bar{s}} (nJ_M) + \varepsilon^2 \bar{\mathbf{A}} \nabla_{\bar{s}} \bar{\mathcal{Z}}_2 + \varepsilon^2 \bar{\mathcal{Z}}_2 + \mathcal{O}(\varepsilon^3).$$

Neglecting the terms of order higher than 1 in the power series (60), the mean variables can be computed as

$$\bar{s} = \bar{s} - \mathbf{W}_1(\bar{s}) - \mathbf{W}_2(\bar{s} - \mathbf{W}_1(\bar{s})) - \mathbf{W}_3(\bar{s} - \mathbf{W}_1(\bar{s}) - \mathbf{W}_2(\bar{s} - \mathbf{W}_1(\bar{s}))).$$

The generators of the three Lie transformations can also be used to estimate the remainder  $\mathbf{R}$ , i.e. the difference between the original and the transformed vector fields, and, thus, to determine the higher-order term  $\mathbf{R}_p$  to include in the averaged model, increasing its accuracy. The remainder term of the third order in  $\varepsilon$  is

$$\mathbf{R}_3 = \mathcal{L}_{\bar{\mathbf{W}}_1} (\bar{\mathbf{A}} \nabla_{\bar{s}} (nJ_M)) + \mathcal{L}_{\bar{\mathbf{W}}_2} (\bar{\mathbf{A}} \nabla_{\bar{s}} (nJ_M)) + \frac{1}{2} \mathcal{L}_{\bar{\mathbf{W}}_3} (\bar{\mathbf{A}} \nabla_{\bar{s}} \mathcal{Z}_2 + \bar{\mathcal{Z}}_2 + \bar{\mathbf{A}} \nabla_{\bar{s}} \bar{\mathcal{Z}}_2 + \bar{\mathcal{Z}}_2).$$

Since the average of the three generators  $W_1$ ,  $W_2$  and  $W_3$  is null and the terms  $\bar{A}\nabla_{\bar{s}}(nJ_M)$ ,  $\bar{A}\nabla_{\bar{s}}\bar{Z}_2$ ,  $\bar{Z}_2$  do not depend on  $(\psi_l, \psi_g, M)$ , it is straightforward that the average  $\bar{R}_3$  over the fast angles is

$$\bar{R}_3 = \frac{1}{2(2\pi)^3} \iiint_0^{2\pi} \tilde{\mathcal{L}}_{W_3} (\bar{A}\nabla_{\bar{s}}\bar{Z}_2 + \bar{Z}_2) d\psi_l d\psi_g dM.$$

More specifically,  $\bar{R}_3$  can be split in the sum of the following terms:

$$\begin{aligned} \bar{R}_{3,1} &= \frac{1}{2(2\pi)^3} \iiint_0^{2\pi} \tilde{\mathcal{L}}_{W_{3H} - \bar{W}_{3H}} (\bar{A}\nabla_{\bar{s}}\bar{Z}_2) d\psi_l d\psi_g dM, \\ \bar{R}_{3,2} &= \frac{1}{2(2\pi)^3} \iiint_0^{2\pi} \tilde{\mathcal{L}}_{W_{3NH} - \bar{W}_{3NH}} (\bar{Z}_2) d\psi_l d\psi_g dM, \\ \bar{R}_{3,3} &= \frac{1}{2(2\pi)^3} \iiint_0^{2\pi} \tilde{\mathcal{L}}_{W_{3NH} - \bar{W}_{3NH}} (\bar{A}\nabla_{\bar{s}}\bar{Z}_2) d\psi_l d\psi_g dM, \\ \bar{R}_{3,4} &= \frac{1}{2(2\pi)^3} \iiint_0^{2\pi} \tilde{\mathcal{L}}_{W_{3H} - \bar{W}_{3H}} (\bar{Z}_2) d\psi_l d\psi_g dM. \end{aligned}$$

Considering that the dependence of the light pressure perturbation on the orbital mean anomaly occurs only through the shadow function, one can easily find that  $\bar{R}_{3,2}$  is null. Thus,

$$\bar{R}_3 = \bar{R}_{3,1} + \bar{R}_{3,3} + \bar{R}_{3,4}.$$

As previously discussed, the light pressure torque has typically smaller effects than the gravity-gradient and the residual magnetic torques. These perturbations become more comparable at higher altitudes, where their effects are less significant and, thus, the necessity of higher-order corrections reduces. Hence, we include only  $\bar{R}_{3,1}$  in the averaged model:

$$R_p = \bar{R}_{3,1}.$$

Considering  $\bar{R}_{3,3}$ ,  $\bar{R}_{3,4}$  and also the average of remainder terms of order higher than 3 in  $\epsilon$  would certainly benefit the accuracy of the model. However, this would imply introducing a prohibitive number of terms in the model which would negatively affect the computational time required to propagate the dynamics.

### 5.3. Non-singular variables

The attitude equations of motion in Eq. (36) are characterised by three singularities: i)  $\mu = 0$ , appearing in the time derivatives of  $\psi_l$  and  $\psi_g$ ; ii)  $\mu = 1$ , in the time derivatives of  $\psi_l$  and  $\psi_g$ ; iii)  $\sin \delta = 0$  in the time derivatives of  $\psi_g$  and  $\psi_h$ . Only the last two singularities survive in the averaged model (55). Indeed, even though the averaged model has terms with  $\mu$  at the denominator, these have a finite limit when  $\mu$  tends to zero. For example, one of the terms appearing in the time derivative of the mean  $\psi_l$  variable is

$$\frac{9\pi\mu_{\oplus}AQ_1^2Q_2 \sin(2\delta) \cos \psi_h \sqrt{1-\zeta}}{8a^3\eta^3(Q_1^2 + Q_2^2 + 1)^2 \sqrt{1+kJ_g(1-\mu)}} \frac{(E(\mu) - K(\mu)(1-\mu))^2}{\mu K(\mu)^2}$$

where

$$\lim_{\mu \rightarrow 0} \frac{(E(\mu) - K(\mu)(1-\mu))^2}{\mu K(\mu)^2} = 0,$$

as it follows from L'Hôpital's rule.

The singularity  $\mu = 1$  is peculiar. Indeed, since it occurs when  $J_d = B$ , as follows from Eq. (6), it denotes the separatrix between the SAMs and the LAMs in the torque-free problem.

When external torques perturb the free rotation of the satellite, the region of the phase space in the neighbourhood of the separatrix becomes chaotic: the attitude motion becomes recurrent aperiodic and extremely sensitive to initial conditions (see [21]). Small variations in the initial conditions result in huge differences in the dynamical evolution, which has no regular pattern. The dynamics becomes comparable to a stochastic process. When the rotational state of the satellite falls in the chaotic region, the averaged model is quantitatively inaccurate and becomes unsuitable. Thus, the singularity  $\mu = 1$  is not an issue.

The singularity  $\sin \delta = 0$  does not identify any attractive equilibrium point of the rotational dynamics. It constitutes a problem only for initial conditions such that the value of  $\sin \delta$  is close to zero, or if, during the propagation of the dynamics, the singularity is slowly approached. As a solution, we introduce alternative variables  $s_I$  obtained by a suitable combination of the  $s$  variables. A possible set is  $s_I = (\zeta, J_g, J_h, \psi_l, I_5, I_6, I_7)$  with

$$I_5 = \psi_g + \frac{J_h}{J_g} \psi_h, \quad I_6 = \sqrt{J_g^2 - J_h^2} \cos \psi_h, \quad I_7 = \sqrt{J_g^2 - J_h^2} \sin \psi_h.$$

The attitude equations of motion in the new variables can be obtained by suitably combining the equations of motion (36) in the Sadov variables, using that

$$\begin{aligned}\frac{dI_5}{dt} &= \frac{d\psi_g}{dt} - \frac{J_h}{J_g^2} \psi_h \frac{dJ_g}{dt} + \frac{1}{J_g} \psi_h \frac{dJ_h}{dt} + \frac{J_h}{J_g} \frac{d\psi_h}{dt}, \\ \frac{dI_6}{dt} &= \frac{J_g \cos \psi_h}{\sqrt{J_g^2 - J_h^2}} \frac{dJ_g}{dt} - \frac{J_h \cos \psi_h}{\sqrt{J_g^2 - J_h^2}} \frac{dJ_h}{dt} - \sqrt{J_g^2 - J_h^2} \sin \psi_h \frac{d\psi_h}{dt}, \\ \frac{dI_7}{dt} &= \frac{J_g \sin \psi_h}{\sqrt{J_g^2 - J_h^2}} \frac{dJ_g}{dt} - \frac{J_h \sin \psi_h}{\sqrt{J_g^2 - J_h^2}} \frac{dJ_h}{dt} + \sqrt{J_g^2 - J_h^2} \cos \psi_h \frac{d\psi_h}{dt},\end{aligned}$$

and successively expressing them in terms of the variables  $s_l$ . The equations of motion are explicitly reported in [Appendix E](#). With the same technique, it is also possible to easily obtain the averaged model in the new variables. This could be used in place of the averaged equations of motion discussed above. However, this is convenient when the singularity is problematic as previously discussed.

The averaged equations of motion expressed both in the  $s$  variables and in the non-singular variables are available open source at the following link:

[https://github.com/strath-ace/smart-astro/tree/opensource\\_release/JULIA](https://github.com/strath-ace/smart-astro/tree/opensource_release/JULIA).

In this paper we include the generators of the Lie transformations, which are used to compute the higher-order correction terms and perform the transformation from osculating to mean variables. Once the transformation from osculating to mean variables is performed through the successive application of the Lie transformations, as discussed in [Section 5.2](#), it is possible to integrate the averaged equations of motion, using the mean variables as initial conditions, to get the evolution of the attitude averaged dynamics. The higher-order correction term may or may not be added to the averaged model. In the numerical simulations discussed in [Sections 7 and 8](#), the higher-order correction term is always included in the averaged model.

## 6. Coupling attitude and orbital dynamics

We introduce the effect of the variation of the orbital elements on the attitude and vice versa, via the Gauss non-singular planetary equations:

$$\frac{da}{dt} = \frac{2}{\eta} \sqrt{\frac{a^3}{\mu_\oplus}} \left( (P_2 \sin \Lambda - P_1 \cos \Lambda) a_R + \frac{a\eta^2}{r} a_T \right), \quad (68)$$

$$\frac{dP_1}{dt} = \frac{r}{\eta \sqrt{a\mu_\oplus}} \left( -\frac{a\eta^2 \cos \Lambda}{r} a_R + \left( P_1 + \sin \Lambda + \frac{a\eta^2 \sin \Lambda}{r} \right) a_T - P_2 (Q_1 \cos \Lambda - Q_2 \sin \Lambda) a_N \right), \quad (69)$$

$$\frac{dP_2}{dt} = \frac{r}{\eta \sqrt{a\mu_\oplus}} \left( \frac{a\eta^2 \sin \Lambda}{r} a_R + \left( P_2 + \cos \Lambda + \frac{a\eta^2 \cos \Lambda}{r} \right) a_T + P_1 (Q_1 \cos \Lambda - Q_2 \sin \Lambda) a_N \right), \quad (70)$$

$$\frac{dQ_2}{dt} = \frac{r}{2\eta \sqrt{a\mu_\oplus}} (1 + Q_1^2 + Q_2^2) \sin \Lambda a_N, \quad (71)$$

$$\frac{dQ_1}{dt} = \frac{r}{2\eta \sqrt{a\mu_\oplus}} (1 + Q_1^2 + Q_2^2) \cos \Lambda a_N. \quad (72)$$

where the components  $(a_R, a_T, a_N)$  of the perturbing acceleration are expressed in a radial-transverse-normal reference frame attached to the orbiting object (see [\[27\]](#)). The semi-analytical propagation of the attitude dynamics is coupled with the analytical integration of a first-order averaged model of the orbital dynamics. This is derived by averaging Eqs. [\(68\)–\(72\)](#) over the orbital mean anomaly, as described in [\[27,28\]](#). This model accounts for the perturbations due to the Earth's zonal harmonics  $J_2, J_3, J_4, J_5$ , the gravitational influence of the Moon and the Sun, and light pressure. In [Zuiani and Vasile \[27\]](#) the authors model the perturbing acceleration as

$$\mathbf{a}_{\text{ip,ZV}} = -K_{\text{ip}} \mathbf{R}_{\text{i2b}}^T \bar{\mathbf{u}}, \quad K_{\text{ip}} = P_{\text{ip}} C_R \frac{S}{m},$$

where  $S$  is the cross-section area,  $C_R$  is a coefficient depending on the optical properties of the space object, and  $\bar{\mathbf{u}}$  is defined in [Eq. \(46\)](#). Note that  $\mathbf{a}_{\text{ip,ZV}}$  does not depend on the orbital mean anomaly. For the sake of consistency between the orbital and the attitude averaged models, we replace  $\mathbf{a}_{\text{ip,ZV}}$  with

$$\mathbf{a}_{\text{ip}} = \frac{1}{4\pi^2 m} \int_0^{2\pi} \int_0^{2\pi} \mathbf{R}_{\text{i2b}}^T \mathbf{f}_{\text{ip}} d\psi_g d\psi_l,$$

with  $\mathbf{f}_{\text{ip}}$  given in [Eq. \(47\)](#). Also  $\mathbf{a}_{\text{ip}}$  is independent of the orbital mean anomaly, so this replacement introduces minimal changes in the analytical model by [Zuiani and Vasile \[27\]](#). The integral in is computed with the same procedure described in [Section 5.1](#).

## 7. Numerical simulations

We consider a few test cases to compare the outcome of the semi-analytical propagation, against the outcome of the numerical integration of the full non-averaged attitude dynamics in [\(36\)](#). In all the simulations, the averaged model includes the higher-order correction term discussed in [Section 5.2](#). To avoid singularity, the propagation of the non-averaged dynamics is performed by integrating the following Euler's equations in quaternions (see [\[29\]](#)):

$$\frac{d\mathbf{w}}{dt} = \begin{bmatrix} \frac{1}{A} & 0 & 0 \\ 0 & \frac{1}{B} & 0 \\ 0 & 0 & \frac{1}{C} \end{bmatrix} \left( \mathbf{M} - \mathbf{w} \times \begin{bmatrix} A & 0 & 0 \\ 0 & B & 0 \\ 0 & 0 & C \end{bmatrix} \mathbf{w} \right),$$

$$\begin{bmatrix} \frac{dq_1}{dt} \\ \frac{dq_2}{dt} \\ \frac{dq_3}{dt} \\ \frac{dq_4}{dt} \end{bmatrix} = \frac{1}{2} \begin{bmatrix} -q_2 & -q_3 & -q_4 \\ q_1 & -q_4 & q_3 \\ q_4 & q_1 & -q_2 \\ -q_3 & q_2 & q_1 \end{bmatrix} \mathbf{w},$$

with  $\mathbf{w}$  the satellite’s angular velocity, given by

$$\mathbf{w} = \mathbf{J}_g \begin{bmatrix} \frac{\sqrt{1-\zeta}}{A} \operatorname{cn}(u, \mu) \\ -\frac{\sqrt{1-\zeta}\sqrt{1+\kappa}}{B} \operatorname{sn}(u, \mu) \\ \frac{\sqrt{\zeta}}{C} \operatorname{dn}(u, \mu) \end{bmatrix},$$

and  $(q_1, q_2, q_3, q_4)$  the quaternions. From the evolution of the angular velocity and the quaternions, one can derive the evolution of the corresponding  $s$  variables, by passing through the transformation in Andoyer–Serret variables and, then, exploiting the relationships in Section 2.2. Then, it is possible to numerically compute the evolution of the mean slow variables by performing a double average over the time intervals  $T_a$  and  $T_o$ , defined as

$$T_a = \max\left(\frac{2\pi}{n_{\psi_l}}, \frac{2\pi}{n_{\psi_g}}\right), \quad T_o = \frac{2\pi}{n},$$

(see (61), (63), (64) for the definitions of  $n_{\psi_l}$  and  $n_{\psi_g}$ ). The percentage difference, or error, between the semi-analytical propagation and the numerical average of  $s$  is defined as:

$$\Delta\zeta = 100 \left| \frac{\bar{\zeta}_O - \bar{\zeta}_{SA}}{\bar{\zeta}_O} \right|, \tag{73}$$

$$\Delta J_g = 100 \left| \frac{\bar{J}_{gO} - \bar{J}_{gSA}}{\bar{J}_{gO}} \right|, \tag{74}$$

$$\Delta J_h = 100 \left| \frac{\bar{J}_{hO} - \bar{J}_{hSA}}{\bar{J}_{hO}} \right|, \tag{75}$$

$$\Delta\psi_h = 100 \left| \frac{\bar{\psi}_{hO} - \bar{\psi}_{hSA}}{\bar{\psi}_{hO}} \right|, \tag{76}$$

where the subscripts SA and O imply that the value of the mean slow variables is computed through the semi-analytical propagation or the numerical averaged procedure, respectively.

In this work, the propagation of the averaged dynamics is performed using the JULIA’s Feagin14 numerical integrator with  $1e-13$  absolute and relative tolerances. The propagation of the non-averaged dynamics is performed using MATLAB’s ODE113 numerical propagator with  $5e-14$  absolute and relative tolerances, after checking the consistency with the outcomes obtained with the same numerical propagator used for the averaged dynamics. When the shadow effects are considered, in the propagation of the non-averaged dynamics, the shadow is modelled through a numerical smoothing function as described in [30]. Instead, in the averaged-model the shadow function is modelled and treated as described in the previous sections.

While the transformation from osculating to mean variables is necessary at the initial instant of time, once the integration of the averaged model is performed, computing the back-transformation from mean to osculating variables at each instant of time could be disadvantageous in terms of computational time. This would also introduce a further increasing source of error, as the variable transformation is based on a Fourier expansion of the equations of motion. Thus, it would be extremely advantageous to approximate the evolution of the non-averaged dynamics directly through the outcomes of the semi-analytical integration, without performing any further transformation. The discrepancy between the averaged dynamics and the non-averaged dynamics is here represented using quantities with an immediate physical meaning. In particular, the satellite’s angular velocity and the axis-angle representation of the rotations are employed. At each considered instant of time, we compute

$$\Delta w = \frac{|\bar{w}_{SA} - w_O|}{w_O}, \quad \begin{bmatrix} \Delta w_x \\ \Delta w_y \\ \Delta w_z \end{bmatrix} = \frac{1}{2} \left| \frac{\bar{\mathbf{w}}_{SA}}{\bar{w}_{SA}} - \frac{\mathbf{w}_O}{w_O} \right|, \tag{77}$$

where  $w = |\mathbf{w}|$ . Note that  $\Delta w$  is a quantity related to the magnitude of the angular velocity, while  $\Delta w_x$ ,  $\Delta w_y$  and  $\Delta w_z$  are related to its direction cosines, and are defined so that their maximum value is equal to one. Concerning the orientation of the body, we measure the rotation that would be required to bring the attitude computed through the semi-analytical propagation to the non-averaged numerically-computed attitude. At each instant of time, this rotation is defined by the matrix

$$\mathbf{R}_{SA2O} = \overline{\mathbf{R}}_{12bSA}^T \mathbf{R}_{12bO},$$

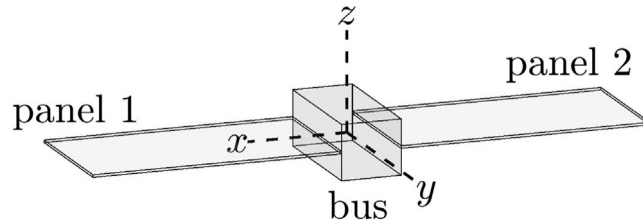


Fig. 2. Fictitious triaxial satellite employed in the test cases.

where  $\mathbf{R}_{12b}$  is the rotation matrix from  $OXYZ$  to  $Oxyz$ . The rotation can be represented as an elementary rotation of angle  $\beta$  equal to

$$\beta = 2 \arccos \left( \frac{\sqrt{T_r + 1}}{2} \right), \tag{78}$$

with  $T_r$  the trace of  $\mathbf{R}_{SA20}$ . Let us remark that  $\Delta w$ ,  $\Delta w_x$ ,  $\Delta w_y$ ,  $\Delta w_z$  and  $\beta$  are not properly errors, as they are used to compare different kinds of variables, i.e. mean variables and osculating variables.

As a test case, we consider a fictitious satellite along an orbit with initial osculating Keplerian elements

$$a = 29600 \text{ km}, \quad e = 0.01, \quad I = 56 \text{ deg}, \quad \omega = 0 \text{ deg}, \quad \Omega = 60 \text{ deg}, \tag{79}$$

in a SAM, with initial angular velocity and quaternions

$$\mathbf{w} = \begin{bmatrix} 0.05 \\ 0.1 \\ 5 \end{bmatrix} \frac{\text{deg}}{s}, \quad \begin{bmatrix} q_1 \\ q_2 \\ q_3 \\ q_4 \end{bmatrix} = \begin{bmatrix} -0.392862 \\ 0.160367 \\ 0.527825 \\ 0.735860 \end{bmatrix}. \tag{80}$$

In terms of the  $s$  variables, the attitude initial conditions are

$$\begin{aligned} \zeta &= 0.999993, \\ J_g &= 233.774 \text{ kg m}^2/\text{s}, \\ J_h &= 94.3974 \text{ kg m}^2/\text{s}, \\ \psi_l &= 298.620 \text{ deg}, \\ \psi_g &= 16.6746 \text{ deg}, \\ \psi_h &= 190.460 \text{ deg}. \end{aligned} \tag{81}$$

The satellite is shown in Fig. 2. Its mass, moments of inertia, and intrinsic magnetic moment are

$$\begin{aligned} m &= 500 \text{ kg}, \\ A &= 334.042 \text{ kg m}^2, \\ B &= 2404.958 \text{ kg m}^2, \\ C &= 2678.416 \text{ kg m}^2, \\ I_m &= [0.1, 0.1, 0.1] \text{ A m}^2. \end{aligned}$$

Its bus has a total reflectivity  $\rho_i = 0.6$  and the fraction of  $\rho_i$  which is specular is  $s_i = 1$ ; the front of panels 1 and 2 has  $\rho_i = 0.27$  and  $s_i = 1$ ; the back of panels 1 and 2 has  $\rho_i = 0.07$  and  $s_i = 0$ . The initial value of  $\mu$  is  $\sim 4 \cdot 10^{-4}$ , and, thus the initial conditions fall in a region of the phase space far from the chaotic region discussed in Section 5.3. The averaged model is expected to be suitable.

Figs. 3, 4 show the evolution of  $(\Delta\zeta, \Delta J_g, \Delta J_h, \Delta\psi_h)$  and  $(\Delta\omega, \Delta\omega_x, \Delta\omega_y, \Delta\omega_z, \beta)$  when the satellite is assumed along a Keplerian orbit. In this simulation as well as in the following ones, the geocentric position of the Sun, and thus the unit vector  $\tilde{u}$ , are derived from the Earth's ephemeris (see [31]). The evolution of the mean slow variables is well-reproduced:  $\Delta\zeta$ ,  $\Delta J_g$ ,  $\Delta J_h$  and  $\Delta\psi_h$  remain smaller than  $10^{-6}\%$ ,  $10^{-6}\%$ ,  $10^{-1}\%$  and  $10^{-3}\%$ , respectively. It is possible to observe a first fast sudden increase of the relative errors  $\Delta\zeta$  and  $\Delta J_g$  around 150 days. Even though this growth is relatively small, it impacts the evolution of the quantities  $(\Delta\omega, \Delta\omega_x, \Delta\omega_y, \Delta\omega_z)$ , which are functions of mean and osculating  $(\zeta, J_g, \psi_l)$  variables. The angular speed of  $\psi_l$  mainly depends on  $(\zeta, J_g)$ , thus the growth of  $\Delta\zeta$  and  $\Delta J_g$  causes a phase shift of the fast angle, which is reflected in the faster increase of  $(\Delta\omega, \Delta\omega_x, \Delta\omega_y, \Delta\omega_z)$ . Anyway, these are still reasonably small after one year. The same occurs for  $\beta$ , which is a function of all the variables  $s$ . The trend of  $(\Delta\omega, \Delta\omega_x, \Delta\omega_y, \Delta\omega_z, \beta)$  is worsened by the effects of the Earth's shadow. Indeed, if the satellite is constantly assumed in light, while  $\beta$  is comparable, the other quantities are smaller, as shown in Figs. 5 and 6.

Fig. 8 shows the evolution of the errors in the more realistic case in which also the orbital dynamics is affected by environmental perturbations. In particular, the effects of the Earth's zonal harmonics  $(J_2, J_3, J_4, J_5)$ , the lunar gravity, the solar gravity, and the light pressure acceleration are considered. Because of the error accumulation related to both the attitude and the orbital averaged



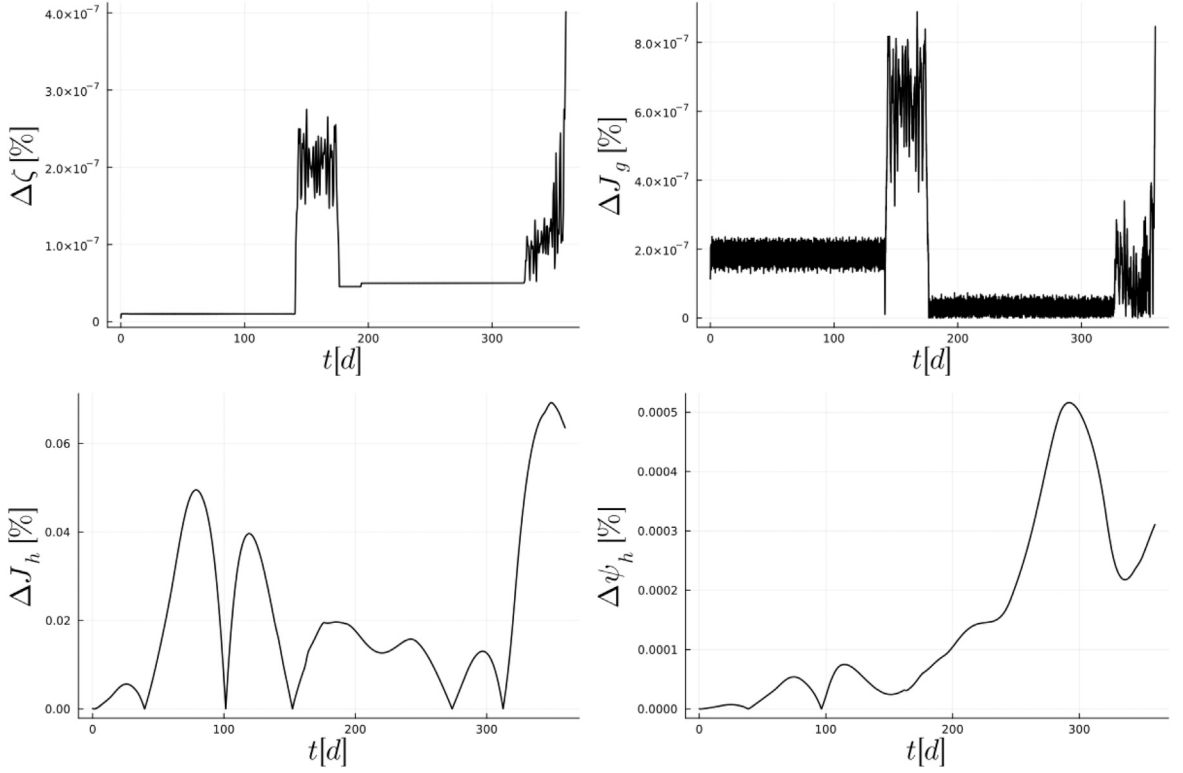


Fig. 3. Evolution of the errors (73)–(76) for the triaxial satellite in Fig. 2 for the initial conditions in (79) and (81). The satellite's orbit is here assumed Keplerian.

models, the errors  $(\Delta\zeta, \Delta J_g, \Delta J_h, \Delta\psi_h)$  are larger, and  $(\Delta\omega, \Delta\omega_x, \Delta\omega_y, \Delta\omega_z, \beta)$  increase faster. However, they are still acceptable after one year.

We slightly change the initial conditions, imposing an initial angular velocity equal to

$$\mathbf{w} = \begin{bmatrix} 0.1 \\ 0.2 \\ 5 \end{bmatrix} \frac{\text{deg}}{\text{s}}.$$

The initial  $s$  variables are

$$\begin{aligned} \zeta &= 0.999973, \\ J_g &= 233.887 \text{ kg m}^2/\text{s}, \\ J_h &= 97.3184 \text{ kg m}^2/\text{s}, \\ \psi_l &= 298.627 \text{ deg}, \\ \psi_g &= 16.940 \text{ deg}, \\ \psi_h &= 189.712 \text{ deg}, \end{aligned} \tag{82}$$

and the new initial value of  $\mu$  is  $\sim 0.00185$ , so that, even though still far from the chaotic region, the initial rotational state is slightly closer to it. We consider the effects of both attitude and orbital perturbations. By comparing Figs. 9 and 10 with Figs. 7 and 8, it is possible to observe that while  $(\Delta\zeta, \Delta J_g, \Delta J_h, \Delta\psi_h)$  and  $\beta$  are comparable,  $(\Delta\omega, \Delta\omega_x, \Delta\omega_y, \Delta\omega_z)$  grow faster. Instead, all the quantities in Figs. 11, 12 are larger than those in Figs. 7, 8. In particular,  $\beta$  increases significantly faster. The outcomes in Figs. 11, 12 are obtained by modifying only the semi-major axis in the initial conditions in (79) and (80), imposing it equal to  $a = 10000$  km, and considering the effects of both orbital and attitude perturbations. The smaller semi-major axis implies that the perturbations by the gravity gradient and residual magnetic torques are larger. In Fig. 11, the errors  $\Delta J_h$  and  $\Delta\psi_h$  can reach quite large values at certain instants of time. Most of the peaks are related to the definitions of the errors themselves as they occur in the neighbourhood of singularities for the mean variables  $\bar{J}_h$  and  $\bar{\psi}_h$ . Nevertheless, the trend of these variables is well reproduced as one can see from Fig. 13, showing the evolution of the mean  $\bar{J}_h$  and  $\bar{\psi}_h$  computed through the semi-analytical propagation and the osculating  $J_h$  and  $\psi_h$  obtained by integrating the full-dynamics.

From the numerical simulations, it is clear that  $\beta$  grows faster than the quantities related to the angular velocity. This trend is justified by the dependence of these quantities on the Sadov fast variables. Indeed, typically, the error tends to increase significantly

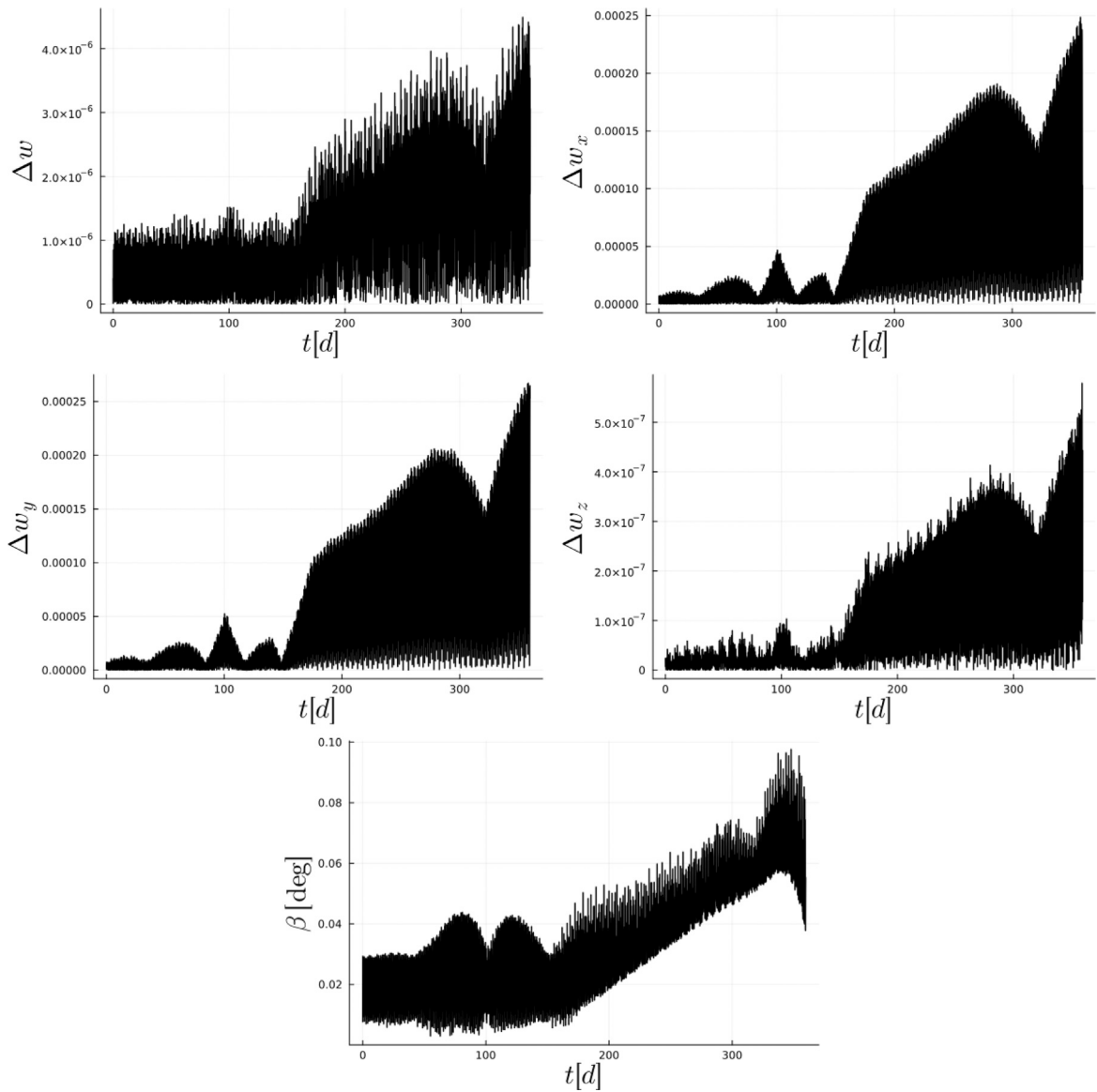


Fig. 4. Evolution of the quantities in (77)–(78) for the triaxial satellite in Fig. 2 for the initial conditions in (79) and (81). The satellite’s orbit is here assumed Keplerian.

faster for the fast variables ( $\psi_l, \psi_g$ ) than for the slow variables ( $\zeta, J_g, J_h, \psi_h$ ) and while the angular velocity depends on the only  $\psi_l$ , the attitude depends on both  $\psi_l$  and  $\psi_g$ . The evolution of the slow variables is typically well reproduced. This is advantageous, as it allows to compute the evolution of mean angular momentum in the inertial reference frame. Indeed,  $J_g$  corresponds to the magnitude of  $\mathbf{G}$ , while  $\sqrt{J_g^2 - J_h^2} \sin \psi_h$ ,  $-\sqrt{J_g^2 - J_h^2} \cos \psi_h$  and  $J_h$  are its projections on the  $X$ ,  $Y$  and  $Z$  axes, respectively. On the contrary, the small increments of errors  $\Delta\zeta$  and  $\Delta J_g$ , which occur as expected with time, cause a significant increase in the error rate of the fast variables, reflected by the quantities ( $\beta, \Delta\omega, \Delta\omega_x, \Delta\omega_y, \Delta\omega_z$ ). Such an increase is worsened when eclipse effects are taken into account.

In terms of computational times, the propagation of the full non-averaged dynamics takes  $\sim 2.16$  h for the test case in Figs. 7, 8,  $\sim 2.4$  h for the test case in Figs. 9, 10, and  $\sim 2.12$  for the test case in Figs. 11, 12. Integrating the semi-analytical model is significantly faster, as it takes  $\sim 54.1$  s,  $\sim 64.4$  s and  $\sim 37.3$  s, respectively.

The test case with initial conditions in (79) and (80) is repeated for the axisymmetric satellite in Fig. 14. Its mass, moments of inertia, and intrinsic magnetic moment are

$$m = 800 \text{ kg,}$$

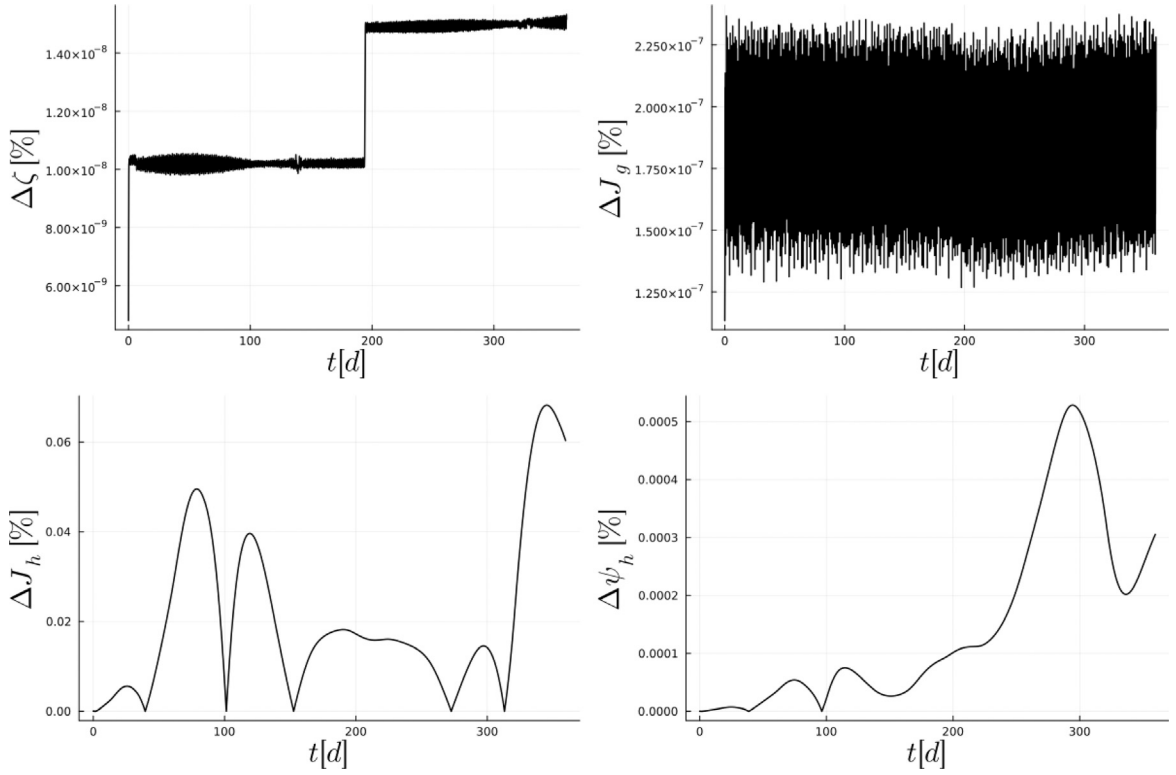


Fig. 5. Evolution of the errors (73)–(76) for the triaxial satellite in Fig. 2 for the initial conditions in (79) and (81). The satellite is assumed to be along a Keplerian and constantly in light.

$$\begin{aligned}
 A &= 483.33 \text{ kg m}^2, \\
 B &= 483.33 \text{ kg m}^2, \\
 C &= 833.33 \text{ kg m}^2, \\
 \mathbf{I}_m &= [0.1, 0.1, 0.1] \text{ A m}^2.
 \end{aligned}$$

The external surface of the satellite has  $\rho_i = 0.6$  and  $s_i = 1$  except for the dark grey panel which has  $\rho_i = 0.27$  and  $s_i = 1$ . The effects of both attitude and orbital perturbations are considered. The new initial  $s$  variables are

$$\begin{aligned}
 \zeta &= 0.999832, \\
 J_g &= 72.7282 \text{ kg m}^2/\text{s}, \\
 J_h &= 29.2844 \text{ kg m}^2/\text{s}, \\
 \psi_l &= 296.565 \text{ deg}, \\
 \psi_g &= 18.5372 \text{ deg}, \\
 \psi_h &= 190.9434 \text{ deg}.
 \end{aligned} \tag{83}$$

Figs. 15, 16 show the evolution of  $(\Delta\zeta, \Delta J_g, \Delta J_h, \Delta\psi_h)$  and  $(\Delta\omega, \Delta\omega_x, \Delta\omega_y, \Delta\omega_z, \beta)$ . They increase in time, but also in this case they maintain acceptable values after one year.

## 8. Accuracy of the attitude semi-analytical propagation

As discussed in 5.3, the accuracy of the semi-analytical propagation depends on the rotational state vector of the satellite. Indeed, if it belongs to a chaotic region of the phase space, i.e. the value of  $\mu$  is close to 1, the averaged model is not suitable. There are also other sources of error. If the hypothesis at the basis of the averaged model are not fulfilled, the integration results to be inaccurate. For example, near a resonance or if the magnitude of the external torques is too large to be considered as a perturbation in comparison to the rotational kinetic energy of the satellite, the averaged model may not be accurate enough. Indeed, as observed in Section 7, the larger the perturbation, the larger the errors and the faster the growth of the discrepancy between the averaged and the non-averaged dynamics.

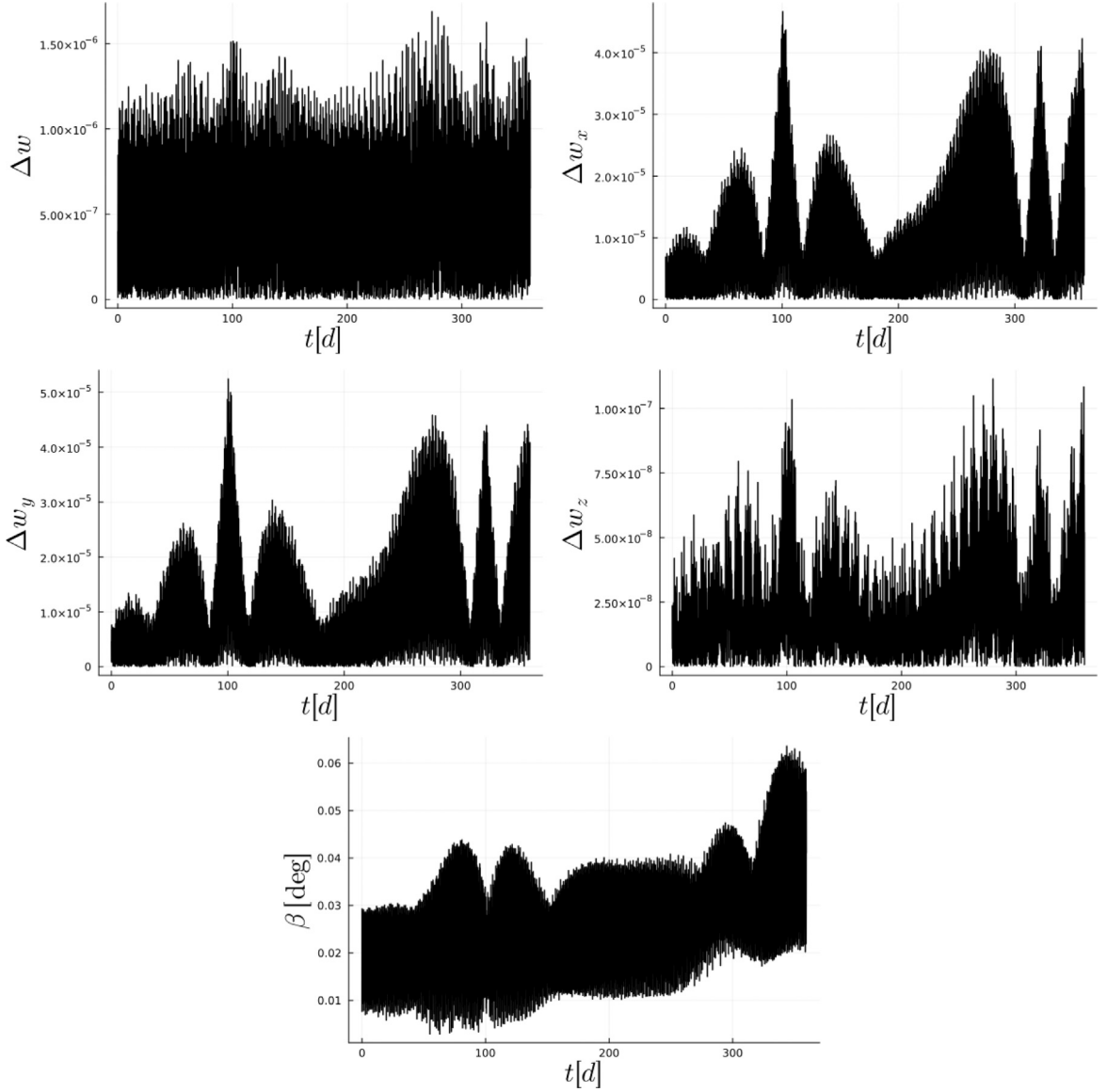


Fig. 6. Evolution of the quantities in (77) and (78), for the triaxial satellite in Fig. 2 for the initial conditions in (79) and (81). The satellite is assumed to be along a Keplerian and constantly in light.

In this section we introduce qualitative accuracy maps to quantify the discrepancy between the outcomes of the semi-analytical propagation and the full non-averaged dynamics over a range of possible initial conditions and perturbing torques. The maps are numerically computed and are suitable for any triaxial satellite. A map is formally defined as

$$\Theta : (\mathcal{M}, T_k, \mu) \mapsto \mathcal{E}$$

where  $\mathcal{M}$  is a quantity used to estimate the magnitude of the perturbation,  $T_k$  is the value of the torque-free Hamiltonian coinciding with the kinetic energy of the satellite, and  $\mathcal{E}$  is a quantity that allows comparing the evolution of the average attitude dynamics with the evolution of the non-averaged dynamics, similarly to  $(\Delta\omega, \Delta\omega_x, \Delta\omega_y, \Delta\omega_z, \beta)$  discussed in the previous section. In the following, we employ the subscripts SA and O to specify whether the value of a considered quantity is computed through the semi-analytical propagation or by numerically integrating the full non-averaged dynamics (see Section 7), we define  $\mathcal{E}$  as

$$\mathcal{E} = \log_{10} \left( \max_{i \in T} \sqrt{\Delta_1^2 + \Delta_2^2 + \Delta_3^2 + \sum_{i=1}^3 \sum_{j=1}^3 (\Delta r_{i,j})^2} \right), \tag{84}$$

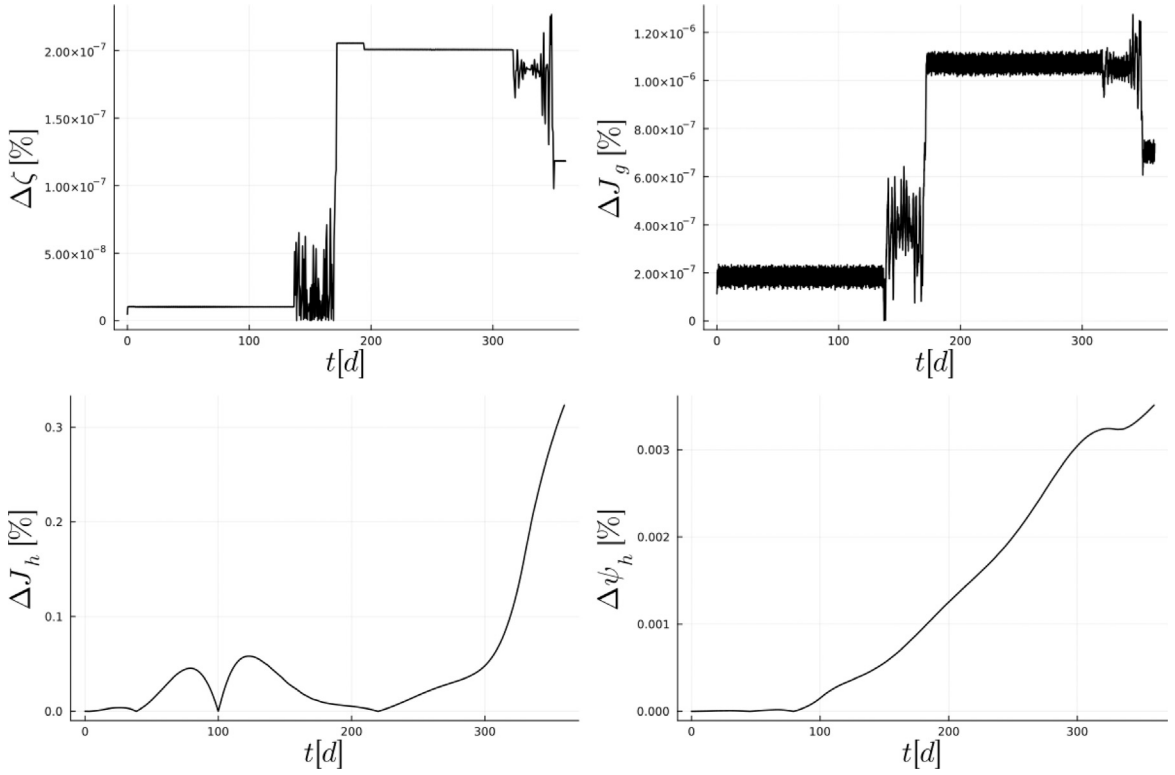


Fig. 7. Evolution of the errors (73)–(76) for the triaxial satellite in Fig. 2 for the initial conditions in (79) and (81). Here, the effects of both environmental perturbing torques and accelerations are considered.

where

$$\begin{bmatrix} \Delta_1 \\ \Delta_2 \\ \Delta_3 \end{bmatrix} = \frac{\mathbf{w}_O - \bar{\mathbf{w}}_{SA}}{w_O},$$

with  $w = |\mathbf{w}|$ ,  $\Delta r_{i,j}$  are the components of

$$\Delta \mathbf{R}_{12b} = \mathbf{R}_{12bO} - \overline{\mathbf{R}}_{12bSA},$$

and  $T$  is the time of propagation. The upper bound of quantity  $\mathcal{E}$  is computed by first deriving an upper bound of the perturbation magnitude. Initial conditions leading to a perturbation magnitude close to such an upper bound should be selected. To this aim, we separately consider the contribution of each perturbing torque. For the gravity-gradient torque, an upper bound can be derived from (43):

$$\mathcal{M}_g = \frac{3\mu_\oplus}{2a^3 \left(1 - \sqrt{P_1^2 + P_2^2}\right)^3} \max(A, B, C). \quad (85)$$

Similarly, for the residual magnetic torque, an upper bound, derived from (44), is:

$$\mathcal{M}_m = \frac{|I_m|\mu_m}{a^3 \left(1 - \sqrt{P_1^2 + P_2^2}\right)^3} \sqrt{1 + \frac{12(Q_1^2 + Q_2^2)}{(1 + Q_1^2 + Q_2^2)^2}}. \quad (86)$$

For the effect of light pressure, an upper bound, derived from Eq. (48), is:

$$\mathcal{M}_{srp} = \max_{\mathbf{u}} \left| \sum_{i=1}^{n_f} S_i \varepsilon_i \rho_i \times (c_{a,i} \mathbf{u} + c_{d,i} \hat{\mathbf{n}}_i + c_{s,i} (\mathbf{u} \cdot \hat{\mathbf{n}}_i) \hat{\mathbf{n}}_i) \right|, \quad (87)$$

Fig. 17 shows three maps for the gravity-gradient torque on the  $(\mathcal{M}_g, T_k)$  plane, each obtained for a different value of  $\mu$ . The first one is  $\mu \sim 4 \cdot 10^{-4}$ , corresponding to the initial value of  $\mu$  in the test case described in Section 7. The other two values are randomly selected. The quantity  $\mathcal{E}$  is represented with a colour code. Warmer colours correspond to larger values of  $\mathcal{E}$ . The maps are computed using grids of  $(200 \times 160)$  points, imposing a propagation time  $T$  equal to 2 days, and assuming the satellite is Keplerian

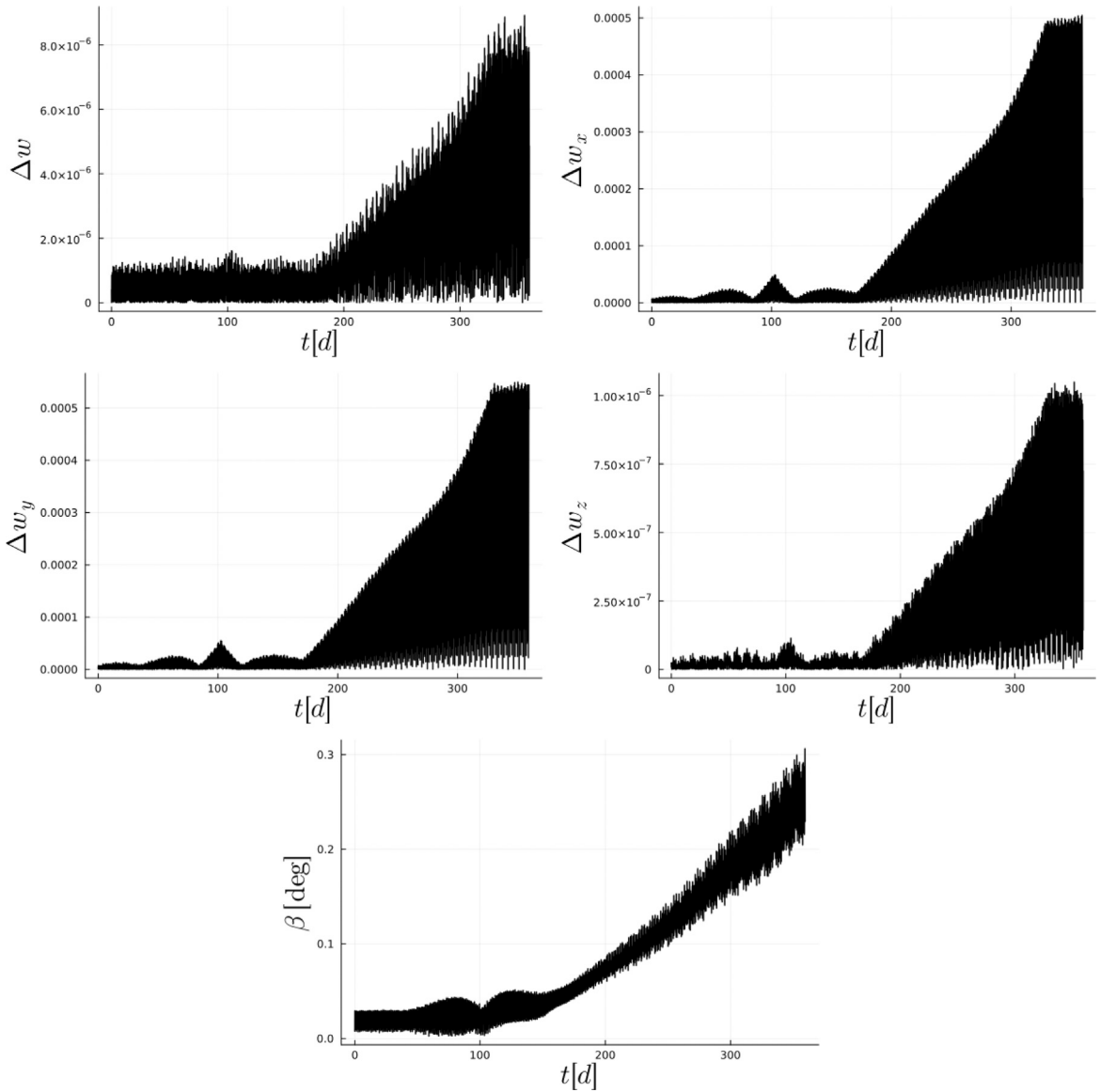


**Fig. 8.** Evolution of the quantities in (77) and (78) for the triaxial satellite in Fig. 2 with the initial conditions in (79) and (81). Here, the effects of both environmental perturbing torques and accelerations are considered.

orbits. As expected, the value of  $\mathcal{E}$  increases at the increase of both  $\mathcal{M}_g$  and  $\mu$ . In particular, for the largest value of  $\mu$ , the map seems less regular, especially in the region with the largest value of  $\mathcal{M}_g$ , where it is also possible to observe the presence of stripes. At the increase of the perturbations, chaotic regions in the phase space typically tend to extend. Thus, the phenomenon may be related to the chaoticity of the dynamics. The specific nature of these interesting features would deserve an accurate analysis, that we reserve to perform in the future.

Figs. 18 and 19 respectively show the maps computed for the residual magnetic torque and the light pressure torque perturbations, for the smaller value of  $\mu$ ,  $\mu \sim 4 \cdot 10^{-4}$ . The map for the residual magnetic torque is computed by using the same grid, and the same time of propagation as the maps for the gravity torque. Also, in this case, the orbits are assumed Keplerian. The map for the light pressure is obtained assuming the satellite is always in light and along Keplerian orbits. Because of the large computational time required by the propagation of the non-averaged dynamics, the grid adopted has a smaller number of points,  $(30 \times 60)$ . This is the reason why it appears discontinuous, differently from the maps for the other perturbations. Furthermore, the propagation time is shorter, equal to 1 day. Since over such a period, the geocentric position of the Sun has a very small variation, it is considered fixed, to save computational time. Finally, to evaluate  $\mathcal{M}_{\text{srp}}$  in (87), we approximate the heliocentric orbit of the Earth as circular and tilted by  $I_E = 23.43928111$  deg over the equatorial plane, so that

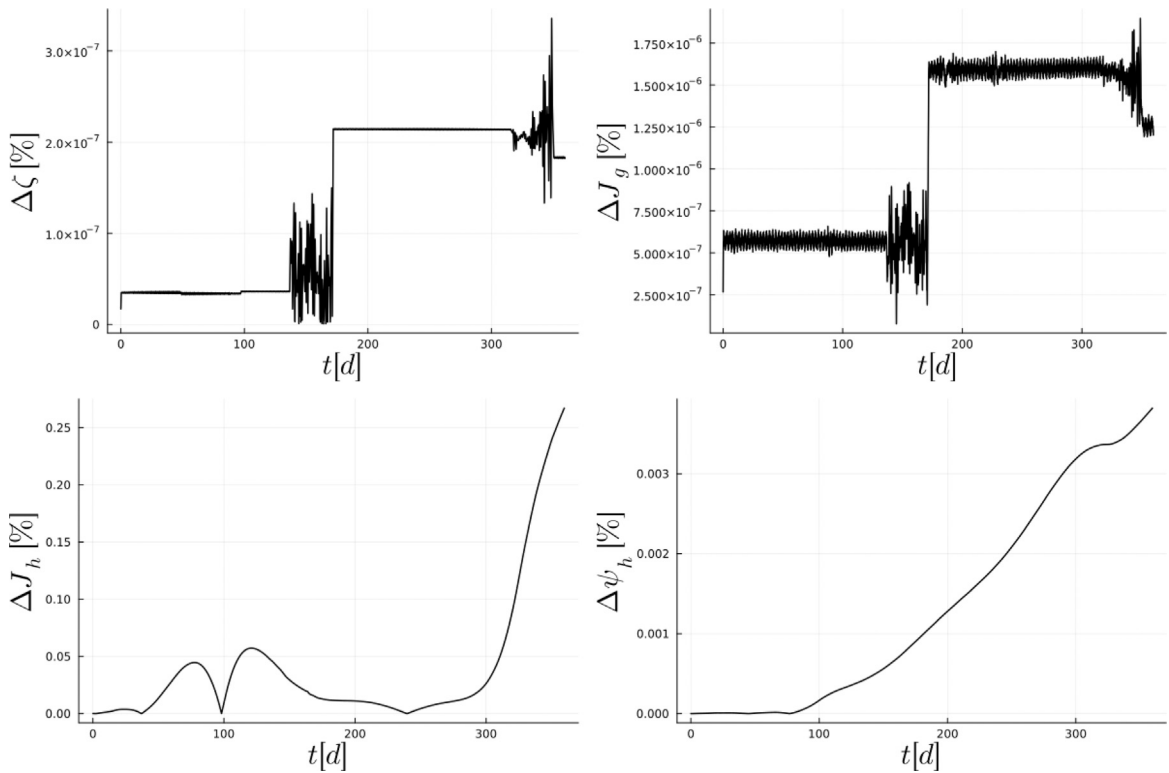


Fig. 9. Evolution of the errors (73)–(76) for the triaxial satellite in Fig. 2, when the initial angular velocity is modified to increase the initial value of  $\mu$ . Here, the effects of both environmental perturbing torques and accelerations are considered.

$$\ddot{\mathbf{u}} \sim -\mathbf{R}_{12b} \begin{bmatrix} 1 & 0 & 0 \\ 0 & \cos I_E & -\sin I_E \\ 0 & \sin I_E & \cos I_E \end{bmatrix} \begin{bmatrix} \cos M_E \\ \sin M_E \\ 0 \end{bmatrix},$$

with  $M_E$  the Earth’s mean anomaly.

Note that the initial conditions (79) and (80) of the test case in Section 7 belong to the blue regions in all three maps 17(a), 18 and 19. The computational time of the averaged model, for all the propagations used to building the accuracy maps, ranges from ~0.7% to 0.9%, of the computational time of the same propagations with the non-averaged model.

### 9. Conclusions

The semi-analytical theory proposed in this paper was developed to be suitable for both triaxial and axisymmetric space objects, which are fast-rotating along geocentric orbits, under the hypothesis that the orbital mean anomaly and the Sadov fast angles ( $\psi_l, \psi_g$ ) are non-resonant. Considering a fictitious triaxial satellite, some numerical tests were performed with different initial values of the attitude or orbital variables. Tests included the coupled effects of perturbations on the orbital and attitude dynamics. A similar numerical test was performed considering an axisymmetric satellite. The results of these tests display a good accuracy vs computational cost with a moderate increase in propagation error over one year. In particular, the results show that the semi-analytical theory can be exploited to well reproduce the evolution of the slow Sadov variables, while the error in the evolution of ( $\psi_l, \psi_g$ ) increases faster. From a further test, where the dynamics was assumed to be affected only by the perturbing torques, and the orbital dynamics was assumed Keplerian, we can speculate that one of the main sources of propagation error comes from the repeated passage through the Earth’s shadow region.

To better evaluate the limits of the semi-analytical theory, we performed a test campaign to assess its accuracy at the variation of the initial conditions and of the magnitude of the perturbations. From the test campaign, we derived accuracy maps showing the accuracy of the semi-analytical propagation as a function of the initial kinetic energy and of an upper estimate of the magnitude of the perturbations. As expected, it was found that the accuracy decreases for larger perturbations and at the decrease of the initial kinetic energy. Furthermore, the error depends also on the dynamic stability of the object: the model is not suitable for rotational states close to the chaotic regions of the phase space.

Future work is required to improve the approach to take into account the Earth’s shadowing effects. Moreover, in this paper, we excluded any atmospheric component of the torque and force. In the future, these effects need to be included to study the long-term

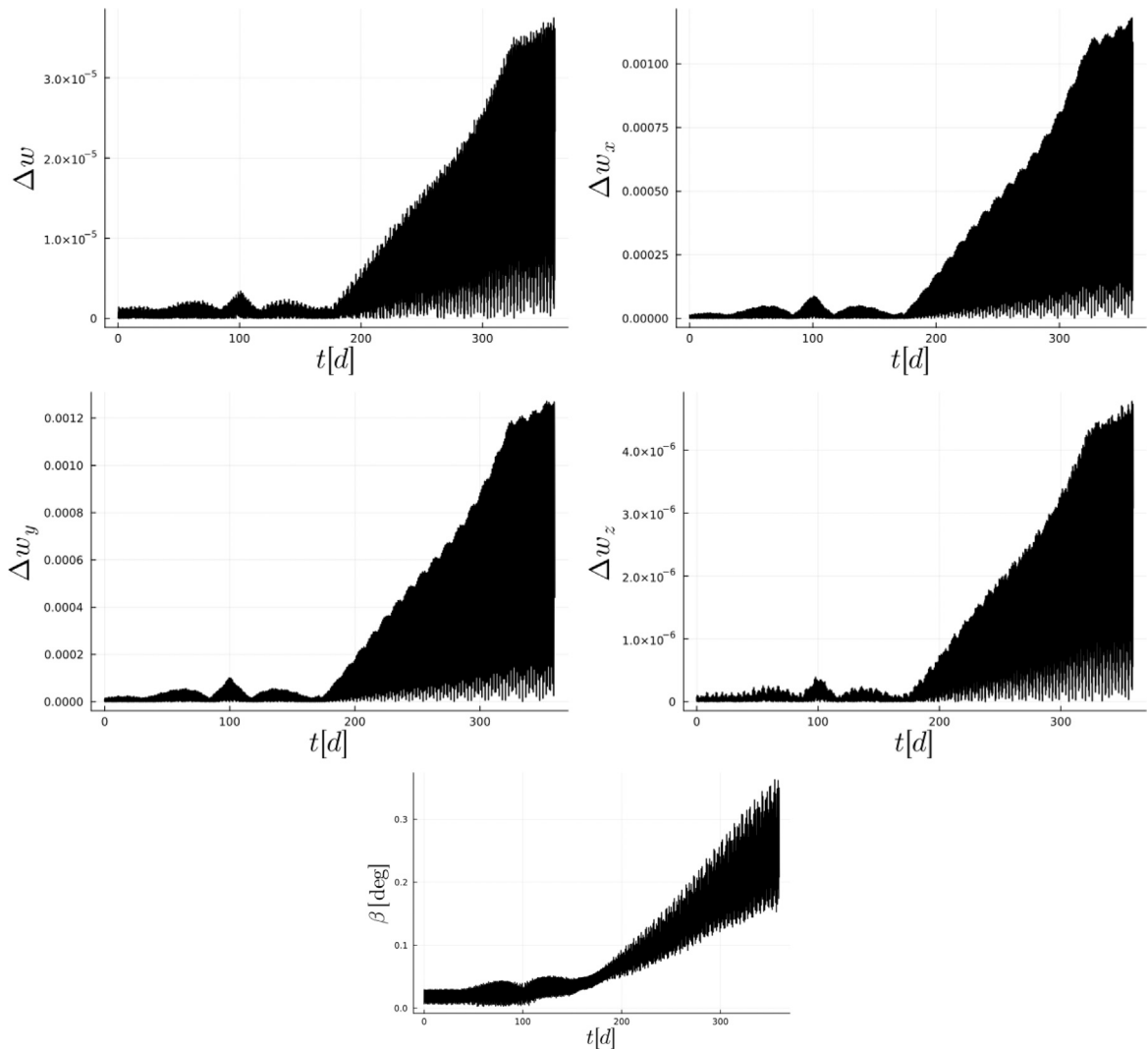


Fig. 10. Evolution of the quantities in (77) and (78) for the triaxial satellite in Fig. 2, when the initial angular velocity is modified to increase the initial value of  $\mu$ . Here, the effects of both environmental perturbing torques and accelerations are considered.

evolution of the motion of Low Earth Orbits. Finally, for the sake of completeness, it would also be interesting to treat the rare case of axisymmetric satellites with equal the principal moments of inertia.

### CRedit authorship contribution statement

**I. Cavallari:** Writing – review & editing, Writing – original draft, Methodology, Formal analysis, Data curation, Conceptualization. **J. Feng:** Writing – review & editing, Supervision, Methodology, Conceptualization. **M. Vasile:** Writing – review & editing, Validation, Supervision, Methodology, Funding acquisition, Conceptualization.

### Declaration of competing interest

The authors declare the following financial interests/personal relationships which may be considered as potential competing interests: Irene Cavallari reports financial support was provided by European Space Agency, Grant T811-702SD. Jinglang Feng reports financial support was provided by European Space Agency, Grant T811-702SD. Massimiliano Vasile reports financial support was provided by European Space Agency, Grant T811-702SD. If there are other authors, they declare that they have no known competing financial interests or personal relationships that could have appeared to influence the work reported in this paper.



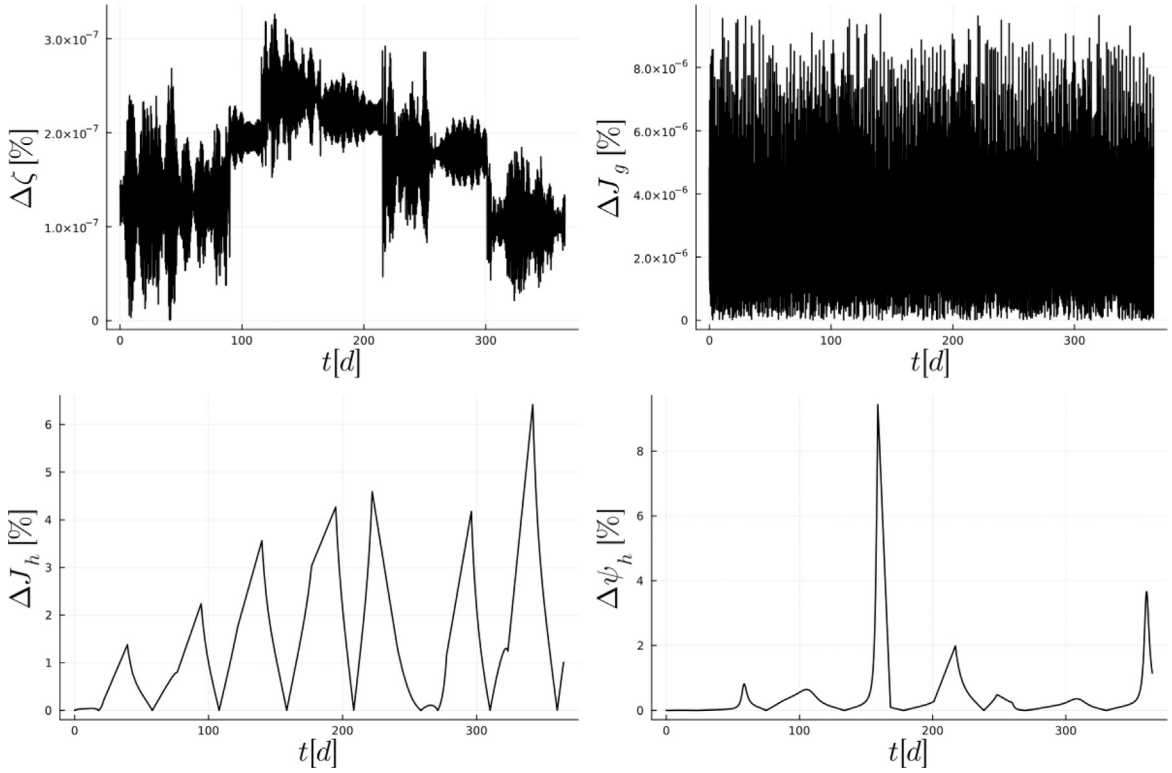


Fig. 11. Evolution of the errors (73)–(76) for the triaxial satellite in Fig. 2, when the initial semi-major axis is reduced. Here, the effects of both environmental perturbing torques and accelerations are considered.

**Acknowledgements**

This work was supported through the ESA Contract No. 4000138557/22/D/SR, ITT Semi-Analytic Attitude Propagation Theory - T811-702SD. The authors also acknowledge Ewan Smith, Simão Da Graça Marto and Thomas McIlwraith for their precious help and collaboration in the project, and Professor Antonio Elife for having kindly supplied enlightening material useful for the work. We would like to thank also the technical officers at the European Space Operations Centre, Jan Siminski and Matteo Losacco for their feedback.

**Appendix A. From the attitude dynamics in the Andoyer–Serret variables to the attitude dynamics in the *s* variables**

Setting  $\mathbf{a} = (L, G, H, l, g, h)$ , the attitude equations of motion expressed in the Andoyer–Serret variables are

$$\frac{d\mathbf{a}}{dt} = \begin{bmatrix} 0 & -\mathbf{I} \\ \mathbf{I} & 0 \end{bmatrix} \nabla_{\mathbf{a}} (\mathcal{H} + \tilde{\mathcal{V}}) + \mathbf{C}\mathbf{M}, \tag{88}$$

where  $\nabla_{\mathbf{a}}$  is the gradient operator,  $\mathbf{I}$  is the  $3 \times 3$  identity matrix,  $\mathcal{H}$  is the Hamiltonian in (2),  $\tilde{\mathcal{V}}$  is the potential energy of the total conservative external torque,  $\mathbf{M}$  is the total non-conservative torque, and

$$\mathbf{C} = \begin{bmatrix} 0 & 0 & 1 \\ \cos \tilde{\delta} \tilde{b}_{13} + \sin \tilde{\delta} \tilde{b}_{12} & \cos \tilde{\delta} \tilde{b}_{23} + \sin \tilde{\delta} \tilde{b}_{22} & \cos \tilde{\delta} \tilde{b}_{33} + \sin \tilde{\delta} \tilde{b}_{32} \\ \frac{\cos l}{G \sin \sigma} & -\frac{\sin l}{G \sin \sigma} & 0 \\ -\frac{\cos \sigma \cos l}{G \sin \sigma} - \frac{\cos \tilde{\delta} \tilde{b}_{11}}{G \sin \tilde{\delta}} & \frac{\cos \sigma \sin l}{G \sin \sigma} - \frac{\cos \tilde{\delta} \tilde{b}_{21}}{G \sin \tilde{\delta}} & -\frac{\cos \tilde{\delta} \tilde{b}_{31}}{G \sin \tilde{\delta}} \\ \frac{\tilde{b}_{11}}{G \sin \tilde{\delta}} & \frac{\tilde{b}_{21}}{G \sin \tilde{\delta}} & \frac{\tilde{b}_{31}}{G \sin \tilde{\delta}} \end{bmatrix},$$

where

$$\cos \sigma = \frac{L}{G}, \quad \cos \tilde{\delta} = \frac{H}{G},$$

and

$$\begin{aligned} \tilde{b}_{11} &= \cos g \cos l - \sin g \sin l \cos \sigma, \\ \tilde{b}_{12} &= \sin g \cos l + \cos g \sin l \cos \sigma, \end{aligned}$$

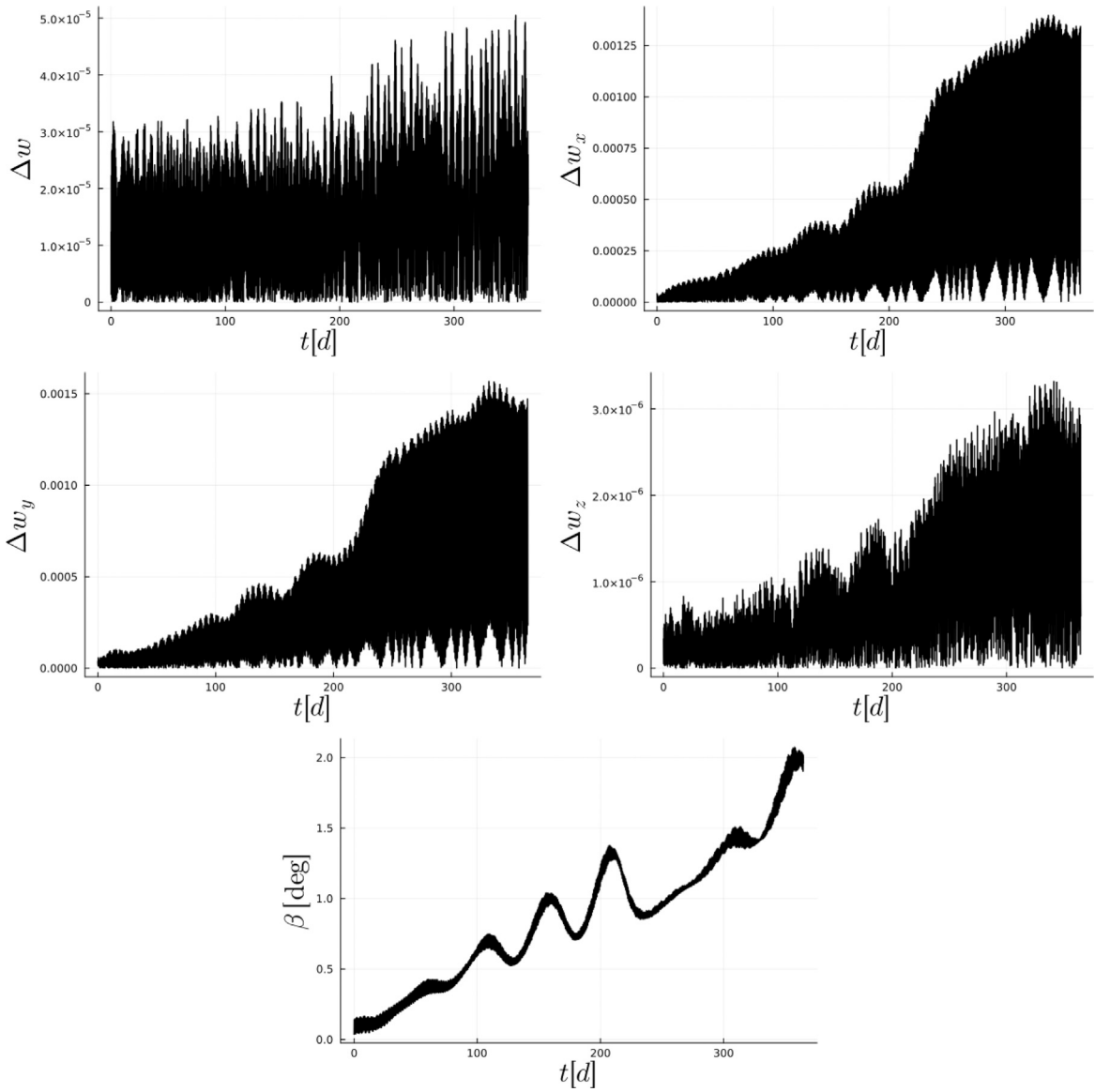


Fig. 12. Evolution of the errors defined in (77) and (78) for the triaxial satellite in Fig. 2, when the initial semi-major axis is reduced. Here, the effects of both environmental perturbing torques and accelerations are considered.

$$\begin{aligned}
 \tilde{b}_{13} &= \sin \sigma \sin l, \\
 \tilde{b}_{21} &= -\cos g \sin l - \sin g \cos l \cos \sigma, \\
 \tilde{b}_{22} &= -\sin g \sin l + \cos g \cos l \cos \sigma, \\
 \tilde{b}_{23} &= \sin \sigma \cos l, \\
 \tilde{b}_{31} &= \sin g \sin \sigma, \\
 \tilde{b}_{32} &= -\cos g \sin \sigma, \\
 \tilde{b}_{33} &= \cos \sigma.
 \end{aligned}$$

(see [32]).

If the problem was conservative, i.e. the contribution of the total non-conservative torque  $\mathbf{M}$  was not present, computing the equations of motion in the  $s$  variables is straightforward, as one can exploit the canonical nature of the transformation from the Andoyer–Serret variables to the Sadov variables, described in Section 2.2. Setting  $s_V = (J_l, J_g, J_h, \psi_l, \psi_g)$ , and considering the canonical transformation

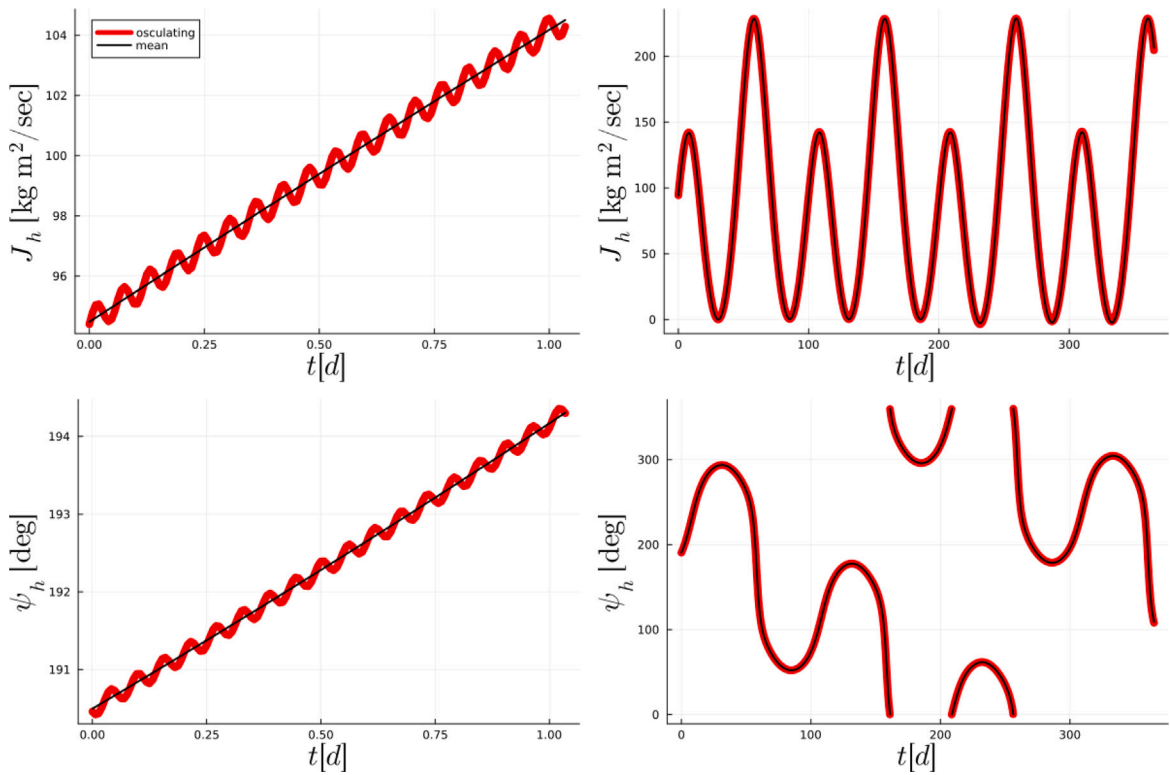


Fig. 13. One-day and One-year evolutions of the mean  $\bar{J}_h$  and  $\bar{\psi}_h$ , computed through the semi-analytical propagation, and of the osculating  $J_h$  and  $\psi_h$ . Here, we consider the triaxial satellite in Fig. 2, when the initial semi-major axis is reduced. The dynamics is affected by environmental perturbing torques and accelerations.

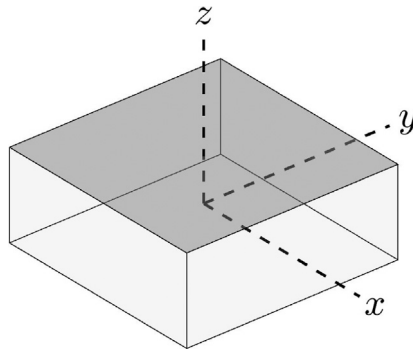


Fig. 14. Fictitious axisymmetric satellite employed in the test cases.

$$\Psi : s_V \mapsto \mathbf{a},$$

which is the inverse transformation of (19), we have

$$\frac{ds_V}{dt} = \begin{bmatrix} 0 & \mathbf{I} \\ -\mathbf{I} & 0 \end{bmatrix} \nabla_{s_V} (\Phi + \mathcal{V}),$$

where

$$\begin{aligned} \mathcal{V} &= \tilde{\mathcal{V}}(\Psi(s_V)) \\ \Phi &= \mathcal{H}(\Psi(s_V)), \end{aligned}$$

with  $\Phi$  given in (8). From Eqs. (18), (16), (17), it follows that

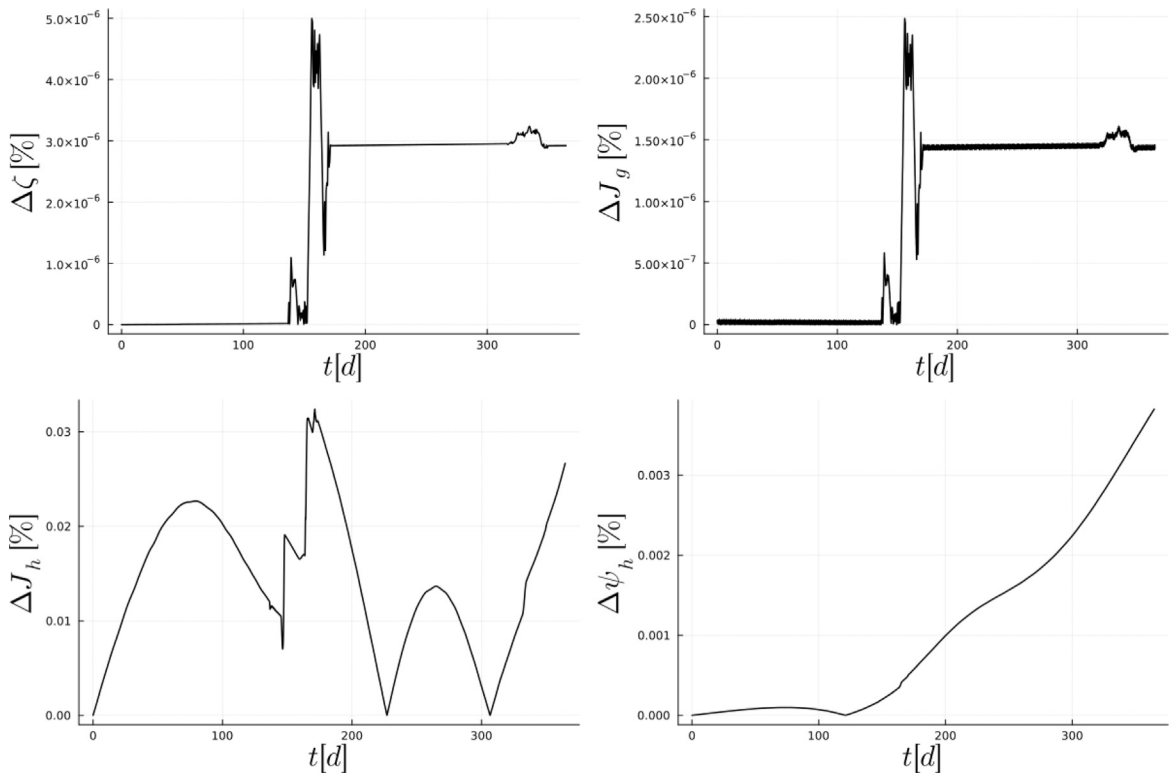


Fig. 15. Evolution of the errors (73)–(76) for the axisymmetric satellite in Fig. 14 with initial conditions (79), (83). Here, the effects of both environmental perturbing torques and accelerations are considered.

$$\frac{\partial \zeta}{\partial J_l} = -\frac{\zeta^2}{\kappa} \frac{d\mu}{dJ_l} = \frac{\pi}{J_g} \frac{\zeta^{\frac{1}{2}}}{\sqrt{1+\kappa}} \frac{1}{K(\mu)}, \quad \frac{\partial \zeta}{\partial J_g} = -\frac{\zeta^2}{\kappa} \frac{dm}{dJ_g} = -\frac{2(\Pi(-\kappa, \mu) - (1-\zeta)K(\mu))}{J_g K(\mu)}.$$

Thus, using the chain rule, we have

$$\frac{d\zeta}{dt} = \frac{\partial \zeta}{\partial J_l} \frac{dJ_l}{dt} + \frac{\partial \zeta}{\partial J_g} \frac{dJ_g}{dt}.$$

Furthermore,

$$\nabla_{s_V}(\cdot) = \begin{bmatrix} \frac{\partial \zeta}{\partial J_l} & 0 & 0 & 0 & 0 & 0 \\ \frac{\partial \zeta}{\partial J_g} & 1 & 0 & 0 & 0 & 0 \\ 0 & 0 & 1 & 0 & 0 & 0 \\ 0 & 0 & 0 & 1 & 0 & 0 \\ 0 & 0 & 0 & 0 & 1 & 0 \\ 0 & 0 & 0 & 0 & 0 & 1 \end{bmatrix} \nabla_s(\cdot)$$

Then,

$$\frac{ds}{dt} = \begin{bmatrix} \frac{\partial \zeta}{\partial J_l} & \frac{\partial \zeta}{\partial J_g} & 0 & 0 & 0 & 0 \\ 0 & 1 & 0 & 0 & 0 & 0 \\ 0 & 0 & 1 & 0 & 0 & 0 \\ 0 & 0 & 0 & 1 & 0 & 0 \\ 0 & 0 & 0 & 0 & 1 & 0 \\ 0 & 0 & 0 & 0 & 0 & 1 \end{bmatrix} \begin{bmatrix} 0 & -\mathbf{I} \\ \mathbf{I} & 0 \end{bmatrix} \begin{bmatrix} \frac{\partial \zeta}{\partial J_l} & 0 & 0 & 0 & 0 & 0 \\ \frac{\partial \zeta}{\partial J_g} & 1 & 0 & 0 & 0 & 0 \\ 0 & 0 & 1 & 0 & 0 & 0 \\ 0 & 0 & 0 & 1 & 0 & 0 \\ 0 & 0 & 0 & 0 & 1 & 0 \\ 0 & 0 & 0 & 0 & 0 & 1 \end{bmatrix} \nabla_s(\Phi + \mathcal{V}) = \mathbf{A} \nabla_s(\Phi + \mathcal{V}),$$

with  $\mathbf{A}$  in (37).

Now, consider the non-conservative contribution in the equations of motion (88), i.e.,

$$\left[ \frac{da}{dt} \right]_{\text{NC}} = \mathbf{C} \mathbf{M}.$$

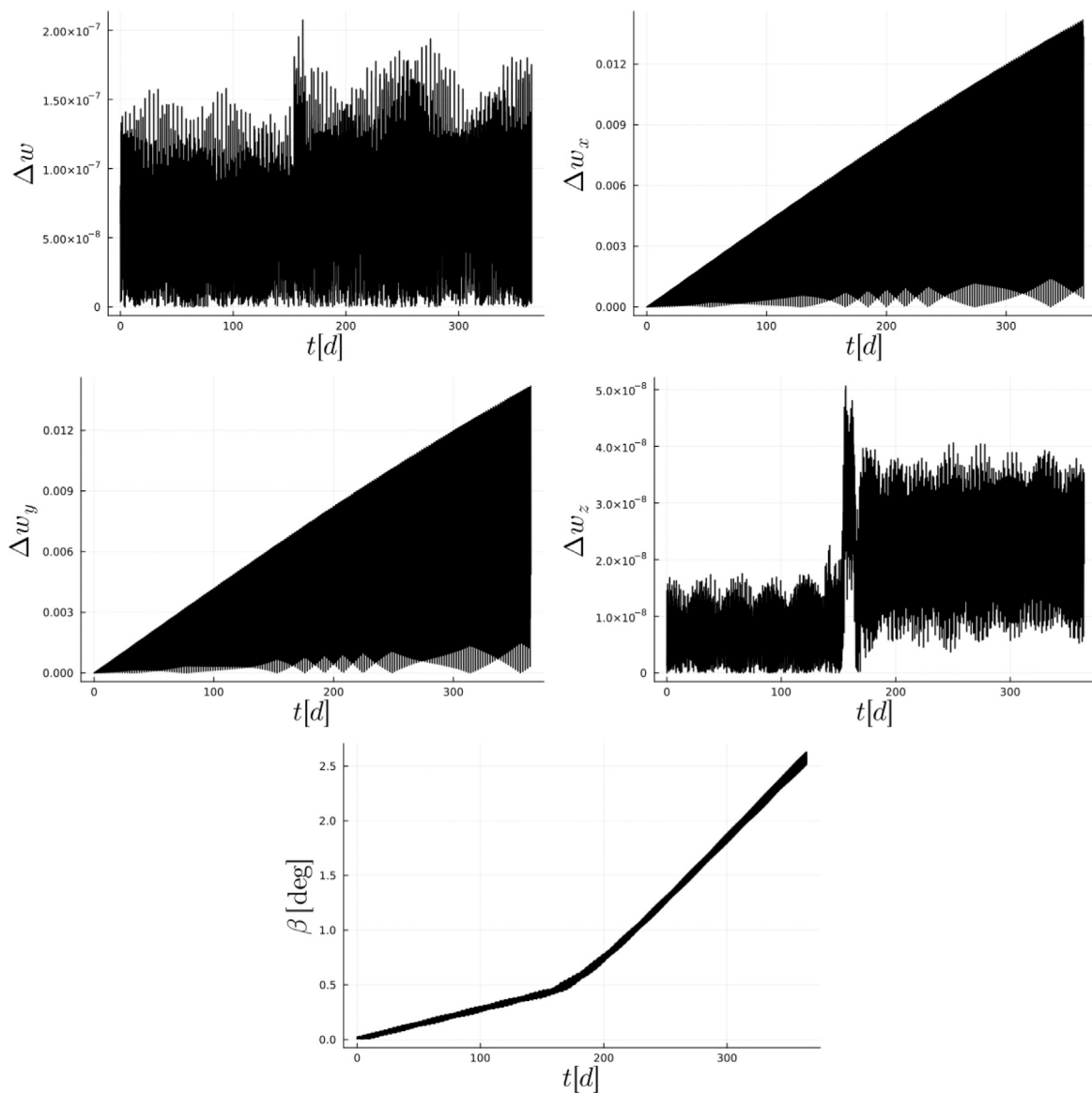


Fig. 16. Evolution of the errors defined in (77) and (78) for the axisymmetric satellite in Fig. 14 with initial conditions (79), (83). Here, the effects of both environmental perturbing torques and accelerations are considered.

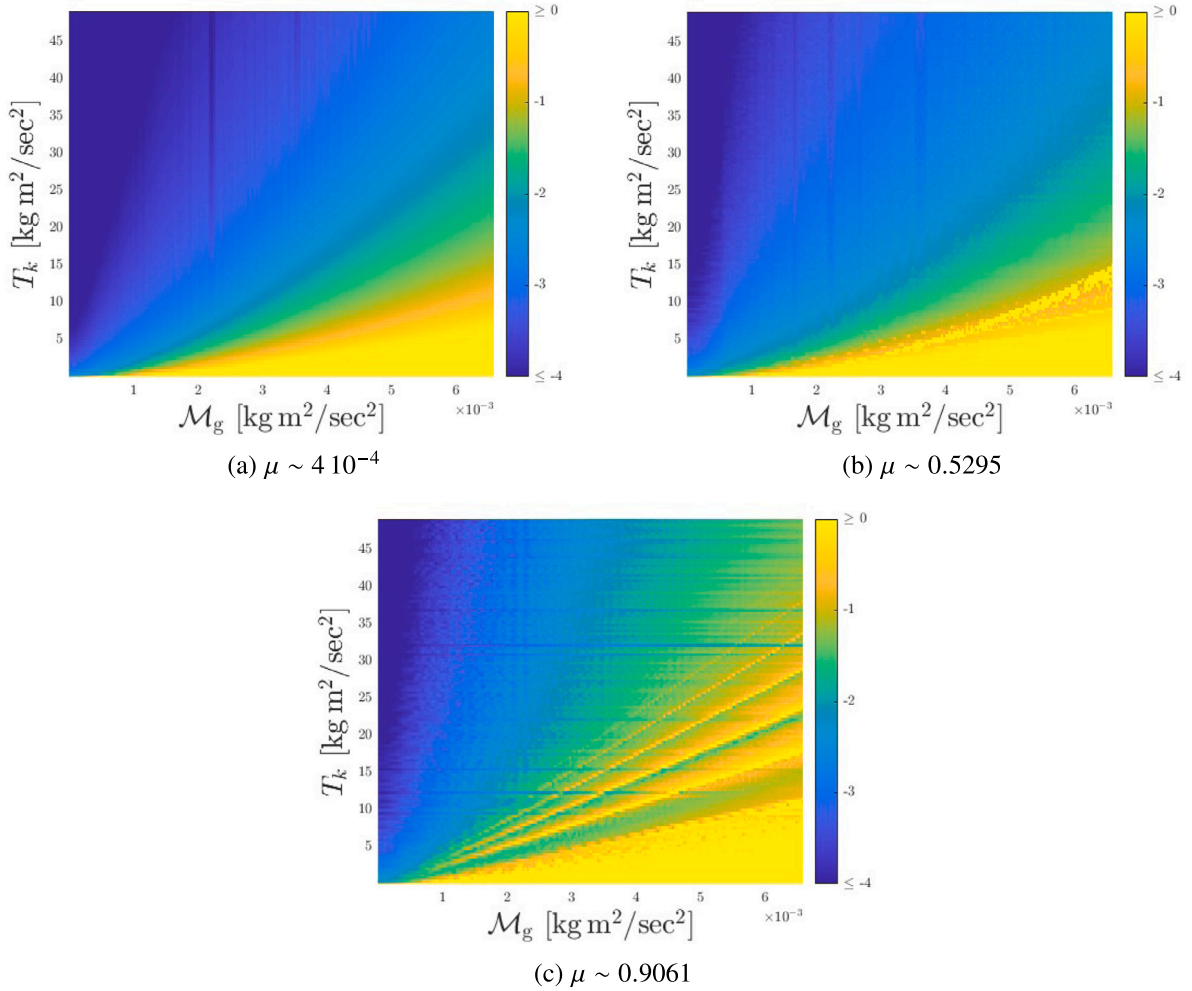


Fig. 17. Accuracy maps of the semi-analytical propagation for the gravity-gradient torque perturbation. The quantity defined in (84) is represented with a colour code on the  $(\mathcal{M}_g, T_k)$  plane for a fixed value of  $\mu$ , with  $\mathcal{M}_g$  given in (85) and  $T_k$  the satellite's kinetic energy.

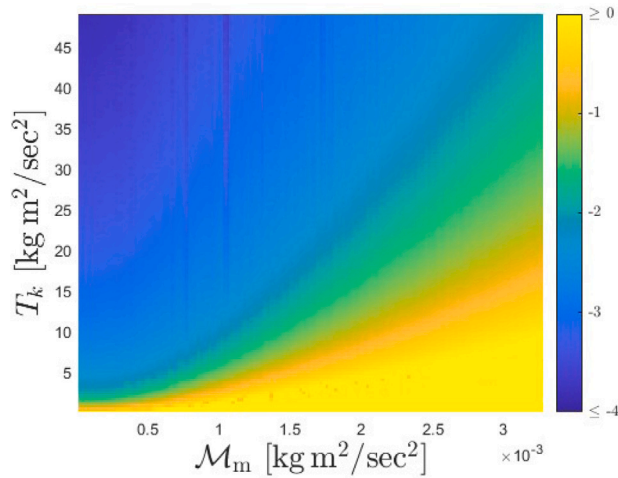


Fig. 18. Accuracy map of the semi-analytical propagation for the residual magnetic torque perturbation. The error defined in (84) is represented with a colour code on the  $(\mathcal{M}_m, T_k)$  plane for a fixed value of  $\mu$ ,  $\mu \sim 4 \cdot 10^{-4}$ , with  $\mathcal{M}_m$  given in (86) and  $T_k$  the satellite's kinetic energy.

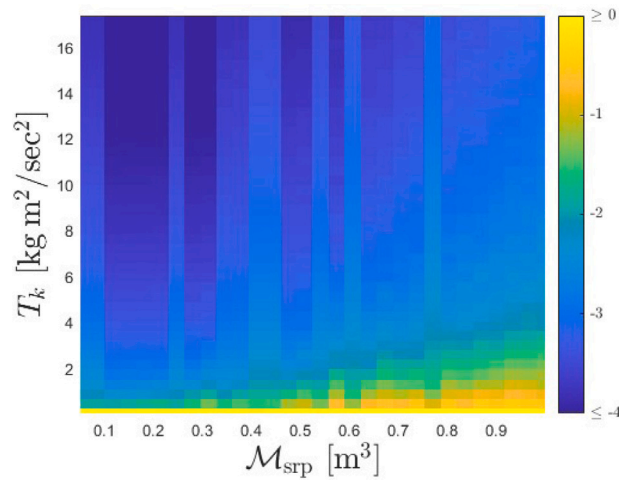


Fig. 19. Accuracy map of the semi-analytical propagation for the light pressure torque perturbation. The error defined in (84) is represented with a colour code on the  $(\mathcal{M}_{\text{srp}}, T_k)$  plane for a fixed value of  $\mu$ ,  $\mu \sim 4 \cdot 10^{-4}$ , with  $\mathcal{M}_{\text{srp}}$  given in (87) and  $T_k$  the satellite's kinetic energy.

Given the transformation (19) and using the chain rule, it is possible to determine the non-conservative contribution to the time derivatives of the  $s$  variables. Consider the transformation

$$\Psi^{-1} : \mathbf{a} \mapsto s_V.$$

The quantity  $\mu$  in (6) expressed in terms of the Andoyer–Serret variables is

$$\tilde{\mu} = \mu(\Psi^{-1}(\mathbf{a})) = \frac{(-AC(\cos^2(l)) + B(-C(\sin^2(l)) + A))C(A - B)(G + L)(G - L)}{A(-C + B)((G^2 - L^2)A - BG^2)C(\cos^2(l)) + BL^2(-C(\sin^2(l)) + A)}.$$

It follows that

$$\frac{d\tilde{\mu}}{dt} = \frac{\partial \tilde{\mu}}{\partial l} \frac{dl}{dt} + \frac{\partial \tilde{\mu}}{\partial L} \frac{dL}{dt} + \frac{\partial \tilde{\mu}}{\partial G} \frac{dG}{dt}.$$

Doing some algebra and considering only the non-conservative contribution of the time derivatives, we obtain

$$\left[ \frac{d\tilde{\mu}}{dt} \right]_{\text{NC}} = \frac{2\tilde{b}_{13}(\tilde{\mu} + \kappa)}{G} M_x + \frac{2\tilde{b}_{23}(1 - \tilde{\mu})(\tilde{\mu} + \kappa)}{G(1 + \kappa)} M_y - \frac{2\tilde{\mu}\tilde{b}_{33}(\tilde{\mu} + \kappa)}{G\kappa},$$

with  $(M_x, M_y, M_z)$  the components of  $\mathbf{M}$ . Applying the transformation

$$\tilde{\Psi} : \mathbf{a} \mapsto s,$$

and, in particular, using Eqs. (19) and (21), one obtains that  $G(\tilde{\Psi}(\mathbf{a})) = J_g$  and  $\tilde{b}_{ij}(\tilde{\Psi}(\mathbf{a})) = b_{ij}$  for each  $i, j \in [1, 3]$ , with  $b_{ij}$  in (25)–(33). Thus,

$$\left[ \frac{d\tilde{\mu}}{dt} \right]_{\text{NC}} = \frac{2b_{13}(\mu + \kappa)}{J_g} M_x + \frac{2b_{23}(1 - \mu)(\mu + \kappa)}{J_g(1 + \kappa)} M_y - \frac{2\mu b_{33}(\mu + \kappa)}{J_g\kappa}.$$

From (18), it follows

$$\left[ \frac{d\zeta}{dt} \right]_{\text{NC}} = \frac{\partial \zeta}{\partial \mu} \left[ \frac{d\tilde{\mu}}{dt} \right]_{\text{NC}} = -\frac{k}{(k + \mu)^2} \left[ \frac{d\tilde{\mu}}{dt} \right]_{\text{NC}} = -\frac{2b_{13}\zeta}{J_g} M_x - \frac{2b_{23}(1 - \mu)\zeta}{J_g(1 + \kappa)} M_y + \frac{2b_{33}(1 - \zeta)}{J_g}.$$

The time derivative of  $\psi_l$  can be obtained by considering that it depends on  $\tilde{\mu}(L, G, l)$  and  $\lambda(l)$ , with  $\lambda(l)$  defined in (5). In particular, by directly applying the transformation  $\tilde{\Psi}$ ,

$$\frac{\partial \psi_l}{\partial \tilde{\mu}} = \frac{\pi(\text{dn}(u, \mu)\text{zn}(u, \mu) - \mu \text{cn}(u, \mu)\text{sn}(u, \mu))}{4K(\mu)(1 - m)\text{dn}(u, \mu)\mu},$$

$$\frac{\partial \psi_l}{\partial l} = \frac{\pi(\kappa \text{sn}(u, \mu)^2 + 1)}{2\sqrt{1 + \kappa}K(\mu)\text{dn}(u, \mu)},$$

with  $u$  in (20), so that

$$\left[ \frac{d\psi_l}{dt} \right]_{\text{NC}} = \frac{\partial \psi_l}{\partial \tilde{\mu}} \left[ \frac{d\tilde{\mu}}{dt} \right]_{\text{NC}} + \frac{\partial \psi_l}{\partial l} \left[ \frac{dl}{dt}(\tilde{\Psi}(s)) \right]_{\text{NC}}.$$

Performing some algebra, we obtain

$$\left[ \frac{d\psi_l}{dt} \right]_{\text{NC}} = -\frac{\pi (\text{dn}(u, \mu)\text{sn}(u, \mu) - \text{cn}(u, \mu)\text{zn}(u, \mu))}{2(1 - \mu)J_g \sqrt{1 - \zeta} K(\mu)} M_x - \frac{\pi (\text{cn}(u, \mu)\text{dn}(u, \mu) + \text{sn}(u, \mu)\text{zn}(u, \mu))}{2K(\mu)\sqrt{1 + \kappa}\sqrt{1 - \zeta} J_g} M_y - \frac{\pi (\text{dn}(u, \mu)\text{zn}(u, \mu) - \mu \text{cn}(u, \mu)\text{sn}(u, \mu))}{2J_g \sqrt{\zeta} K(\mu)(1 - \mu)} M_z.$$

Similarly,  $\psi_g$  can be seen as a function of  $\tilde{\mu}(L, G, l)$ ,  $\lambda(l)$ , and  $g$ :

$$\frac{\partial \psi_g}{\partial \tilde{\mu}} = \frac{(\text{dn}(u, \mu)\text{zn}(u, \mu) - \mu \text{cn}(u, \mu)\text{sn}(u, \mu)) \mathcal{T} J_g}{2 \text{dn}(u, \mu)(1 - \mu)},$$

$$\frac{\partial \psi_g}{\partial l} = \frac{\text{dn}k \left( \frac{1}{\text{dn}k} - \frac{J_g \mathcal{T} \sqrt{\zeta}}{1 + \kappa} - (1 - \zeta) \right)}{\sqrt{\zeta} \text{dn}(u, \mu)}$$

$$\frac{\partial \psi_g}{\partial g} = 1,$$

with  $\mathcal{T}$  in (39). Then,

$$\left[ \frac{d\psi_g}{dt} \right]_{\text{NC}} = \frac{\partial \psi_g}{\partial \tilde{\mu}} \left[ \frac{d\tilde{\mu}}{dt} \right]_{\text{NC}} + \frac{\partial \psi_g}{\partial l} \left[ \frac{dl}{dt} (\tilde{\Psi}(s)) \right]_{\text{NC}} + \frac{\partial \psi_g}{\partial g} \left[ \frac{dg}{dt} (\tilde{\Psi}(s)) \right]_{\text{NC}},$$

i.e., after performing some algebra,

$$\begin{aligned} \left[ \frac{d\psi_g}{dt} \right]_{\text{NC}} &= \left( \frac{\mathcal{T} (\text{dn}(u, \mu)\text{sn}(u, \mu) - \text{cn}(u, \mu)\text{zn}(u, \mu))}{(1 - \mu)\sqrt{1 - \zeta}} - \frac{\cos(\delta)b_{11}}{J_g \sin(\delta)} \right) M_x \\ &+ \left( \frac{\mathcal{T} (\text{cn}(u, \mu)\text{dn}(u, \mu) + \text{sn}(u, \mu)\text{zn}(u, \mu))}{\sqrt{1 + \kappa}\sqrt{1 - \zeta}} - \frac{\cos(\delta)b_{21}}{J_g \sin(\delta)} \right) M_y \\ &+ \left( \frac{\mathcal{T} (\text{dn}(u, \mu)\text{zn}(u, \mu) - \mu \text{cn}(u, \mu)\text{sn}(u, \mu))}{\sqrt{\zeta}(1 - \mu)} - \frac{\cos(\delta)b_{31}}{J_g \sin(\delta)} \right) M_z, \end{aligned}$$

with  $\cos \delta = \cos \tilde{\delta}(\tilde{\Psi}(s)) = \frac{J_h}{J_g}$ . Concerning  $J_g, J_h, \psi_h$ , we have

$$\frac{\partial J_g}{\partial G} = 1, \quad \frac{\partial J_h}{\partial H} = 1, \quad \frac{\partial \psi_h}{\partial h} = 1,$$

so that

$$\left[ \frac{dJ_g}{dt} \right]_{\text{NC}} = \left[ \frac{dG}{dt} (\tilde{\Psi}(s)) \right]_{\text{NC}}, \quad \left[ \frac{dJ_h}{dt} \right]_{\text{NC}} = \left[ \frac{dH}{dt} (\tilde{\Psi}(s)) \right]_{\text{NC}}, \quad \left[ \frac{d\psi_h}{dt} \right]_{\text{NC}} = \left[ \frac{dh}{dt} (\tilde{\Psi}(s)) \right]_{\text{NC}},$$

i.e.

$$\left[ \frac{dJ_g}{dt} \right]_{\text{NC}} = b_{13} M_x + b_{23} M_y + b_{33} M_z,$$

$$\left[ \frac{dJ_h}{dt} \right]_{\text{NC}} = (\cos \delta b_{13} + \sin \delta b_{12}) M_x + (\cos \delta b_{23} + \sin \delta b_{22}) M_y + (\cos \delta b_{33} + \sin \delta b_{32}) M_z,$$

$$\left[ \frac{d\psi_h}{dt} \right]_{\text{NC}} = -\frac{b_{11}}{J_g \sin(\delta)} M_x - \frac{b_{21}}{J_g \sin(\delta)} M_y - \frac{b_{31}}{J_g \sin(\delta)} M_z.$$

### Appendix B. Proof of Proposition 1

Consider the term  $f_a$  given in (59). Its average over  $\psi_g$  is equal to

$$\begin{aligned} \langle f_a \rangle_{\psi_g} &= \frac{1}{2\pi} \mathcal{F}_a(\zeta) \text{dn}^o(u, \mu) \text{sn}^s(u, \mu) \text{cn}^k(u, \mu) \text{dn}k^{\frac{p_i+p_j}{2}} \text{zn}^w(u, \mu) \mathcal{I}, \\ \mathcal{I} &= \int_0^{2\pi} \sin^i(\psi_g + \delta g) \cos^j(\psi_g + \delta g) d\psi_g. \end{aligned}$$

Consider the integral  $\mathcal{I}$ . By the variable change  $g = \psi_g + \delta g$ , we obtain

$$\mathcal{I} = \int_{\delta g}^{\delta g + 2\pi} \sin^i g \cos^j g dg.$$

$\mathcal{I}$  can be written as the sum of two integrals, i.e.

$$\mathcal{I} = \int_{\delta g}^{\delta g + \pi} \sin^i g \cos^j g dg + \int_{\delta g + \pi}^{\delta g + 2\pi} \sin^i g \cos^j g dg.$$



Setting  $g = \tilde{g} + \pi$ , the periodicity of the trigonometric functions implies

$$\int_{\delta g + \pi}^{\delta g + 2\pi} \sin^i g \cos^j g dg = (-1)^{i+j} \int_{\delta g}^{\delta g + \pi} \sin^i \tilde{g} \cos^j \tilde{g} d\tilde{g}.$$

Thus, if  $i$  is odd and  $j$  is even or vice versa, it follows

$$I = \int_{\delta g}^{\delta g + \pi} \sin^i g \cos^j g dg - \int_{\delta g}^{\delta g + \pi} \sin^i \tilde{g} \cos^j \tilde{g} d\tilde{g} = 0.$$

Instead, if both  $i$  and  $j$  are odd,  $I$  can be written as

$$I = 2 \int_{\delta g}^{\delta g + \pi} \sin^i g \cos^j g dg. \tag{89}$$

Similarly as before,  $I$  in (89) can be expressed as the sum of two integrals

$$I = 2 \int_{\delta g}^{\delta g + \frac{\pi}{2}} \sin^i g \cos^j g dg + 2 \int_{\delta g + \frac{\pi}{2}}^{\delta g + \pi} \sin^i g \cos^j g dg.$$

Performing the variable change  $\hat{g} = g - \frac{\pi}{2}$  in the second integral, we get

$$2 \int_{\delta g + \frac{\pi}{2}}^{\delta g + \pi} \sin^i g \cos^j g dg = 2 \int_{\delta g}^{\delta g + \frac{\pi}{2}} (-1)^j \cos^i \hat{g} \sin^j \hat{g} d\hat{g}.$$

Since  $j$  is odd,

$$I = 2 \int_{\delta g}^{\delta g + \frac{\pi}{2}} \sin^i g \cos^j g dg - 2 \int_{\delta g}^{\delta g + \frac{\pi}{2}} \cos^i \hat{g} \sin^j \hat{g} d\hat{g} = 0.$$

This brings to the conclusion that if either  $i$  or  $j$  are odd,  $\langle f_a \rangle_{\psi_g} = 0$ .

Now, suppose that  $i$  and  $j$  are both even. Since  $i = 2\tilde{i}$ , with  $\tilde{i} \in \mathbb{N}$ ,

$$I = \int_{\delta g}^{\delta g + 2\pi} \sin^{2\tilde{i}} g \cos^j g dg = \int_{\delta g}^{\delta g + 2\pi} (1 - \cos^2 g)^{\tilde{i}} \cos^j g dg.$$

By the binomial theorem [see33, Section 1.2], it follows

$$I = \sum_{d=0}^{\tilde{i}} \binom{\tilde{i}}{d} (-1)^d \int_{\delta g}^{\delta g + 2\pi} \cos^{2d+j} g dg,$$

where  $2d + j$  is an even number for every  $d$  so that we can write  $2d + j = 2\tilde{j}$ , with  $\tilde{j} \in \mathbb{N}$ . Consider the integral

$$\tilde{I} = \int_{\delta g}^{\delta g + 2\pi} \cos^{2\tilde{j}} g dg.$$

Applying the integration by parts, we get

$$\tilde{I} = \frac{1}{2\tilde{j}} \left( \sin g \cos^{2\tilde{j}-1} g \Big|_{\delta g}^{\delta g + 2\pi} + (2\tilde{j} - 1) \int_{\delta g}^{\delta g + 2\pi} \cos^{2(\tilde{j}-1)} g dg \right).$$

The same procedure can be applied to the integral

$$\int_{\delta g}^{\delta g + 2\pi} \cos^{2(\tilde{j}-1)} g dg.$$

By recursively applying the integration by parts, it follows

$$\tilde{I} = \left[ \frac{\sin g \cos^{2\tilde{j}-1} g}{2\tilde{j}} + \prod_{\nu=0}^{\tilde{j}-1} \frac{2\tilde{j} - 2\nu - 1}{2(\tilde{j} - \nu)} g + \frac{\sin g}{2\tilde{j}} \prod_{q=1}^{\tilde{j}-1} \prod_{\nu=1}^q \frac{2\tilde{j} - 2\nu + 1}{2(\tilde{j} - \nu)} \cos^{2\tilde{j}-1-2q} g \right]_{\delta g}^{\delta g + 2\pi}.$$

Since  $\sin(\delta g + 2\pi) = \sin(\delta g)$  and  $\cos(\delta g + 2\pi) = \cos(\delta g)$ ,

$$\tilde{I} = 2\pi \prod_{\nu=0}^{\tilde{j}-1} \frac{2\tilde{j} - 2\nu - 1}{2(\tilde{j} - \nu)},$$

so that

$$I = 2\pi \sum_{d=0}^{\tilde{i}} \binom{\tilde{i}}{d} (-1)^d \prod_{\nu=0}^{d+\frac{\tilde{i}-1}{2}} \frac{2d + j - 2\nu - 1}{2d + j - 2\nu}.$$

Since  $p_i$  has the same parity as  $i$  and  $p_j$  has the same parity as  $j$ , when  $I$  is different from zero, they are both even numbers, which implies that  $(p_i + p_j)/2$  is an integer number. This concludes the proof of Proposition 1.

### Appendix C. Proof of Proposition 2

Consider the integral

$$\mathcal{J} = \int_0^{4K(\mu)} \text{dn}^o(u, \mu) \text{sn}^s(u, \mu) \text{cn}^k(u, \mu) \text{dn}k^p \text{zn}(u, \mu) \text{du},$$

with  $o, s, k, \in \mathbb{N}$ ,  $p \in \mathbb{Z}$  and  $dnk$  defined in (23). It is possible to write  $\mathcal{J}$  as the sum of two integrals:

$$\mathcal{J} = \mathcal{J}_1 + \mathcal{J}_2,$$

with

$$\mathcal{J}_1 = \int_0^{2K(\mu)} \text{dn}^o(u, \mu) \text{sn}^s(u, \mu) \text{cn}^k(u, \mu) \text{dn}k^p \text{zn}(u, \mu) \text{du}$$

and

$$\mathcal{J}_2 = \int_{2K(\mu)}^{4K(\mu)} \text{dn}^o(u, \mu) \text{sn}^s(u, \mu) \text{cn}^k(u, \mu) \text{dn}k^p \text{zn}(u, \mu) \text{du}.$$

Functions  $\text{dn}(u, \mu)$ , and  $\text{cn}(u, \mu)$  are even and periodic, while  $\text{zn}(u, \mu)$  and  $\text{sn}(u, \mu)$  are odd and periodic. The period of  $\text{dn}(u, \mu)$  and  $\text{zn}(u, \mu)$  is  $2K(\mu)$ , while the period of  $\text{cn}(u, \mu)$  and  $\text{sn}(u, \mu)$  is  $4K(\mu)$  [see34, Sections 120.01, 140.03]. Thus, performing the change of variables  $u = -\tilde{u} + 4K(\mu)$  in  $\mathcal{J}_2$  results in

$$\mathcal{J}_2 = (-1)^{s+1} \int_0^{2K(\mu)} \text{dn}^o(\tilde{u}, \mu) \text{sn}^s(\tilde{u}, \mu) \text{cn}^k(\tilde{u}, \mu) \text{dn}k^p \text{zn}(\tilde{u}, \mu) \text{d}\tilde{u}.$$

It is straightforward that  $\mathcal{J} = 0$  if  $s$  is even. On the contrary, if  $s$  is odd it is possible to write

$$\mathcal{J} = 2(\tilde{\mathcal{J}}_1 + \tilde{\mathcal{J}}_2),$$

with

$$\tilde{\mathcal{J}}_1 = \int_0^{K(\mu)} \text{dn}^o(u, \mu) \text{sn}^s(u, \mu) \text{cn}^k(u, \mu) \text{dn}k^p \text{zn}(u, \mu) \text{du}$$

and

$$\tilde{\mathcal{J}}_2 = \int_{K(\mu)}^{2K(\mu)} \text{dn}^o(u, \mu) \text{sn}^s(u, \mu) \text{cn}^k(u, \mu) \text{dn}k^p \text{zn}(u, \mu) \text{du}.$$

Performing the variables change  $u = -\hat{u} + 2K(\mu)$ , and considering that

$$\text{sn}(-\hat{u} + 2K(\mu), \mu) = \text{sn}(\hat{u}, \mu),$$

$$\text{cn}(-\hat{u} + 2K(\mu), \mu) = -\text{cn}(\hat{u}, \mu),$$

(see [34, Sections 122.00, 122.04], it follows

$$\tilde{\mathcal{J}}_2 = (-1)^{k+1} \int_0^{K(\mu)} \text{dn}^o(\hat{u}, \mu) \text{sn}^s(\hat{u}, \mu) \text{cn}^k(\hat{u}, \mu) \text{dn}k^p \text{zn}(\hat{u}, \mu) \text{d}\hat{u}.$$

Thus,  $\mathcal{J} = 0$  if  $k$  is even.

Now, consider the case in which both  $s$  and  $k$  are odd. Set

$$\mathcal{I} = \int \text{dn}^o(u, \mu) \text{sn}^s(u, \mu) \text{cn}^k(u, \mu) \text{dn}k^p \text{du},$$

so that it is possible to write  $\mathcal{J}$  as

$$\mathcal{J} = \int_0^{4K(\mu)} \frac{\text{d}\mathcal{I}}{\text{du}} \text{zn}(u, \mu) \text{du}.$$

Since

$$\frac{\text{dzn}(u, \mu)}{\text{du}} = \text{dn}^2(u, \mu) - \frac{E(\mu)}{K(\mu)},$$

by applying the integration by parts, it follows

$$\begin{aligned} \mathcal{J} &= [\mathcal{I} \text{zn}(u, \mu)]_0^{4K(\mu)} - \int_0^{4K(\mu)} \mathcal{I} \left( \text{dn}^2(u, \mu) - \frac{E(\mu)}{K(\mu)} \right) \text{du} \\ &= - \int_0^{4K(\mu)} \mathcal{I} \left( \text{dn}^2(u, \mu) - \frac{E(\mu)}{K(\mu)} \right) \text{du}, \end{aligned}$$

as  $\text{zn}(0, \mu) = \text{zn}(4K(\mu), \mu) = 0$ . This concludes the proof of Proposition 2.

#### Appendix D. Fourier expansion

Here, we summarise the method described in [2,25] to perform the Fourier expansions of combinations of Jacobi elliptic functions, specifically the Jacobi elliptic sine, the Jacobi elliptic cosine, and the Jacobi elliptic delta amplitude. Unless differently stated, all the relations presented in this section previously appeared and were proven in [2,25]. To apply the method, the Jacobi elliptic functions have to be expressed in terms of the Jacobi theta functions, defined as

$$\vartheta_1(\xi, \kappa) = 2 \sum_{i=0}^{\infty} (-1)^i q^{(i+1/2)^2} \sin((2i+1)\xi),$$

$$\vartheta_2(\xi, \kappa) = 2 \sum_{i=0}^{\infty} q^{(i+1/2)^2} \cos((2i+1)\xi),$$

$$\vartheta_3(\xi, \kappa) = 1 + 2 \sum_{i=1}^{\infty} q^{i^2} \cos(2i\xi),$$

$$\vartheta_0(\xi, \kappa) = 1 + 2 \sum_{i=1}^{\infty} (-1)^i q^{i^2} \cos(2i\xi),$$

where  $q$  is the Jacobi nome, i.e.

$$q = \exp(2i\tau),$$

with  $i$  the imaginary unit and

$$\tau = i \frac{\pi}{2} \frac{K(1-\kappa)}{K(\kappa)},$$

with  $K(\kappa)$  the complete elliptic integral of the first kind. In particular, the relations

$$\operatorname{sn}(v, \kappa) = \frac{1}{\kappa^{1/4}} \frac{\vartheta_1(\xi, \kappa)}{\vartheta_0(\xi, \kappa)}, \tag{90}$$

$$\operatorname{cn}(v, \kappa) = \frac{(1-\kappa)^{1/4}}{\kappa^{1/4}} \frac{\vartheta_2(\xi, \kappa)}{\vartheta_0(\xi, \kappa)}, \tag{91}$$

$$\operatorname{dn}(v, \kappa) = (1-\kappa)^{1/4} \frac{\vartheta_3(\xi, \kappa)}{\vartheta_0(\xi, \kappa)}, \tag{92}$$

hold for

$$\xi = \frac{\pi}{2K(\kappa)} v.$$

The method is suitable for computing the Fourier expansions of functions like

$$\mathcal{R}(\xi, \kappa) = \prod_{i,j,k} \frac{\vartheta_i^k(\xi + i j \zeta, \kappa)}{\vartheta_0^k(\xi, \kappa)}, \tag{93}$$

with  $i \in \{1, 2, 3\}$ ,  $j \in \{0, 1, -1\}$ , and  $k \in \mathbb{N}^+$ . The expansion is given by

$$\mathcal{R}(\xi, \kappa) = \sum_{k=-\infty}^{+\infty} A_k \exp\left(\frac{2\pi}{T} i k \xi\right), \tag{94}$$

with  $T$  the period of  $\mathcal{R}(\xi, \kappa)$  and

$$A_k = \frac{1}{T} \int_0^T \mathcal{R}(\xi, \kappa) \exp\left(-\frac{2\pi}{T} i k \xi\right) d\xi. \tag{95}$$

The integral (95) is determined through a technique based on the periodicity of the theta functions and the following two properties of  $\mathcal{R}(\xi, \kappa)$ :

1. since  $\vartheta_1$  and  $\vartheta_2$  have period  $2\pi$ , and  $\vartheta_3$  and  $\vartheta_0$  have period  $\pi$ ,  $\mathcal{R}(\xi, \kappa)$  has either  $T = \pi$  or  $T = 2\pi$ ;
2. since  $\mathcal{R}(\xi, \kappa)$  possesses an exponentiation with base  $\theta_0(\xi, \kappa)$  at the denominator, it has complex poles  $j\pi + (2i+1)\tau$ , with  $i, j$  integers.

The technique consists of two main steps:

- (1) the computation of the quadrature

$$A_k = \oint_{\Gamma} \mathcal{R}(\xi, \kappa) \exp\left(-\frac{2\pi}{T} i k \xi\right) d\xi, \tag{96}$$

where  $\Gamma = \text{ABCD}$  is the closed path in the complex field with

$$\begin{aligned} A = 0, \quad B = \pi, \quad C = \pi + 2\tau, \quad D = 2\tau, \quad & \text{if } T = \pi, \\ A = 0, \quad B = \pi, \quad C = 2\pi + 2\tau, \quad D = 2\tau, \quad & \text{if } T = 2\pi. \end{aligned}$$

- (2) the computation of (95) as

$$A_k = \frac{1}{T} \frac{A_k}{1 - Q(q)q^{-\frac{2\pi}{T}k}},$$

where

$$Q(q) = \frac{\mathcal{R}(\xi + 2\tau, \kappa)}{\mathcal{R}(\xi, \kappa)}. \tag{97}$$

The quadrature  $\mathcal{A}_k$  in (96) is determined by applying Cauchy's theorem, for which

$$\mathcal{A}_k = 2\pi i \sum \text{res}$$

where res are the residues of the integrand  $\mathcal{R}(\xi, \kappa) \exp(-2\pi i k \xi / T)$  at its poles inside the closed path  $\Gamma$ . We have

$$\sum \text{res} = \begin{cases} \text{res}|_{\xi=\tau} & \text{if } T = \pi, \\ \text{res}|_{\xi=\tau} + \text{res}|_{\xi=\pi+\tau} & \text{if } T = 2\pi. \end{cases}$$

Expressing

$$\mathcal{R}(\xi, \kappa) \exp\left(-\frac{2\pi}{T} i k \xi\right) = \frac{F}{G^p},$$

with  $p \in \mathbb{N}^+$  the exponent of  $\theta_0(\xi, \kappa)$  at the denominator of  $\mathcal{R}(\xi, \kappa)$ , Abad et al. [25] gives the recurrent formula to determine the expression of the residue, obtained by applying L'Hôpital's rule:

$$\begin{aligned} \text{res}\left(\frac{F}{G^o}\right) &= \frac{1}{(o-1)G'} \left( \text{res}\left(\frac{F}{G^{o-1}}\right) \right)', \quad o > 1, \\ \text{res}\left(\frac{F}{G}\right) &= \frac{F}{G'}, \end{aligned} \tag{98}$$

where the subscript ' is here used to represent the derivative with respect to  $\xi$ . In particular, to compute the derivatives in (98), consider that

$$\begin{aligned} \theta_1'(\xi, \kappa) &= \frac{2K(\kappa)}{\pi\theta_0(\xi, \kappa)} \left( \theta_1(\xi, \kappa)\theta_0(\xi, \kappa)\text{zn}(v, \kappa) + \sqrt{1-\kappa} \theta_2(\xi, \kappa)\theta_3(\xi, \kappa) \right), \\ \theta_2'(\xi, \kappa) &= \frac{2K(\kappa)}{\pi\theta_0(\xi, \kappa)} \left( \theta_2(\xi, \kappa)\theta_0(\xi, \kappa)\text{zn}(v, \kappa) - \theta_1(\xi, \kappa)\theta_3(\xi, \kappa) \right), \\ \theta_3'(\xi, \kappa) &= \frac{2K(\kappa)}{\pi\theta_0(\xi, \kappa)} \left( \theta_3(\xi, \kappa)\theta_0(\xi, \kappa)\text{zn}(v, \kappa) - \sqrt{\kappa} \theta_1(\xi, \kappa)\theta_2(\xi, \kappa) \right), \\ \theta_0'(\xi, \kappa) &= \frac{2K(\kappa)}{\pi} \text{zn}(v, \kappa) \theta_0(\xi, \kappa), \end{aligned}$$

with  $v = 2K(\kappa)\xi/\pi$ . To evaluate the residues at the poles  $\xi = \tau$  and  $\xi = \pi + \tau$ , the following relations are useful:

$$\begin{aligned} \theta_1(\xi + \tau + ij\zeta, \kappa) &= i q^{-\frac{1}{4}} \exp(j\sigma) \exp(-i\xi) \theta_0(\xi + ij\zeta, \kappa), \\ \theta_2(\xi + \tau + ij\zeta, \kappa) &= q^{-\frac{1}{4}} \exp(j\sigma) \exp(-i\xi) \theta_3(\xi + ij\zeta, \kappa), \\ \theta_3(\xi + \tau + ij\zeta, \kappa) &= q^{-\frac{1}{4}} \exp(j\sigma) \exp(-i\xi) \theta_2(\xi + ij\zeta, \kappa), \\ \theta_0(\xi + \tau + ij\zeta, \kappa) &= i q^{-\frac{1}{4}} \exp(j\sigma) \exp(-i\xi) \theta_1(\xi + ij\zeta, \kappa), \\ \text{zn}\left(\frac{2K(\kappa)(\xi + \tau + ij\zeta)}{\pi}, \kappa\right) &= \text{zn}\left(v + i \frac{2K(\kappa)j\zeta}{\pi}, \kappa\right) - \frac{i\pi}{K(\kappa)}, \\ \theta_1(0, \kappa) = \theta_1(\pi, \kappa) &= 0, \\ \theta_2(0, \kappa) = -\theta_2(\pi, \kappa) &= \kappa^{\frac{1}{4}} \sqrt{\frac{2K(\kappa)}{\pi}}, \\ \theta_3(0, \kappa) = \theta_3(\pi, \kappa) &= \sqrt{\frac{2K(\kappa)}{\pi}}, \\ \theta_0(0, \kappa) = \theta_0(\pi, \kappa) &= (1-\kappa)^{\frac{1}{4}} \sqrt{\frac{2K(\kappa)}{\pi}}, \\ \text{zn}(0, \kappa) = \text{zn}(2K(\kappa), \kappa) &= 0, \end{aligned}$$

with  $j \in (0, 1, -1)$  (see Byrd and Friedman [34], Section 141.01; Olver et al. [33], Section 20.2). Instead, the function of the nome  $Q(q)$  in (97) can be determined using the periodicity properties of the theta functions, i.e.

$$\begin{aligned} \theta_1(\xi + 2j\tau) &= \frac{\exp(-2ji\xi)}{q^j} (-1)^j \theta_1(\xi, \kappa), \\ \theta_2(\xi + 2j\tau) &= \frac{\exp(-2ji\xi)}{q^j} \theta_2(\xi, \kappa), \\ \theta_3(\xi + 2j\tau) &= \frac{\exp(-2ji\xi)}{q^j} \theta_3(\xi, \kappa), \\ \theta_0(\xi + 2j\tau) &= \frac{\exp(-2ji\xi)}{q^j} (-1)^j \theta_0(\xi, \kappa), \end{aligned}$$

$j \in \mathbb{Z}$ . Note that the method can be applied to evaluate all the coefficients  $A_0$  of the Fourier expansions (94) if  $Q(q) \neq 1$ . On the contrary, if  $Q(q) = 1$ , the method can be used for all the terms, but  $A_0$ , which has to be classically computed. This can be easily done by re-writing the integrand of  $A_0$  in terms of the Jacobi elliptic functions and employing the support of a symbolic manipulator.

In the problem of interest, it is necessary to compute the Fourier expansions of combinations of the elements  $b_{ij}$  in (25)–(33), potentially multiplied by one of the terms  $(S_x, S_y, S_z)$  in (40)–(42). Vallejo [2] gives the expression of the elements  $b_{ij}$  suitable for applying the method:

$$\begin{aligned}
 b_{11} &= i \frac{B_{11} \exp(i\psi_g) - B_{21} \exp(-i\psi_g)}{2}, \\
 b_{12} &= \frac{B_{11} \exp(i\psi_g) + B_{21} \exp(-i\psi_g)}{2}, \\
 b_{13} &= B_{13}, \\
 b_{21} &= i \frac{B_{12} \exp(i\psi_g) - B_{22} \exp(-i\psi_g)}{2}, \\
 b_{22} &= \frac{B_{12} \exp(i\psi_g) + B_{22} \exp(-i\psi_g)}{2}, \\
 b_{23} &= B_{23}, \\
 b_{31} &= i \frac{B_{13} \exp(i\psi_g) - B_{23} \exp(-i\psi_g)}{2}, \\
 b_{32} &= \frac{B_{13} \exp(i\psi_g) + B_{23} \exp(-i\psi_g)}{2}, \\
 b_{33} &= B_{33},
 \end{aligned}$$

where

$$\begin{aligned}
 B_{11} &= i \sqrt{\frac{2K(\mu)}{\pi(\kappa + \mu)}} \frac{(\mu(1 - \mu))^{\frac{1}{4}}}{\theta_0(i\hat{\zeta}, \mu)} \frac{\theta_1(\psi_l - i\hat{\zeta}, \mu)}{\theta_0(\psi_l, \mu)}, \\
 B_{12} &= i \sqrt{\frac{2K(\mu)}{\pi(\kappa + \mu)}} \frac{(\mu(1 - \mu)^2)^{\frac{1}{4}}}{\theta_0(i\hat{\zeta}, \mu)} \frac{\theta_2(\psi_l - i\hat{\zeta}, \mu)}{\theta_0(\psi_l, \mu)}, \\
 B_{13} &= -\sqrt{\frac{2K(\mu)}{\pi(\kappa + \mu)}} \frac{(\mu^2(1 - \mu))^{\frac{1}{4}}}{\theta_0(i\hat{\zeta}, \mu)} \frac{\theta_0(\psi_l - i\hat{\zeta}, \mu)}{\theta_0(\psi_l, \mu)}, \\
 B_{21} &= -i \sqrt{\frac{2K(\mu)}{\pi(\kappa + \mu)}} \frac{(\mu(1 - \mu))^{\frac{1}{4}}}{\theta_0(i\hat{\zeta}, \mu)} \frac{\theta_1(\psi_l + i\hat{\zeta}, \mu)}{\theta_0(\psi_l, \mu)}, \\
 B_{22} &= -i \sqrt{\frac{2K(\mu)}{\pi(\kappa + \mu)}} \frac{(\mu(1 - \mu)^2)^{\frac{1}{4}}}{\theta_0(i\hat{\zeta}, \mu)} \frac{\theta_2(\psi_l + i\hat{\zeta}, \mu)}{\theta_0(\psi_l, \mu)}, \\
 B_{23} &= -\sqrt{\frac{2K(\mu)}{\pi(\kappa + \mu)}} \frac{(\mu^2(1 - \mu))^{\frac{1}{4}}}{\theta_0(i\hat{\zeta}, \mu)} \frac{\theta_0(\psi_l + i\hat{\zeta}, \mu)}{\theta_0(\psi_l, \mu)}, \\
 B_{31} &= \frac{(\mu(1 - \mu))^{\frac{1}{4}}}{\sqrt{\mu + \kappa}} \frac{\theta_2(\psi_l, \mu)}{\theta_0(\psi_l, \mu)}, \\
 B_{32} &= -\frac{\mu^{\frac{1}{4}} \sqrt{1 + \kappa}}{\sqrt{\mu + \kappa}} \frac{\theta_1(\psi_l, \mu)}{\theta_0(\psi_l, \mu)}, \\
 B_{33} &= (1 - \mu)^{\frac{1}{4}} \sqrt{\frac{\kappa}{\mu + \kappa}} \frac{\theta_3(\psi_l, \mu)}{\theta_0(\psi_l, \mu)},
 \end{aligned}$$

and

$$\hat{\zeta} = \frac{\pi}{2K(\mu)} F \left( \arctan \left( \sqrt{\frac{\kappa}{\mu}} \right), 1 - \mu \right).$$

In particular, to evaluate the coefficients of the Fourier expansions, it is convenient to use the following equations:

$$\begin{aligned}
 \operatorname{sn} \left( i \frac{2K(\mu)\hat{\zeta}}{\pi}, \mu \right) &= i \sqrt{\frac{\kappa}{\mu}}, \\
 \operatorname{cn} \left( i \frac{2K(\mu)\hat{\zeta}}{\pi}, \mu \right) &= \sqrt{\frac{1}{1 - \zeta}}, \\
 \operatorname{dn} \left( i \frac{2K(\mu)\hat{\zeta}}{\pi}, \mu \right) &= \sqrt{1 + \kappa},
 \end{aligned}$$

$$\begin{aligned} \operatorname{zn}\left(\frac{2K(\mu)\zeta}{\pi}, \mu\right) &= -i \frac{\sqrt{1+\kappa}(\Pi(-k, \mu) - K(\mu))}{\sqrt{\zeta}K(\mu)}, \\ \operatorname{cn}\left(\frac{2K(\mu)\zeta}{\pi}, 1-\mu\right) &= \sqrt{1-\zeta}, \\ \operatorname{sn}\left(\frac{2K(\mu)\zeta}{\pi}, 1-\mu\right) &= \sqrt{\zeta}. \end{aligned}$$

The method described in [2,25] can be applied to expand the combinations of Jacobi elliptic sine, cosine and delta amplitude contained in the elements  $S_x, S_y, S_z$ , with  $\kappa = \mu$  and  $\xi = \psi_l$ . However, the same method does not apply to the Jacobi zeta function, therefore, one needs to directly replace it with its own Fourier expansion, i.e.

$$\operatorname{zn}(u, \mu) = \frac{2\pi}{K(\mu)} \sum_{k=1}^{\infty} \frac{q^k}{1-q^{2k}} \sin(2k\psi_l),$$

(see [34, Section 905.01]).

### Appendix E. Attitude equations of motion in Sadov-like non-singular variables

With the variables  $s_I = (\zeta, J_g, J_h, \psi_l, I_5, I_6, I_7)$  introduced in Section 5.3, the equations of motion for the attitude dynamics can be shortly written as

$$\frac{ds_I}{dt} = \mathbf{A}_I \nabla_{s_I} \Phi + \mathbf{A}_I \nabla_{s_I} \mathcal{V} + \mathbf{B}_I \mathbf{M}$$

with  $\Phi$  in (8),  $\mathcal{V}$  the potential energy of a conservative external torque and  $\mathbf{M}$  an external non-conservative torque.  $\mathbf{A}_I$  is an anti-symmetric matrix equal to

$$\mathbf{A}_I = \mathbf{T}_A - \mathbf{T}_A^T,$$

with  $\mathbf{T}_A = (a_{ij})_{i=1\dots7, j=1\dots7}$  an upper triangular matrix whose non-null elements are

$$\begin{aligned} a_{14} &= -\frac{\pi}{J_g} \frac{\zeta^{\frac{1}{2}}}{\sqrt{1+\kappa}} \frac{1}{K(\mu)}, \\ a_{15} &= \frac{2(\Pi(-\kappa, \mu) - (1-\zeta)K(\mu))}{J_g K(\mu)}, \\ a_{25} &= -1, \\ a_{35} &= -\frac{J_h}{J_g}, \\ a_{36} &= I_7, \\ a_{37} &= -I_6, \\ a_{56} &= \frac{I_6 + I_7 \arctan\left(\frac{I_7}{I_6}\right)}{J_g}, \\ a_{57} &= \frac{I_7 - I_6 \arctan\left(\frac{I_7}{I_6}\right)}{J_g}, \\ a_{67} &= J_h. \end{aligned}$$

We recall that  $\mu = (1-\zeta)\kappa/\zeta$  is a function of the variable  $\zeta$  and  $\kappa$  is the constant defined in (7).  $\mathbf{B}_I$  is equal to

$$\mathbf{B}_I = \begin{bmatrix} -\frac{2\zeta}{J_g} b_{13} & -\frac{2\zeta(1-\mu)}{J_g(1+\kappa)} b_{23} & \frac{2(1-\zeta)}{J_g} b_{33} \\ b_{13} & b_{23} & b_{33} \\ \frac{J_h}{J_g} b_{13} + \Delta b_{31} & \frac{J_h}{J_g} b_{23} + \Delta b_{32} & \frac{J_h}{J_g} b_{33} + \Delta b_{33} \\ -\frac{\pi S_x}{2J_g K(\mu)(1-\mu)} & -\frac{\pi S_y}{2J_g K(\mu)} & -\frac{\pi S_z}{2J_g K(\mu)(1-\mu)} \\ \frac{\mathcal{T} S_x}{1-\mu} + \Delta b_{51} & \mathcal{T} S_y + \Delta b_{52} & \frac{\mathcal{T} S_z}{1-\mu} + \Delta b_{53} \\ \frac{I_6}{J_g} b_{13} + \Delta b_{61} & \frac{I_6}{J_g} b_{23} + \Delta b_{62} & \frac{I_6}{J_g} b_{33} + \Delta b_{63} \\ \frac{I_7}{J_g} b_{13} + \Delta b_{71} & \frac{I_7}{J_g} b_{23} + \Delta b_{72} & \frac{I_7}{J_g} b_{33} + \Delta b_{73} \end{bmatrix},$$

with  $b_{13}$  in (27),  $b_{23}$  in (30),  $b_{33}$  in (33), and

$$\Delta b_{31} = -\frac{\sqrt{I_6^2 + I_7^2}}{J_g} \left( K_1 \cos\left(I_5 - \frac{J_h}{J_g} \arctan\left(\frac{I_7}{I_6}\right) + \delta g\right) - K_2 \sin\left(I_5 - \frac{J_h}{J_g} \arctan\left(\frac{I_7}{I_6}\right) + \delta g\right) \right),$$

$$\begin{aligned} \Delta b_{32} &= -\frac{\sqrt{I_6^2 + I_7^2}}{J_g} \left( K_3 \cos \left( I_5 - \frac{J_h}{J_g} \arctan \left( \frac{I_7}{I_6} \right) + \delta g \right) - K_4 \sin \left( I_5 - \frac{J_h}{J_g} \arctan \left( \frac{I_7}{I_6} \right) + \delta g \right) \right), \\ \Delta b_{33} &= -\frac{\sqrt{I_6^2 + I_7^2}}{J_g} K_5 \cos \left( I_5 - \frac{J_h}{J_g} \arctan \left( \frac{I_7}{I_6} \right) + \delta g \right), \\ \Delta b_{51} &= -\frac{\sqrt{I_6^2 + I_7^2}}{J_g^2} \left( K_1 \cos \left( I_5 - \frac{J_h}{J_g} \arctan \left( \frac{I_7}{I_6} \right) + \delta g \right) - K_2 \sin \left( I_5 - \frac{J_h}{J_g} \arctan \left( \frac{I_7}{I_6} \right) + \delta g \right) \right) \arctan \left( \frac{I_7}{I_6} \right), \\ \Delta b_{52} &= -\frac{\sqrt{I_6^2 + I_7^2}}{J_g^2} \left( K_3 \cos \left( I_5 - \frac{J_h}{J_g} \arctan \left( \frac{I_7}{I_6} \right) + \delta g \right) - K_4 \sin \left( I_5 - \frac{J_h}{J_g} \arctan \left( \frac{I_7}{I_6} \right) + \delta g \right) \right) \arctan \left( \frac{I_7}{I_6} \right), \\ \Delta b_{53} &= -\frac{\sqrt{I_6^2 + I_7^2}}{J_g^2} K_5 \cos \left( I_5 - \frac{J_h}{J_g} \arctan \left( \frac{I_7}{I_6} \right) + \delta g \right) \arctan \left( \frac{I_7}{I_6} \right), \\ \Delta b_{61} &= \frac{K_1}{2} \left( \left( \frac{J_h}{J_g} + 1 \right) \cos \left( I_5 - \frac{J_h - J_g}{J_g} \arctan \left( \frac{I_7}{I_6} \right) + \delta g \right) + \left( \frac{J_h}{J_g} - 1 \right) \cos \left( I_5 - \frac{J_h + J_g}{J_g} \arctan \left( \frac{I_7}{I_6} \right) + \delta g \right) \right) \\ &\quad - \frac{K_2}{2} \left( \left( \frac{J_h}{J_g} + 1 \right) \sin \left( I_5 - \frac{J_h - J_g}{J_g} \arctan \left( \frac{I_7}{I_6} \right) + \delta g \right) + \left( \frac{J_h}{J_g} - 1 \right) \sin \left( I_5 - \frac{J_h + J_g}{J_g} \arctan \left( \frac{I_7}{I_6} \right) + \delta g \right) \right), \\ \Delta b_{62} &= \frac{K_3}{2} \left( \left( \frac{J_h}{J_g} + 1 \right) \cos \left( I_5 - \frac{J_h - J_g}{J_g} \arctan \left( \frac{I_7}{I_6} \right) + \delta g \right) + \left( \frac{J_h}{J_g} - 1 \right) \cos \left( I_5 - \frac{J_h + J_g}{J_g} \arctan \left( \frac{I_7}{I_6} \right) + \delta g \right) \right) \\ &\quad - \frac{K_4}{2} \left( \left( \frac{J_h}{J_g} + 1 \right) \sin \left( I_5 - \frac{J_h - J_g}{J_g} \arctan \left( \frac{I_7}{I_6} \right) + \delta g \right) + \left( \frac{J_h}{J_g} - 1 \right) \sin \left( I_5 - \frac{J_h + J_g}{J_g} \arctan \left( \frac{I_7}{I_6} \right) + \delta g \right) \right), \\ \Delta b_{63} &= \frac{K_5}{2} \left( \left( \frac{J_h}{J_g} + 1 \right) \cos \left( I_5 - \frac{J_h - J_g}{J_g} \arctan \left( \frac{I_7}{I_6} \right) + \delta g \right) + \left( \frac{J_h}{J_g} - 1 \right) \cos \left( I_5 - \frac{J_h + J_g}{J_g} \arctan \left( \frac{I_7}{I_6} \right) + \delta g \right) \right), \\ \Delta b_{71} &= \frac{K_1}{2} \left( \left( \frac{J_h}{J_g} + 1 \right) \sin \left( I_5 - \frac{J_h - J_g}{J_g} \arctan \left( \frac{I_7}{I_6} \right) + \delta g \right) - \left( \frac{J_h}{J_g} - 1 \right) \sin \left( I_5 - \frac{J_h + J_g}{J_g} \arctan \left( \frac{I_7}{I_6} \right) + \delta g \right) \right) \\ &\quad + \frac{K_2}{2} \left( \left( \frac{J_h}{J_g} + 1 \right) \cos \left( I_5 - \frac{J_h - J_g}{J_g} \arctan \left( \frac{I_7}{I_6} \right) + \delta g \right) - \left( \frac{J_h}{J_g} - 1 \right) \cos \left( I_5 - \frac{J_h + J_g}{J_g} \arctan \left( \frac{I_7}{I_6} \right) + \delta g \right) \right), \\ \Delta b_{72} &= \frac{K_3}{2} \left( \left( \frac{J_h}{J_g} + 1 \right) \sin \left( I_5 - \frac{J_h - J_g}{J_g} \arctan \left( \frac{I_7}{I_6} \right) + \delta g \right) - \left( \frac{J_h}{J_g} - 1 \right) \sin \left( I_5 - \frac{J_h + J_g}{J_g} \arctan \left( \frac{I_7}{I_6} \right) + \delta g \right) \right) \\ &\quad + \frac{K_4}{2} \left( \left( \frac{J_h}{J_g} + 1 \right) \cos \left( I_5 - \frac{J_h - J_g}{J_g} \arctan \left( \frac{I_7}{I_6} \right) + \delta g \right) - \left( \frac{J_h}{J_g} - 1 \right) \cos \left( I_5 - \frac{J_h + J_g}{J_g} \arctan \left( \frac{I_7}{I_6} \right) + \delta g \right) \right), \\ \Delta b_{73} &= \frac{K_5}{2} \left( \left( \frac{J_h}{J_g} + 1 \right) \sin \left( I_5 - \frac{J_h - J_g}{J_g} \arctan \left( \frac{I_7}{I_6} \right) + \delta g \right) - \left( \frac{J_h}{J_g} - 1 \right) \sin \left( I_5 - \frac{J_h + J_g}{J_g} \arctan \left( \frac{I_7}{I_6} \right) + \delta g \right) \right), \end{aligned}$$

where

$$\begin{aligned} K_1 &= -\frac{\sqrt{\zeta} \operatorname{cn}(u, \mu) \operatorname{dn}(u, \mu)}{\sqrt{dnk}}, \\ K_2 &= -\frac{\sqrt{1 + \kappa} \operatorname{sn}(u, \mu)}{\sqrt{dnk}}, \\ K_3 &= \frac{\sqrt{1 + \kappa} \sqrt{\zeta} \operatorname{sn}(u, \mu) \operatorname{dn}(u, \mu)}{\sqrt{dnk}}, \\ K_4 &= -\frac{\operatorname{cn}(u, \mu)}{\sqrt{dnk}}, \\ K_5 &= \sqrt{1 - \zeta} \sqrt{dnk}. \end{aligned}$$

and  $\delta g$ ,  $dnk$  and  $u$  and are given in (22), (20) and (23), respectively. If  $I_6 = I_7 = 0$ , the term  $\arctan(I_7/I_6)$  becomes undefined. However, in the equations of motion, this term is always multiplied by  $I_6$ ,  $I_7$ , or  $J_h - J_g$ , whose value is equal to zero when  $I_6 = I_7 = 0$ . Since  $\arctan(I_7/I_6) = \psi_h$ , which has a finite value, it follows that

$$I_6 \arctan(I_7/I_6) = 0,$$

$$I_7 \arctan(I_7/I_6) = 0,$$

$$(J_h - J_g) \arctan(I_7/I_6) = 0,$$

$$(J_h - J_g) \sin\left(\frac{J_g + J_h}{J_g} \arctan(I_7/I_6)\right) = 0,$$

$$(J_h - J_g) \cos\left(\frac{J_g + J_h}{J_g} \arctan(I_7/I_6)\right) = 0,$$

when  $I_6 = I_7 = 0$ .

## Data availability

Data will be made available on request.

## References

- [1] Ferrandiz J-M, Sansaturio M-E. Elimination of the nodes when the satellite is a non spherical rigid body. *Celest Mech Dyn Astron* 1989;46(4):307–20.
- [2] Vallejo M. Series de Fourier de funciones elípticas aplicacion a la precesion terrestre [Ph.D. thesis], Ministerio de Defensa, Real Instituto y Observatorio de la Armada, Universidad de Zaragoza; 1995.
- [3] Elipse A, Vallejo M. On the attitude dynamics of perturbed triaxial rigid bodies. *Celest Mech Dyn Astron* 2001;81:3–12.
- [4] Lara M, Ferrer S. Closed form perturbation solution of a fast rotating triaxial satellite under gravity-gradient torque. *Cosmic Res* 2013;51(4):289–303.
- [5] Lara M. Complex variables approach to the short-axis-mode rotation of a rigid body. *Appl Math Nonlinear Sci* 2018;3(2):537–52.
- [6] Deprit A. Canonical transformations depending on a small parameter. *Celest Mech Dyn Astron* 1969;1(1):12–30.
- [7] Lara M, Fukushima T, Ferrer S. First-order rotation solution of an oblate rigid body under the torque of a perturber in circular orbit. *Astron Astrophys* 2010;519:A1.
- [8] San Juan J, Lopez L, López R. Higher-order analytical attitude propagation of an oblate rigid body under gravity-gradient torque. *Math Probl Eng* 2012;2012:123138.
- [9] Mohmmmed M, Ahmed M, Owis A, Diwdar H. Analytical solution of the perturbed orbit-attitude motion of a charged spacecraft in the geomagnetic field. *Internat J Adapt Control Signal Process* 2013;4:272–86.
- [10] Zanardi M, Vilhena de Moraes R. Analytical and semi-analytical analysis of an artificial satellite's rotational motion. *Celest Mech Dyn Astron* 1999;75:227–50.
- [11] Benson C, Scheeres D. Averaged rotational dynamics of GEO debris. In: Flohrer T, Lemmens S, Schmitz F, editors. Proceedings of the eighth European conference on space debris, vol. 8. ESA Space Debris Office; 2021.
- [12] Benson C, Scheeres D. Averaged solar torque rotational dynamics for defunct satellites. *J Guid Control Dyn* 2021;44(4).
- [13] Garcia R, Zanardi M, Kuga HK. Spin-stabilized spacecrafts: Analytical attitude propagation using magnetic torques. *Math Probl Eng* 2009;2009:242396.
- [14] Barrio R, Palacià J. Lie transforms for ordinary differential equations: taking advantage of the Hamiltonian form of the perturbation. *Int J Numer Methods Eng* 1997;40:2289–300.
- [15] Sadov IA. The action-angle variables in the Euler-Poinsot problem. *J Appl Math Mech* 1970;34(5):922–5.
- [16] Kinoshita H. First-order perturbations of the two finite body problem. *Publ Astron Soc Japan* 1972;24:423.
- [17] Cavallari I, Feng J, Bi S, Vasile M. Semi-analytical long-term attitude propagation. In: Proceedings of the 2023 AAS/AIAA astrodynamics specialist conference. 2023.
- [18] Andoyer H. Cours de mecanique celeste, vol. 1, Gauthier-Villars et Cie, Paris; 1923.
- [19] Hancock H. Elliptic integrals. New York J. Wiley; 1917.
- [20] Beletsky VV. Motion of an artificial satellite about its center of mass. Nasa technical documents; 1966.
- [21] Liu Y, Chen L. Chaos in attitude dynamics of spacecraft. Springer Berlin, Heidelberg; 2013.
- [22] Ferraz-Mello S. Analytical study of the earth's shadowing effects on satellite orbits. *Celest Mech* 1972;5:80–101.
- [23] Valk S, Lemaître A. Semi-analytical investigations of high area-to-mass ratio geosynchronous space debris including earth's shadowing effects. *Adv Space Res* 2008;42(8):1429–43.
- [24] Henrard J. On a perturbation theory using Lie transforms. *Celest Mech* 1970;3(1):107–20.
- [25] Abad A, Elipse A, Vallejo M. Automated Fourier series expansions for elliptic functions. *Mech Res Commun* 1994;21(4):361–6.
- [26] Efthymiopoulos C. Canonical perturbation theory, stability and diffusion in Hamiltonian systems: applications in dynamical astronomy. In: Cincotta P, Giordano CM, Efthymiopoulos C, editors. La plata international school on astronomy and geophysics: chaos, diffusion and non-integrability in Hamiltonian systems - applications to astronomy, la plata observatory, July 11-15, 2011. AAA Workshop Series, Asociación Argentina de Astronomía; 2012, p. 3–146.
- [27] Zuiani F, Vasile M. Extended analytical formulas for the perturbed Keplerian motion under a constant control acceleration. *Celest Mech Dyn Astron* 2015;121(3):275.
- [28] Di Carlo M, da Graça Marto S, Vasile M. Extended analytical formulae for the perturbed Keplerian motion under low-thrust acceleration and orbital perturbations. *Celest Mech Dyn Astron* 2021;133(3):13.
- [29] Shuster MD. Survey of attitude representations. *J Astronaut Sci* 1993;41(4):439–517.
- [30] Lemaître A. Space debris: from LEO to GEO. In: Baù G, Celletti A, Galeš C, Gronchi G, editors. Satellite dynamics and space missions. Springer; 2019, p. 115–57.
- [31] Dysli P. Analytical ephemeris for planets. *Adv Space Res* 1977.
- [32] Bloch A, Gurfil P, Lum KY. The serret-andoyer formalism in rigid-body dynamics: II. Geometry, stabilization, and control. *Regul Chaotic Dyn* 2007;12(4):426–47.
- [33] Olver FWJ, Lozier DW, Boisvert RF, Clark CW. NIST handbook of mathematical functions. Cambridge University Press; 2010.
- [34] Byrd PF, Friedman M. Handbook of elliptic integrals for engineers and scientists. 2nd ed.. Springer-Verlag New York Berlin Heidelberg; 1971.